Mechanical Reliability Enhancement of Single Crystal Silicon Microstructures by Means of Diamond-Like Carbon Film Coating

ZHANG WENLEI

2019

Mechanical Reliability Enhancement of Single Crystal Silicon Microstructures by Means of Diamond-Like Carbon Film Coating

Submitted by

ZHANG WENLEI

Department of Micro Engineering

In partial fulfillment of the requirements

For the Degree of Doctor of Engineering

Kyoto University

Kyoto, Japan

2019

Abstract

Diamond-like carbon (DLC) film has been widely proposed as a protecting film for reliability enhancement or functional material in micro electro-mechanical systems (MEMS) device, due to its excellent mechanical properties and other functional properties in the field of electrics, photoelectricity, as well as biology. However, due to the difficulties in making specimen for mechanical tests given the high residual stress inherent in DLC film, only a few studies have succeed in the mechanical evolution of DLC coated microstructure.

In this thesis, the full DLC coating method, which deposited DLC film from all-around sides of a microstructure simultaneously, was developed to minimize the possible film spalling or structure deformation caused by unbalanced residual stress. The full coating method was adopted for reliability enhancement of two kinds of single crystal silicon (SCS) microstructures for tensile and torsional tests.

First, the possibility of fully DLC coating method was attempted on SCS microstructure using plasma enhanced chemical vapor deposition (PECVD) method No obvious deformation or fracture was found on coated silicon microstructure. The tensile strength was measured by a custom-made quasi-static tensile tester equipped with an electrostatic gripping system. Results show that both tensile strength and strength deviation were improved by fully DLC coating. The bare SCS microstructure had the average tensile strength of 1.86 GPa and coated one was 2.86 GPa. The feasibility of full DLC coating method was proved.

Second, the deposition bias voltage influence of DLC coating on the tensile properties of coated microstructure was investigate, with the purpose of clarification fracture mechanism as well as repeatability of full coating method. To understand the chemical and mechanical properties of deposited DLC films, the films were characterized by different evolution methods. Tensile test result showed that all of the coated structures had improved tensile properties. Among different deposition bias voltages, -400 V coated microstructure had the highest tensile strength, dominated by fracture toughness of

DLC/silicon system. Moreover, the strength deviation reduced with increasing of bias voltage, which was explained as the crack sealing phenomenon by residual stress inside DLC film and the influence was further discussed theoretically by the knowledge of fracture mechanism.

At last, the fully DLC coated method was used on SCS torsional microstructure to improve its torsional properties. A torsional tester was built and DLC coated SCS microstructure was fabricated. Average torsional fracture strength of DLC coated microstructure was 18.1~27.9% higher than that of the SCS one, with a value of 2.98 GPa. The torsional fracture strength exhibited a good agreement with the tensile fracture strength in DLC coated SCS microstructures. Deviation in torsional fracture strength was also reduced with increasing deposition bias voltage, due to the compressive residual stress of DLC film.

The findings revealed in this thesis are promising to lead the applications of DLC film for increasing the relatability of MEMS devices, as well as provide theoretical and practical information for the design on DLC coated microstructures. More importantly, the evolution, characterization and mechanical analysis method reported in this thesis inspire more research on DLC or even other hard coating material for MEMS application.

Acknowledgements

My efforts alone are not sufficient for this work to become reality without the contributions from many people around me over these years. At the beginning of this thesis, I would like to present my fully gratitude to them, for their guidance, advise, criticism and love.

First, I want to thank my Ph.D. supervisor Professor Osamu Tabata and Professor Toshiyuki Tsuchiya for their consistent guiding and supporting on my work during the past three years. They kindly help me in all the time of research, presentation, poster, publication and daily life by providing so many valuable discussion and comments. This dissertation would not have been possible without their intellectual contribution and remarks.

I would like to acknowledge Professor Yoshikazu Hirai in Tabata Lab. for his comments and questions during lab seminars as well as my publication reviewing. I also thank Professor Takahiro Namazu, Department of Engineering, Aichi Institute of Technology, for his great help on the research proposal. Many thanks give to Professor Dongfeng Diao, Institute of Nanosurface Science and Engineering, Shenzhen University, for his advising on the contents of third chapter.

I am grateful to the staffs who help with my research work, Mr. Tomoaki Mastushima, Mr. Yoshiyuki Inoue, Mr. Eiji Ohmura, Mr. Hiroyuki Seto and Mr. Shinji Kishimura, Nanohub, Kyoto University; Mr. Kosuke Ishikawa, Department of Mechanical Engineering and Science, Kyoto University; Dr. Yusuke Kondo, Mr. Kenichi Miura, and Mr. Yoshiharu Kakehi, Osaka Research Institute of Industrial Science and Technology; Mr. Kunimitsu Maejima and Dr. Kenshi Kimoto, Engineering Division, ESCO Ltd. Without their help, I cannot finish this interesting and meaningful research.

I want to acknowledge my dissertation committee members, Professor Motofumi Suzuki, Department of Micro Engineering, and Professor Hiroyuki Hirakata, Department of Mechanical Engineering and Science, for their interests in this work. They provide their precious time and patience to

review my thesis and invaluable advice that is greatly helpful to shape this thesis and for my future research.

I would like to thank all of the staffs in Tabata Lab. through my stay in Japan, especially grateful for all the help I received from the staffs, Ms. Miri Okino, Ms. Keiko Kawano, Ms. Yukiko Himuro and Ms. Naoe Souma. Special thanks for Dr. Amit Banerjee, for his kindly advice and help with my research, data process, and language modification on my paper and thesis. I thank Dr. Zhipeng Ma, Dr. Akio Uesugi, Mr. Naoki Yamashita, Mr. Tetstuya Hemmi, Mr. Yusuke Shiomi, Ms. Akiko Uno, Mr. Tomoya Nakamura, Mr. Yunyi Shu, Mr. Kazutaka Obitani and Mr. Xiaoyu Wang, Department of Mechanical Engineering and Science, Kyoto University for sharing their knowledge and all the contribution to my research work. I also would like to thank all the lab members for making me a great study and life here.

I would give my deepest thank towards my parents, my fiancee Ying Yin and my other relatives. Because of their inspiration, blessings, sacrifices and will-power, I could overcome one and another difficulty, and finally reach my dream. Special thanks for my best friend, Bo Yang, Tepper School of Business, Carnegie Mellon University, for his encouragement and support all the time. I am also thankful to China Scholarship Council (CSC) for the financial support during my Ph.D. course.

Last but not least, please allow me to present my thank again, to everyone the one who loves me and the one I love in my life. And many thanks for you, the readers who are reading this thesis.

Contents

Contents i

List of Figures v

List of Tables ix

Chapter 1 Introduction 1

1.1 Overview 1

1.2 Motivation 2

1.3 DLC Film 3

1.3.1 Chemical Contents 3

1.3.2 Deposition Methods 5

1.3.3 Mechanical and Other Properties 6

1.3.4 Application 10

1.4 MEMS Reliability 13

1.4.1 Overview 13

1.4.2 Reliability Test on Silicon 14

1.4.3 Reliability Improvement on Silicon Microstructure 17

1.5 Thesis Outline 18

1.6 Conclusion 19

Chapter 2 Tensile Testing of Silicon Microstructure Fully Coated with PECVD DLC Film 23

2.1 Introduction 23

2.2 Experiment 24

2.2.1 Tensile Test System 24

2.2.2 Microstructure Fabrication 25
2.2.3 DLC Deposition 27
2.2.4 Tensile Test 29
2.3 Results 30
2.4 Discussion 34
2.5 Conclusion 36
Chapter 3 Effect of Deposition Bias Voltage on Tensile Properties of DLC Coated Silicon Microstructure 39
3.1 Introduction 39
3.2 Experiment 40
3.2.1 Microstructure Fabrication 40
3.2.2 Characterization of DLC 41
3.2.3 Tensile Test 43
3.3 Results 44
3.3.1 Characterization Results 44
3.3.2 Tensile Properties 52
3.4 Discussion 55
3.4.1 Tensile Strength Improvement 55
3.4.2 Strength Deviation 57
3.5 Conclusion 59
Chapter 4 Torsional Properties of DLC Coated Silicon Microstructure Using Resonant Vibration Testing 63
4.1 Introduction 63

4.2 Experiment 64
4.2.1 Torsional Test System 64
4.2.2 Silicon Torsional Microstructure Design 67
4.2.3 DLC Coated Torsional Microstructure Fabrication 74
4.2.4 Characterization of DLC 76
4.2.5 Torsional Test 77
4.3 Results 77
4.3.1 Characterization Results 77
4.3.2 Torsional Properties 80
4.4 Discussion 85
4.5 Conclusion 88
Chapter 5 Conclusion 91
5.1 Overview 91
5.2 Chapter Summary 92
5.3 Practical Application 94
5.4 Future Work 95
List of Publications 97

List of Figures

Figure 1-1 Number of publications on diamond-like carbon film in four decades. 3

Figure 1-2 Ternary phase diagram of bonding in the family of DLC films. 5

Figure 1-3 Schematic illustration of the working principle for ECR ion irradiation and electron irradiation process. 6

Figure 1-4 SEM picture of an SU8/DLC microcage and captured polystyrene micro-ball 8

Figure 1-5 The schematic illustration of the friction-electrification coupling at sliding interface of DLC film 9

Figure 1-6 Selected engine parts coated with DLC 11

Figure 1-7 (a) SEM micrograph and sketch of DLC coated electrostatic lateral output motor; (b) Life time of DLC coated lateral motor and uncoated one 12

Figure 1-8 Patterning DLC film with different shapes and dimensions 13

Figure 1-9 Photography and and sketch of high temperature tensile test system 15

Figure 1-10 Schematic of pure torsion, uniaxial tension, and tension-torsion combined loading test for investigating the mechanical characteristics of a microscale beam specimen. 16

Figure 1-11 Tensile test on single side DLC coated SCS microstructures. 18

Figure 2-1 Sketch of tensile testing system. 24

Figure 2-2 The principle for electrostatic gripping. 25

Figure 2-3 Mask design of tensile microstructure 26

Figure 2-4 Fabrication flow of tensile microstructure. 27

Figure 2-5 Full coating by adopting PECVD. 28

Figure 2-6 The output-force curve of the loading cell. 30

Figure 2-7 FESEM image of DLC coated tensile microstructures. 31

Figure 2-8 Tensile force-stage displacement curves of SCS and DLC coated microstructures..... 31

Figure 2-9 Tensile strength of SCS and DLC coated microstructures. 32

Figure 2-10 Weibull plots of SCS and DLC coated microstructures. 33

Figure 2-11 Typical fracture surface of microstructures observed at a tilt angle of 45°..... 34

Figure 3-1 Fabrication flow of tensile microstructure. 41

Figure 3-2 Raman spectra of DLC at bias of −200 V and −600 V. 44

Figure 3-3 Comparison between Raman and XPS characterization 46

Figure 3-4 TDS spectra (methane, ethylene and hydrogen contents) of DLC at bias of −200 V. 47

Figure 3-5 Hydrogen atomic density measured with TDS and Raman parameter k/I_G..... 48

Figure 3-6 Nano-indentation curves for DLC film deposited at different bias voltages..... 49

Figure 3-7 The surface quality and roughness of microstructures with different bias voltages 50

Figure 3-8 Fracture toughness measurement.. 52

Figure 3-9 Tensile strength of SCS and DLC coated microstructures with different bias voltage. 53

Figure 3-10 Weibull plot for tensile strength of silicon and DLC microstructures coated at different bias voltages. 54

Figure 3-11 Typical fracture surfaces of microstructures observed at a tile angle of 45° 54

Figure 3-12 Average tensile strength and fracture toughness value for silicon and DLC/silicon system. . 56

Figure 4-1 Sketch of torsional testing system. 65

Figure 4-2 Displacement of piezoelectric actuator with increasing of applied voltage and working frequency of 1 KHz and 2 KHz. 66

Figure 4-3 Sketch of micro displacement measuring system. 66

Figure 4-4 Calibration results from a standard Gonio stage 67

Figure 4-5 Sketch of torsional microstructure. 68

Figure 4-6 The relationship between required displacement and offset parameter. 70

Figure 4-7 FEM simulation model of torsional beam. 73

Figure 4-8 Stress distribution along the torsional beam. 73

Figure 4-9 Fabrication process of torsional microstructure. 74

Figure 4-10 Mask design for one torsional microstructure. 75

Figure 4-11 DLC coated torsional microstructure 76

Figure 4-12 Raman spectra of DLC films with different bias voltages. 78

Figure 4-13 Nano-indentation curve of DLC films 79

Figure 4-14 Typical frequency response of SCS and -400 V coated torsional microstructures. 81

Figure 4-15 Typical loading curves of torsional test of bare and DLC coated SCS microstructures. 81

Figure 4-16 Average torsional fracture strength and tensile fracture strength values of SCS and DLC coated microstructures with different deposition bias voltages. 83

Figure 4-17 Weibull plot of torsional fracture strength of SCS and DLC coated microstructures with different deposition bias voltages. 84

Figure 4-18 Typical fracture surfaces of torsional beam observed at a tile angle of 45° with the fracture origin and fracture planes. 84

List of Tables

Table 2-1 Working parameters of PECVD 29

Table 3-1 Fitting parameters for Raman spectra of DLC film. 46

Table 3-2 Hardness, elastic modulus, residual stress and roughness of SCS and DLC films. 49

Table 3-3 Fracture toughness value of SCS and DLC film. 51

Table 4-1 Main parameters of torsional microstructure. 72

Table 4-2 Fitting parameters of Raman spectra of DLC films. 78

Table 4-3 Mechanical properties of SCS and DLC films. 80

Table 4-4 Resonance properties of bare and DLC coated microstructures with different deposition bias voltages. 86

Chapter 1 Introduction

1.1 Overview

The goal of this thesis is to enhance the reliability of silicon based micro electro-mechanical system (MEMS) structure, including tensile properties and torsional properties, through full diamond-like carbon (DLC) film coating using plasma enhanced chemical vapor deposition (PECVD) method.

The single crystal silicon (SCS) microstructure was fabricated from a 4-inch silicon on insulator (SOI) wafer using a standard MEMS manufacturing technique including metal film deposition, photolithography, deep plasma reactive ion etching (DRIE) and wet etching process. In order to realize full DLC coating, the chip carrying released microstructures was attached on a special fixer with an opening, and the fixer revolved both on its own axis and the center axis of deposition chamber of PECVD machine. In this machine, plasma was generated at the center of the chamber and film was deposited by the negative bias voltage applied on the fixer. The chip was exposed from the both sides to the plasma with the revolutions, which realized a conformal deposition of hundreds of nano-thick DLC film coating. Different bias voltages were adopted to ensure the repeatability of this work as well as to investigate the fracture or reliability improving mechanism.

The tensile and torsional properties of bare SCS and DLC coated microstructures were evaluated in custom-made tensile and torsional test system, respectively. The tensile strength, torsional strength, strength deviation and fracture origination were mainly concentrated.

Since tensile and torsional properties of the microstructure strongly depended on the mechanical properties of surface DLC film, it is very important to explore the best coating parameters for reliability improvement, and to clarify the relationship between coating parameter and fracture mechanism from experimental data. In this work, the chemical contents and mechanical properties, including thickness, elastic modulus, hardness, surface roughness, residual stress and fracture toughness of DLC film were

characterized by various experimental method: Raman spectroscopy, X-ray photoelectron spectroscopy (XPS), thermal desorption spectrometry (TDS), atomic force microscope (AFM), scanning electron microscope (SEM), surface profilometry and nanoindentation. The mechanism was further discussed by the combination of characterization results and theoretical analysis. This work related to reliability of fully coated silicon would open new applications of SCS microstructure especially in corrosive or harsh environment.

1.2 Motivation

Silicon is one of the most commonly used materials in MEMS industry nowadays, due to its well-established processing, high reserves and low cost. However, silicon has its material limitation. In particular, it is a brittle material with relatively low fracture toughness, large coefficient of friction (COF) and high wear rate against many common materials, which influences the reliability of silicon-based MEMS components [1]. Moreover, the comparatively low chemical stability in alkali or some acid environment and poor biocompatibility [2] may restrict silicon from usage of corrosion or biological condition. Since the current MEMS technology is mainly dominated by silicon material, compared with seeking for new materials, a concise way is using coating technology for a surface modification of silicon structure. Among coating materials, DLC film would be the most promising one since it has relatively high hardness, toughness, tribology properties, good chemical stability and biocompatibility, which cooperate with silicon well. Thus, understanding the mechanical properties, including the tensile and torsional properties, is required for optimum design of DLC coated MEMS structure.

However, most of DLC films have a fatal disadvantage, high compressive residual stress. When deposited on one side of microstructure surface, the unbalanced residual stress may cause structure deformation or even direct fracture, leading to an aggravation in the reliability [3]. Thus, the full DLC

coating method is proposed to minimized the deformation from unbalanced residual stress and also take the advantage of compressive residual stress for fracture toughness enhancement [4].

On the other hand, even though DLC film attracts much attention from researchers in the recent 10 years (Fig. 1-1) and is widely used in traditional industry [5], because of the data lacking of basic mechanical properties in micro/nano-scaled usages, DLC film has not been common used in MEMS research field. In this thesis, we aim to first study to these fundamental mechanical properties for DLC coated microstructure, providing a theoretical and practical guideline for the promising applications in MEMS or material research.

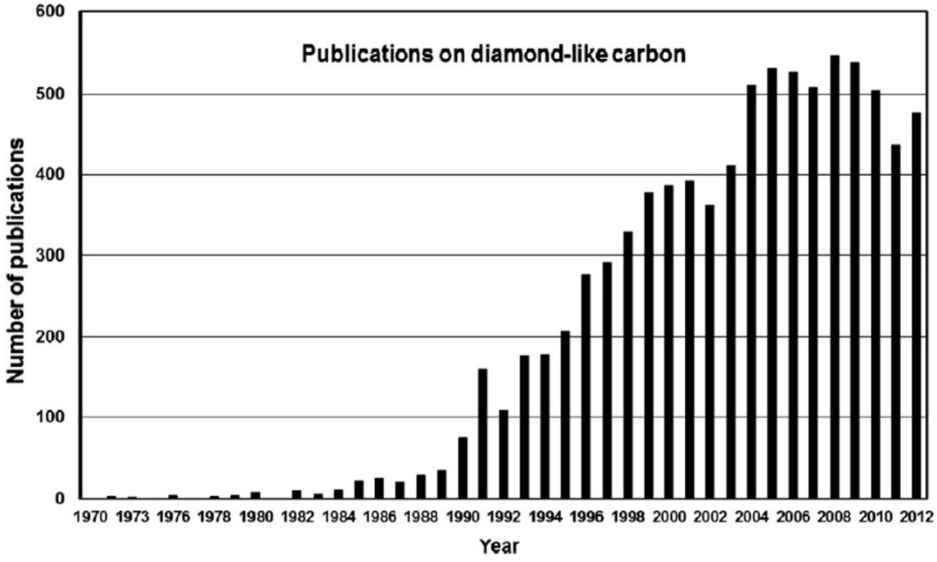

Figure 1-1 Number of publications on diamond-like carbon film in four decades [5].

1.3 DLC Film

1.3.1 Chemical Contents

Carbon is the most shining stars in the material research field and has attracted world-wide interest from research groups and industry in the recent years. One of the most fantasy points of carbon is that it

has two different phase, sp^3 phase and sp^2 phase, which exhibit exactly opposite properties. The sp^3 phase carbon has perfect symmetry of diamond structure, leading to properties like extremely high hardness, residual stress, excellent thermal conductivity, high electrical resistivity, wide band gap, high frication and low wear rate [6, 7]. The sp^2 phase carbon is quite weak in perpendicular direction where only weak Van der Walls force acts, and thus results in low hardness, low electrical resistivity, low frication and high wear rate [8, 9].

By different arrangement of these two phases, researchers have discovered a serious of carbon-based material from macroscopic to microcosmic, including fullerenes, nanotubes, graphene, glassy carbon, graphite, diamond, and amorphous carbon [10].

Amorphous carbon consists of a disordered network of carbon atoms with a mixture of both sp^3 and sp^2 coordinated phase bonds. In should be noticed that even through some carbon films with small graphene or diamond crystal clusters inside are reported recently [11, 12], they are still regarded as amorphous carbon on the whole. And the family of amorphous carbon films regardless of hardness, is called diamond-like carbon, or DLC [13].

Depending on the deposition methods, such as PECVD method, because the film is made from hydrocarbon gases (methane, ethylene or acetylene), some hydrogen atoms are concluded into the film and affect its properties. Jacob et al. first raised a ternary phase diagram to display the contents of various forms in DLC film, as shown in Fig. 1-2 [14]. The sp^3 phase carbon, sp^2 phase carbon and hydrogen are three major contents inside DLC film.

Like silicon, DLC film can be doped by nonmetals or metals atoms to enhance its critical properties. Among them, silicon, nitrogen, fluorine, titanium, and chromium are the most common ones [15]. The influence of doping material on the properties of DLC film is introduced in section 1.3.3.

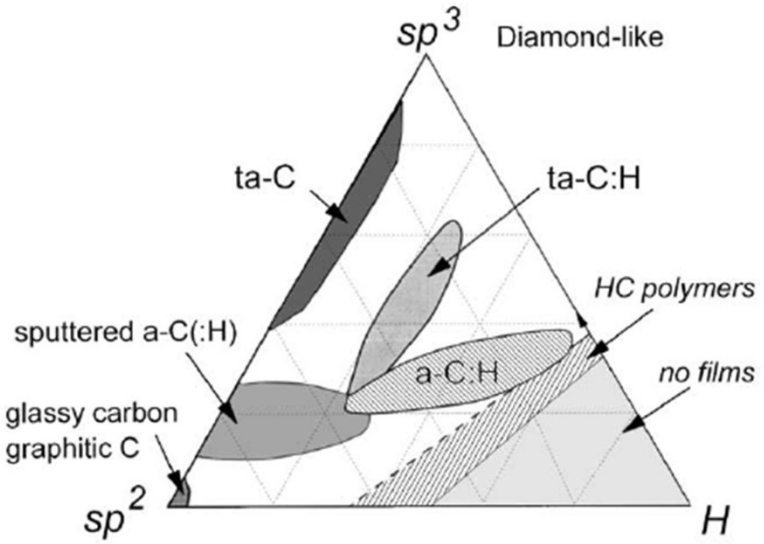

Figure 1-2 Ternary phase diagram of bonding in the family of DLC films [14].

1.3.2 Deposition Methods

Many methods have been developed for producing DLC film, including ion beam deposition, sputtering, cathodic arc deposition, pulsed laser deposition and plasma enhanced chemical vapor deposition [16]. The most common industrial process for the depositions of DLC film are sputtering and PECVD.

Figure 1-3 draws a sketch of one of the typical sputtering methods, electron cyclotron resonance (ECR) sputtering [17]. The Ar^+ plasma is excited by DC or RF power source and hits the graphite target. Magnets are placed near the target to form the shape of the plasma and direct the sputtered carbon atoms towards substrate. A second plasma beam (ion beam or electron beam) is used to bombard the growing film to densify the film or apply energy for film growth. High sputtering energy can extend sp^2 phase towards sp^3 phase and lead to an increasing in film hardness [18]. Hydrogen free DLC film (a-C) can be achieved by sputtering method since the targets are mostly made by pure graphite. However, the sputtering has problems in the high substrate temperature (70~200 °C after ECR sputtering), high film

residual stress [17], and also, since carbon atoms have a relativity strong directivity, the film is hard to be deposited on the side wall of microstructure.

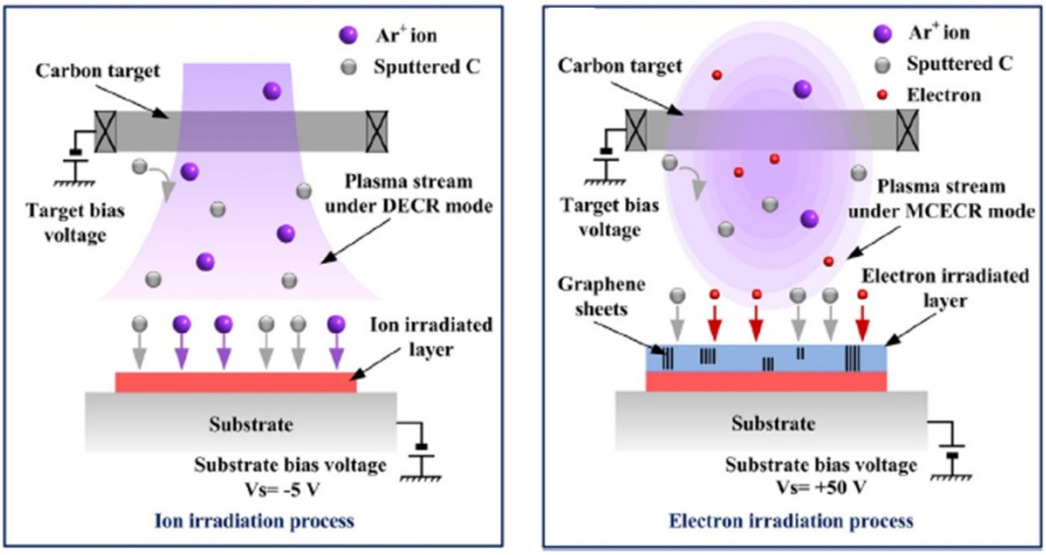

Figure 1-3 Schematic illustration of the working principle for ECR ion irradiation and electron irradiation process [17].

Another deposition method is PECVD, which is achieved by introducing reactant gases between parallel electrodes, a grounded electrode and an RF energized electrode. The capacitive coupling between the electrodes excites the reactant gases into plasma, which induces a chemical reaction and results in the reaction product being deposited on the substrate. Compared with sputtering, PECVD method can only fabricate hydrogen DLC film (a-C:H) for the restriction from reactant gases. PECVD method has less directivity and is promising to form formal coating on the side wall.

1.3.3 Mechanical and Other Properties

DLC film is well known for its excellent mechanical properties, including elastic modulus, hardness, and tribology properties. Recently, the properties in conductive, magnetic, photoelectric and biological

fields also have been reported, which extend the potential usages of DLC film acting as a MEMS functional material besides a protection material.

1.3.3.1 Mechanical Properties

The elastic modulus and hardness of DLC films have a large range from 10~700 GPa and 2~30 GPa respectively [13], decided by their different chemical contents. Among them, Grimm et al. deposited a super hard a-C films with the hardness of 40~50 GPa, elastic modulus of 450 GPa by pulsed vacuum arc discharge, a kind of physical vapor deposition (PVD) method [19]. By using titanium and tungsten doping, Zhang et al. succeed an even harder DLC film with a figure of 53 GPa [20].

DLC films are usually suffer from a high compressive residual stress, due to the temperature changing during deposition or bonding structure [21]. The stress level was around 1~2 GPa for a-C:H films and 8-10 GPa or even higher for a-C films. High residual stress may cause substrate deformation, film fracture or film spalling from the substrate. In most of occasions, the residual stress is not a desirable material property for film deposition and could be reduced by post-annealing [22] or silicon/metal doping [23]. However, some novel devices are able to take advantages from residual stress to form useful 3D microstructures such as the SU-8/DLC microcage shown in Fig. 1-4 [1]. Besides, the fully coating method reported in this thesis gives another example on the usage of compressive residual stress in DLC film.

The most well-known mechanical properties of DLC films are their excellent tribological properties, including low coefficient of friction (COF) and high wear life, in both dry and wet lubricated conditions. The general principle of that can be explained as when two surfaces slide against each other, the surface of DLC film wear out and form a surface layer called transfer layer. This transfer layer is mainly made by graphite and acting as a lubricant between the friction pair, causing low COF and high wear life. The common COF of a-C:H is 0.025~0.22 in the dry air [24]. Recently, Wang et al. doped PECVD DLC film by fluorine/sulfur mixture gas and achieved low COF of 0.01~0.02 [25]. This value becomes even less by

Yue et al. They deposited a kind of DLC film with fullerene-like clusters inside and achieved a super-low friction with a COF of 0.006 [26].

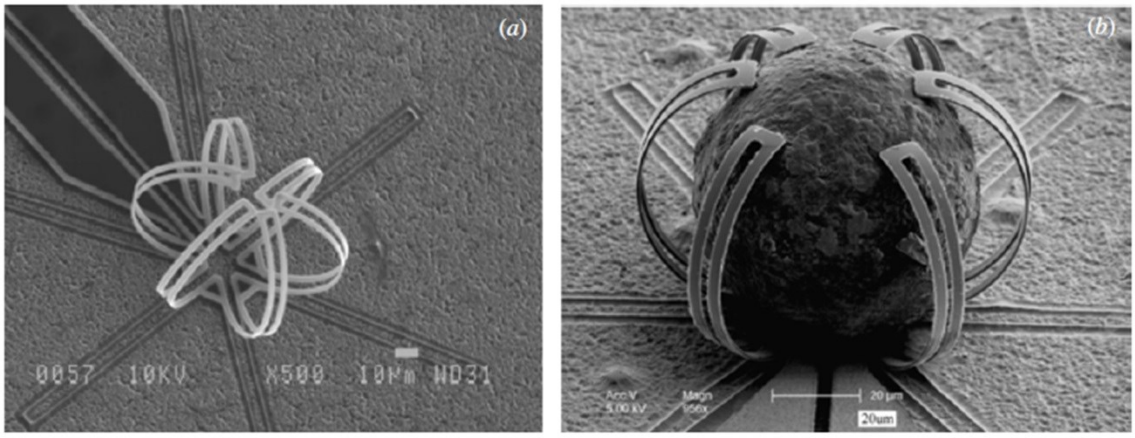

Figure 1-4 SEM picture of (a) an SU8/DLC microcage with a finger length of 100 μm fabricated by the authors and (b) an SEM picture of the microcage and captured polystyrene micro-ball [1].

Besides, DLC film has good antistiction, corrosion resistance and hydrophobic surface, which lead it to other applications in biologic or fluid fields.

1.3.3.2 Functional Properties

Beside excellent mechanical properties, DLC film equipped with other interesting functional properties is also developed in the recent years. Because of the relatively simple fabrication method compared with other carbon-based material like graphene or diamond, the applications of functional DLC film is highly expected.

In most of occasions, DLC films have a very low conductivity because of their amorphous structure. By critical fabrication methods, some graphene clusters may be concluded in the film and change the conductivity of DLC film. Nakao et al. made a conductive DLC film by high power pulsed magnetron

sputtering with bipolar type plasma based ion implantation system, which had an acceptable resistivity of 0.5 Ω·cm and a high hardness of 11 GPa [27].

Zhang et al. deposited a kind of DLC film with friction electrification properties. This DLC film also contented graphene clusters inside and generated as high as 10 V open-circuit voltage between two 25 mm square, 100 nm thick sliding [28]. The film was hopefully to act as a triboelectric nanogenerator in MEMS field (Fig. 1-5).

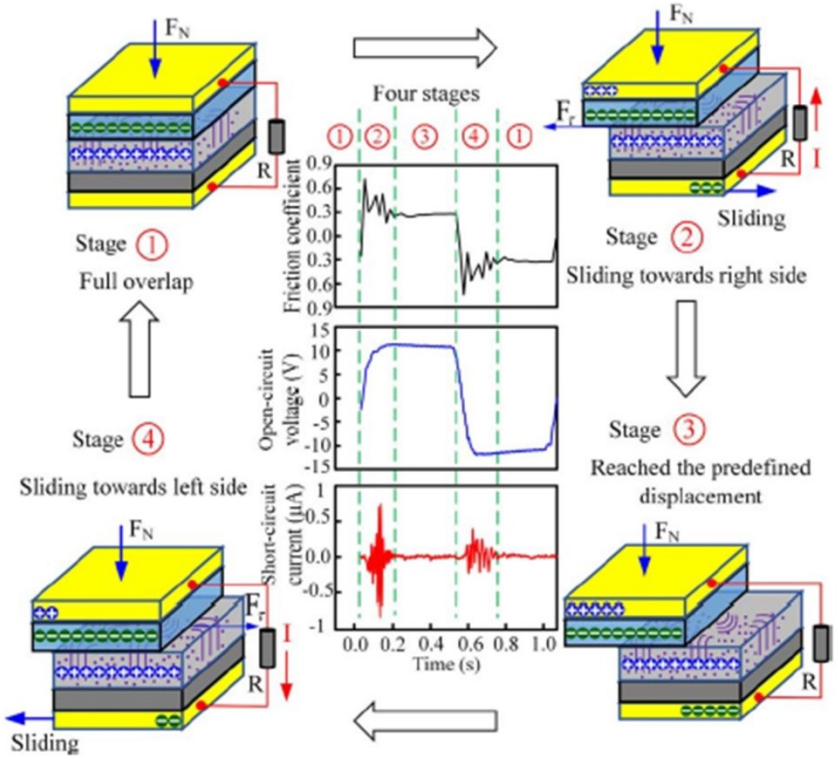

Figure 1-5 The schematic illustration of the friction-electrification coupling at sliding interface of DLC film [28].

The graphene clusters embedded DLC film also has photoelectric behaviors. Yang et al., from the same group, found that the film could generate 8.4 mA/cm^2 current with the illumination of 100 mW/cm^2 [29], which was four times of usual amorphous carbon and even 2.5 times larger than graphene.

DLC film has good biocompatibility and attracts much attention from biomaterial researchers recently. Among them, Subramanian et al. contrasted the biocompatibility of pure PECVD DLC film,

fluorinate, silicon and nitrogen doped DLC film respectively, for the usage of bone implants [30]. The result proved that neither of DLC film had toxic effect on osteoblasts. Moreover, compared with traditional Ti_6Al_4V substrate, the osteoblasts growing on nitrogen doped DLC film produced more alkaline phosphatase and calcium during 28-days observation, which indicated the surface DLC coating was promising to be used as metallic implants for human health.

1.3.4 Application

DLC film has been widely used for traditional industry products, mainly taking advantages of its good mechanical properties, such as high hardness and excellent tribological properties. However, the applications in MEMS are still remaining at research stage. In this section, the applications of DLC film are introduced from these two aspects in detail.

1.3.4.1 Traditional Industry

The biggest mass-produced application of DLC film is automotive parts such as pistons, valves and tappets. These applications began with various types of coatings for high-end racing engines at the beginning of the 1990s. The excellent tribological properties behaviors of DLC coatings on heavily loaded parts result in a decrease of friction loss, preventing adhesive and abrasive wear. Figure 1-6 draws the widely adopted DLC coating parts in an automotive engine [31]. As an example, as early as 2006, the Nissan motor company started to introduce a 1-μm-thick DLC film for the tappets usage in its new car (Nissan V6), and achieved a fuel consumption reduction of 2% by this simple coating [32].

Because of the hard property and corrosion resistance, DLC film has also been used in some consumer products as a protecting layer, for example, razor blades, cooking knives, medical instruments, and cutting tools [5].

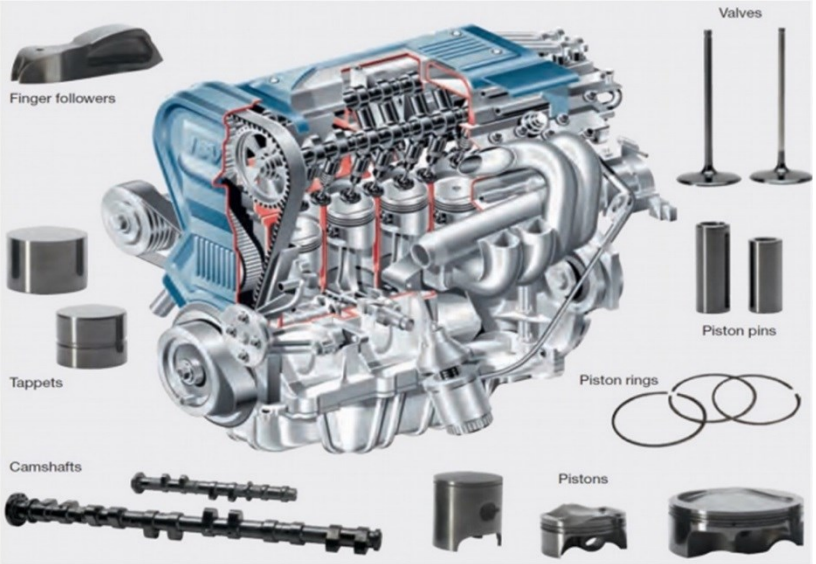

Figure 1-6 Selected engine parts coated with DLC [31].

Besides, DLC film has other interesting applications. Among them, Hakutsuru, a Japanese wine company coated DLC film on the inner surface of their plastic wine bottles to prevent the negative effect of oxygen to the wine taste [33]. Compared with traditional glass bottles, DLC coated plastic bottles have to advantages of in weight, toughness and storage. Moreover, because of its metallic appearance, DLC film is also used for decoration in watches and textiles.

1.3.4.2 MEMS Industry

Till now, DLC film has not been mass-produced for MEMS usages. However, due to its attractive properties and good adhesion with silicon, polymer or other basic MEMS material, the potential applications of DLC film still capture researchers' attention.

The earliest application of DLC film on MEMS related to its excellent tribological properties. Smallwood et al. fabricated a MEMS electrostatic lateral output motor coated with a PECVD DLC film to against wear [34]. The life of DLC coated motor showed a sixteen times increase over the uncoated

device when running in the air, and had a three hundred times increase when running in the vacuum (Fig. 1-7).

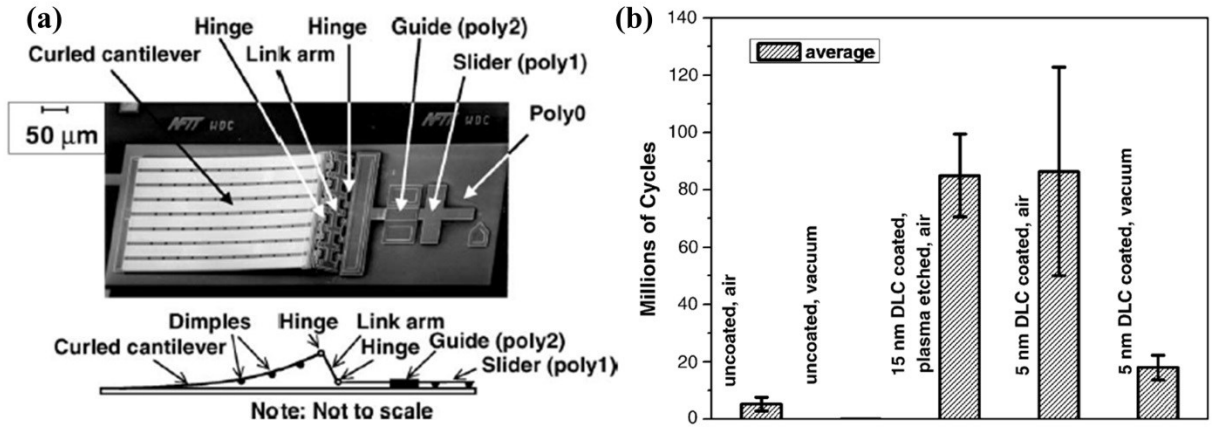

Figure 1-7 (a) SEM micrograph and sketch of DLC coated electrostatic lateral output motor; (b) Life time of DLC coated lateral motor and uncoated one [34].

Silicon-based technologies are always reported to suffer from problems of stiction and abrasion, leading to the poor reliability of silicon MEMS switch. Sumant et al. fabricated a switch made by 400 nm DLC film with a gate pull-in voltage of 90 V [35].The transient switching revealed that a long duration on in the on state did not create a stiction problem even in the air.

DLC film has good biocompatibility as well as changeable hydrophobic surface, which makes it become attractive for microfluidic devices. Murayama et al. coated two kinds of DLC films on microchannel of microfluidic devices and found a good blood compatibility and changeable wettability [36]. Compared with traditional SU-8 devices, DLC coated ones have a maximum contact angle of 89.7° against pure water and the oxygen-doped ones have a minimum value of 1.0°. Moreover, after 24 hours immersed into acetone as an organic solvent, some cracks were observed on the surface of SU-8 devices while no significate change happened on the DLC coated deceives due to its high chemical stability.

The biggest challenge for the applications of DLC film in MEMS device is pattern method. DLC film has high hardness and chemical stability, which restrict its shaping and fabrication. Virganavicius et al. developed a stable pattern method using silicon containing thermoplastic resist (SiPol) as a hard mask and etched DLC film by pure oxygen plasma [37]. As shown in Fig. 1-8, they successfully patterned DLC film with different shapes and smallest dimensions down to 300 nm for sensor applications.

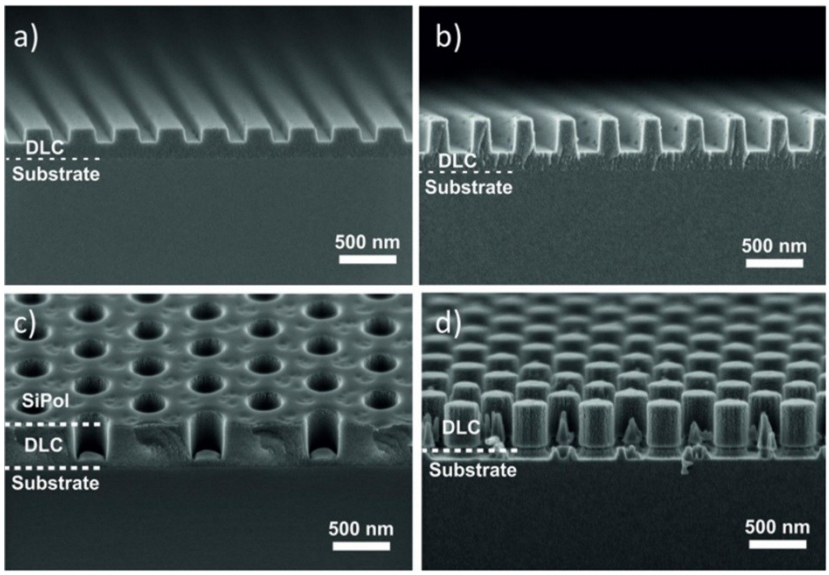

Figure 1-8 Patterning DLC film with different shapes and dimensions [37].

1.4 MEMS Reliability

1.4.1 Overview

MEMS device is expected to penetrate consumer markets in a vast number of areas including accelerometers, gyroscopes, pressure sensors, resonators, relays, switches, micro pumps and valves. MEMS device is attractive because of its high throughput, cost efficiency, small size, and high integration capability with electric circuits. It is expected in the field of RF/microwave, optical communication, energy saving, and bio-medical areas [38].

Within the rapid development of MEMS technology, MEMS device starts to play quite important role around our daily life. Since most of its functions are related to the mechanical movement, the device reliability is more and more important to ensure the safety and quality for our life. Understanding the failure mechanisms is a prerequisite for quantifying and in turn improved the reliability of MEMS devices.

Huang et al. reviewed the different failure mechanisms of MEMS device and their root causes [38]. He concluded MEMS reliability from seven aspects: mechanical fracture, including overload and shock, stiction, charge accumulation, wear, creep and fatigue, electric short and open, and contamination. Tsuchiya et al. distinguished the evolution of MEMS reliability from three different levels from the basic material to real MEMS production: sample-class level, component-class level and production level [39]. Before mass-producing of a new MEMS device, the material and fabrication method influence on reliability should be studied from sample-class level to grasp the basic parameter and fracture mechanism for design and optimization. Then, the evolution on component-class level should be done to examine if the components containing expected properties. At last, some trial productions could be further tested based on the experience from previous two levels.

1.4.2 Reliability Test on Silicon

Silicon is one of the most common used structure materials in the MEMS industry nowadays, due to its well-established process, high reserves and low cost. However, silicon belongs to brittle material, which may become invalid suddenly by mechanical deformation from operations, the evaluation of its mechanical property with high accuracy is important for the reliability improvement. Among different reliability tests on silicon, the most important aspect is mechanical fracture, including tensile, bending and torsional fracture properties.

In previous time, the tensile strength of silicon was mainly obtained by out-of-plane bending or nanoindentation. However, from these tests, researchers cannot get the value directly and also the strength

concertation and substrate effect may cause addition error to the obtained results. Tsuchiya et al. developed a uniaxial tensile tester equipped with an electrostatic gap to hold the SCS microstructure. They found the tensile strength of value was 1.5~4.7 GPa, depending on the dimensions of tensile microstructures [40]. Namazu et al. proposed a tensile specimen assembled with hooking holes and grasped by two hooks [41]. He got the relatively smaller tensile strength of 1.46 GPa, probably because of the large specimen dimensions.

The tensile strength of silicon microstructures is not fixed and highly depends on their crystal orientation and fabrication process. Uesugi et al. studied their influence and found that the microstructures made by <110> and <111> orientation silicon had higher strength than that of <100> orientation silicon [42]. Moreover, longer wet etching for residual removal caused rough structure surface and a decrease in tensile strength. Some silicon-based MEMS devices are designed for in harsh environments, such as engine room sensors, gas sensors, and aerospace sensors. These applications require better understanding of high-temperature tensile properties. Uesugi et al. investigated the tensile behaviors of SCS microstructures in high temperature (Fig. 1-9) and found a strength decreasing when the testing temperature is over 500 °C [43]. A brittle-ductile transition (BDT) was observed at the same time.

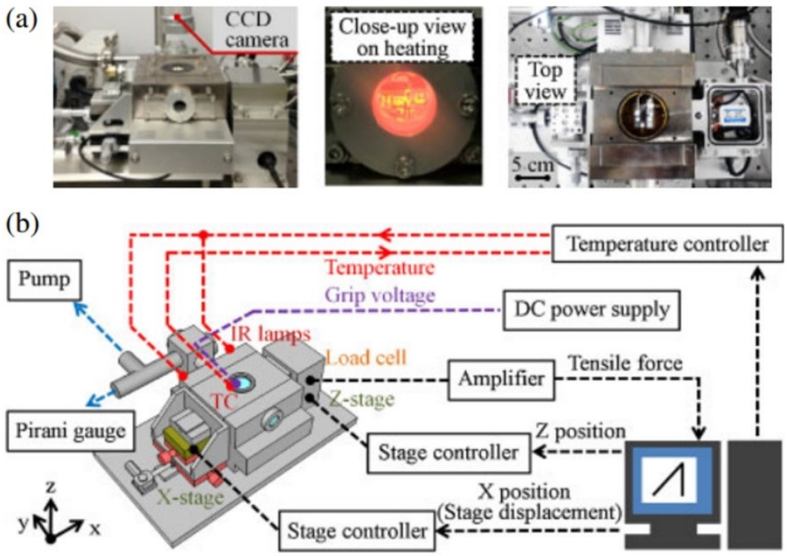

Figure 1-9 Photography and and sketch of high temperature tensile test system [43].

On the aspect of torsional test, Wolter et al. developed a silicon micro scanning mirror driven by electrostatic force from a comb structure [44]. The torsional beam was of 150 μm in length, 6.6 μm in width and 30 μm in height. The torsional strength was calculated from maximum torsional angle, ranging from 2.0 GPa to 2.45 GPa.

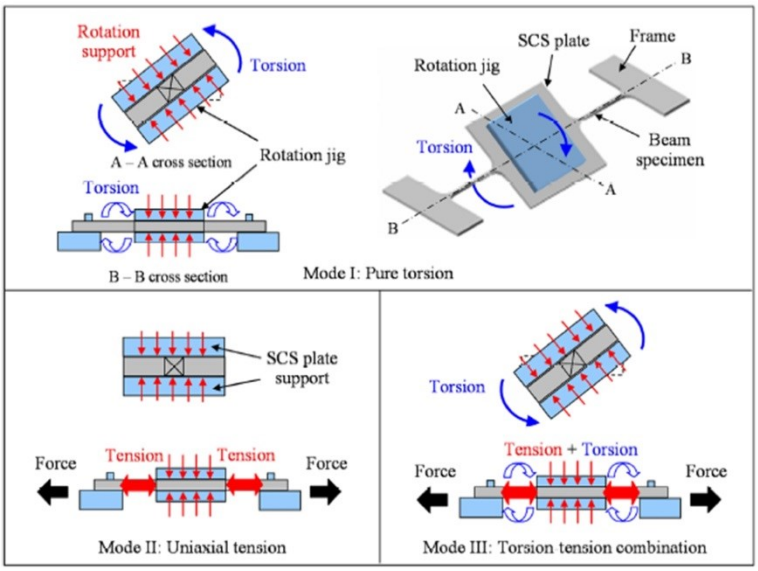

Figure 1-10 Schematic of pure torsion, uniaxial tension, and tension-torsion combined loading test for investigating the mechanical characteristics of a microscale beam specimen [45].

Namazu et al. built a quasi-static tension-torsion combined loading test equipment and contrasted the pure torsion, uniaxial tension, and tension–torsion combined test results for investigating the mechanical characteristics of a microscale beam specimen (Fig. 1-10) [45]. The result showed that the average uniaxial tensile strength of silicon was 0.81 GPa, while the torsional strength was 1.14 GPa. However, due to the lack of specimen types and the number of specimens for each test were not same, it was difficult to evaluate the relationship between tensile and torsional fracture strength.

1.4.3 Reliability Improvement on Silicon Microstructure

In last section, some typical research on the evolution of silicon reliability, especially tensile and torsional strength, was reviewed. Based on these studies, other researchers did some trials to improve the reliability of silicon microstructure by using different surface modification, which are briefly introduced in this section.

Imperfections, like surface roughness and defects, introduced by common manufacturing processes are recognized to favor failure of microfabricated components and systems. Schifferle et al. did comparison among a series of post-treatment, including using wet etching by KOH and HNA, oxidation processes by thermal and hydrogen oxidation, on released silicon tensile microstructures. Authors proved that all of these post treatment can enhance the tensile strength of silicon microstructures [46]. They made remarkable improvements of fracture strain and stress of up to 5.7% and 8.8 GPa, respectively. However, the enhancement results of these surface treatment strongly depended on their working parameters and moreover, most of them had an increasing in strength deviation compared with untreated ones.

Mitwally et al. used localized harsh laser treatment to achieve uniformly smooth surfaces for tensile strength enhancement [47]. Laser annealing resulted in smoother sidewalls by eliminating scallops coming from fabrication. By eliminating stress concentration locations on sidewalls, the tensile strength was improved by 20%. However, the strength deviation still increased two times and additional curvature due to surface tension effects was developed on laser treated surfaces.

Surface coating method is another idea to improve the reliability of silicon microstructures. Isono et al. coated a DLC film on the top surface of SCS tensile microstructure by PECVD method [3]. However, they found a 25~50% decrease in the tensile strength (Fig. 1-11), which may be caused by deformation of silicon microstructures induced by unbalanced residual stress.

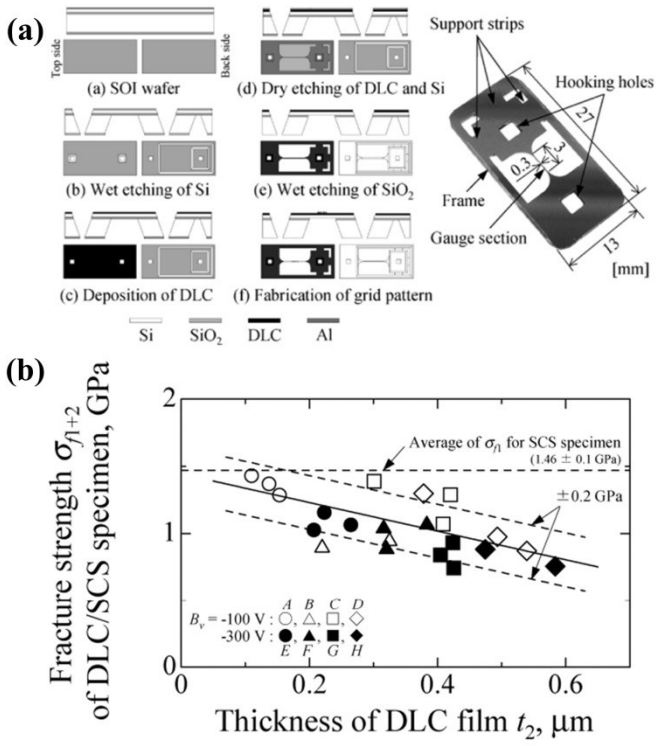

Figure 1-11 Tensile test on single side DLC coated SCS microstructures: (a) Fabrication process; (b) Tensile test results [3].

Several reports have been published on the enhancement of torsional strength. Hajika et al. investigated the strengthening effect of hydrogen annealing for two kinds of silicon torsional beams driven by moving-magnet method [48]. The authors concluded that the fracture strength and the strength deviation of beams made by SCS wafer was enhanced with longer anneal time, while no significant improvement was observed on the torsional beam made by SOI wafer.

1.5 Thesis Outline

In chapter 1, the overview, motivation and innovation of this thesis are concluded and a review on DLC film and reliability of silicon microstructures is provided. In Chapter 2, the fully DLC coating method is introduced in detail and a comparison in tensile properties between bare silicon and DLC

coated microstructure is done briefly. Chapter 3 depicts the coating bias influence on tensile properties and discusses the fracture mechanism thorough the characterization of DLC film. Chapter 4 describes the torsional fracture properties of silicon microstructures fully coated by DLC film and discusses the fracture mechanism. At last, conclusions are presented in chapter 5 together with recommendations on future work.

1.6 Conclusion

In this chapter, the overview, motivation and innovation of this thesis were presented. The review on chemical contents, properties and application of DLC film showed that DLC film had excellent mechanical properties as well as interesting functional properties, which were promising to be used in MEMS industry. Recent research findings on the reliability of silicon MEMS device were also reviewed in this chapter. At last, the outline of this thesis was introduced.

Reference

[1] J.K. Luo, Y.Q. Fu, J.A. Williams, S.M. Spearing, W.I. Milne, Diamond and diamond-like carbon MEMS, J. Micromech. Microeng. 17 (2007) S147-S163.

[2] A. Grill, Tribology of diamond like carbon and related materials: an updated review, Surf. Coatings Technol. 94-95 (1997) 507-513.

[3] Y. Isono, T. Namazu, N. Terayama, Development of AFM tensile test technique for evaluating mechanical properties of sub-micron thick DLC films, J. Microelectromech. Sci. 15 (2006) 169-180.

[4] Y. Zhang, W.H. Wang, A.L. Greer, Making metallic glasses plastic by control of residual stress, Nat. Mater. 5 (2006) 857-860.

[5] J. Vetter, 60 years of DLC coatings: Historical highlights and technical review of cathodic arc processes to synthesize various DLC types, and their evolution for industrial applications, Surf. Coatings Technol. 257 (2014) 213-240.

[6] P. Merel, M. Tabbal, M.Chaker, S. Moisa, J. Margot, Direct evaluation of the sp^3 content in diamond-like-carbon films by XPS, Appl. Surf. Sci. 136 (1998) 105-110.

[7] R. Kalish, Y. Lifshitz, K. Nugent, S. Prawer, Thermal stability and relaxation in diamond-like-carbon. A Raman study of films with different sp^3 fractions (ta-C to a-C), Appl. Phys. Lett. 74 (1999) 2936-2938.

[8] X. Yan, T. Xu, G. Chen, S. Yang, H. Liu, Study of structure, tribological properties and growth mechanism of DLC and nitrogen-doped DLC films deposited by electrochemical technique, Appl. Surf. Sci. 236 (2004) 328-335.

[9] R. Paul, S.N. Das, S. Dalui, R.N. Gayen, R.K. Roy, R. Bhar, A.K. Pal, Synthesis of DLC films with different sp^2/sp^3 ratios and their hydrophobic behavior, J. Phy. D. Appl. Phys. 41 (2008) 055309.

[10] S. Nasir, M.Z. Hussein, Z. Zainal, N.A. Yusof, Carbon-based nanomaterials/allotropes: a glimpse of their symthesis properties and some applications, Materlals 11 (2018) 295.

[11] C. Wang, D. Diao, X. Fan, C. Chen, Graphene sheets embedded carbon film prepared by electron irradiation in electron cyclotron resonance plasma, Appl. Phys. Lett. 74 (2012) 231909.

[12] X. Fan, K. Nose, D. Diao, T. Yoshida, Nanoindentation behaviors of amorphous carbon films containing nanocrystalline graphite and diamond clusters prepared by radio frequency sputtering, Appl. Surf. Sci. 273 (2013) 816-823.

[13] K. Bewilogua, D. Hofmann, History of diamond-like carbon films-from first experiments to worldwide applications, Surf. Coat. Technol. 242 (2014) 214-225.

[14] W. Jacob, W. Moller, On the structure of thin hydrocarbon films, Appl. Phys. Lett. 74 (1993) 1771-1773.

[15] J.C. Lopez, A. Fernandez, Doping and alloying effects on DLC coatings, in C. Donnet, A. Erdemir (Eds.), Tribology of diamond-like carbon films, Springer, Boston, 2008, pp. 311-338.

[16] K.P. Furlan, A.N. Klein, D. Hotza, Diamond-like carbon films deposited by hydrocarbon plasma sources, Rev. Adv. Mater. Sci. 34 (2013) 165-172.

[17] W. Zhang, D. Diao, X. Fan, Three-layered sandwich structured carbon film prepared by ECR ion/electron/ion alternative irradiation technique, Surf. Coat. Technol. 278 (2015) 12-17.

[18] H. Dai, Z. Chen, R. Xue, T. Li, Y. Xue, Effect of step biasing on diamond-like carbon films deposited by pulsed unbalanced magnetron sputtering, Phys. Status Solidi A 210 (2013) 1874-1880.

[19] W. Grimm, V. Weihnacht, Properties of super-hard carbon films deposited by pulsed arc process, Vacuum 85 (2010) 506-509.

[20] S. Zhang, E. Byon, M. Li, Y. He, F. Cai, L. Wang, H. Li, S. Si, Realization of superhard nanocomposites with sufficient toughness: superlattice nanocrystal-TiN/amorphous-(W, Ti) $C_{0.83}$ films, Thin Solid Films 519 (2011) 1901-1906.

[21] Y. Tokuta, M. Kawaguchi, A. Shimizu, S. Sasaki, Effects of applied heat and stress on structure changes of DLC film, Tribology Online 7 (2012) 119-126.

[22] H.W. Choi, M.W. Moon, T.Y. Kim, K.R. Lee, K.H. Oh, The thermal annealing effect on the residual stress and interface adhesion in the compressive stressed DLC film, Mat. Res. Soc. Symp. Proc. 795 (2004) U11.42.1.

[23] W.J. Wu, M.H. Hon, The effect of residual stress on adhesion of silicon-containing diamond-like carbon coatings, Thin Solid Films 345 (1999) 200-207.

[24] K.A. Mahmud, M.A. Kalam, H.H. Masjuki, H.M. Mobarak, N.W. Zulkfi, An updated overview of diamond-like carbon coating in tribology, Crit. Rev. Solid. State. 40 (2015) 90-118.

[25] C. Wang, S. Yang, Q. Wang, Z. Wang, J. Zhang, Super-low friction and super-elastic hydrogenated carbon films originated from a unique fullerene-like nanostructure, Nanotechnology 19 (2008) 225709.

[26] Z. Yue, Y. Wang, J. Zhang, Microstructure changes of self-mated feremce-like hydrogenated carbon films from low friction to super-low friction with the increasing of normal load, Diam. Relat. Mater. 88 (2018) 276-281.

[27] S. Nakao, T. Kimura, T. Suyama, K. Azuma, Conductive diamond-like carbon films prepared by high power pulsed magnetron sputtering with bipolar type plasma based ion implantation system, Diam. Relat. Mater. 77 (2017) 122-130.

[28] W. Zhang, D. Diao, K. Sun, X. Fan, P. Wang, Study on friction-electrification coupling in sliding-mode triboelectric nanogenerator, Nano Energy 48 (2018) 456-463.

[29] L. Yang, G. Hu, D. Zhang, D. Diao, Nanosized graphene sheets enhanced photoelectric behavior of carbon film on p-silicon substrate, Appl. Phys. Lett. 109 (2016) 031910.

[30] B. Subramanian, S.R. Thanka, P.J. Martin, V. Vaithilingam, A.B. Penelope, M.D. Evans, A. Bendavid, Biomineralization of osteoblasts on DLC coated surfaces for bone implants, Biointerphases, 13 (2018) 041002.

[31] A. Norin, E. Rodriguez Cabeo, J. Vetter, Eco-friendly driving pleasure, Sulzer Technol. Rev. 3 (2012) 14-15.

[32] Nissan's hydrogen-free DLC coatings wins METI award, Nissan Press Release. http://www.nissan-global.com/EN/NEWS/2007/_STORY/070829-02-e.html (accessed 29 August 2007).

[33] Hakutsuru sake pet point, Hakutsuru Sake Brewing co. Ltd. http://www.hakutsuru.co.jp/product/pet/ (accessed 26 September 2018, in Japanese).

[34] S.A. Smallwood, K.C. Eapen, S.T. Patton, J.S. Zabinski, Performance results of MEMS coated with a conformal DLC, Wear 260 (2006) 1179-1189.

[35] A.V. Sumant, O. Auciello, M. Liao, O.A. Williams, MEMS/NEMS based on mono-, nano-, and ultrananocrystalline diamond films, MRS Bull. 36 (2014) 511-514.

[36] Y. Murayama, K. Shiba, Y. Ohgoe, J. Mizuno, S. Shoji, K. Ozeki, K. Sato, A. Alanazi, K. Hirakuri, Improvement of surface properties on microfluidic devices by diamond-like carbon coatings, ICEP-IAAC 2015 Proceedings 16 (2015) 874-877.

[37] D.Virganavicius, V.J. Cadarso, R. Kirchner, L. Stankevicius, T. Tamulevicius, S. Tamulevicius, H. Schift, Patterning of diamond like carbon films for sensor applications using silicon containing thermoplastic resist (SiPol) as a hard mask, Appl. Surf. Sci. 385 (2016) 145-152.

[38] Y. Huang, A.S. Vasan, R. Doraiswami, M. Osterman, MEMS reliability review, IEEE T. Device Mat. Re. 12 (2012) 482-493.

[39] T. Tsuchiya, Evalution of mechanical properties of MEMS materials and their standardization, in O. Tabata, T. Tsuchiya (Eds.), Reliability of MEMS, Southeast University Press, Nanjing, 2009, pp. 17-22 (in Chinese).

[40] T. Tsuchiya, O. Tabata, J. Sakata, Y. Taga, Specimen size effect on tensile strength of surface-micromachined polycrystalline silicon thin films, J. Microelectromech. S. 7 (1998) 106-113.

[41] T. Namazu, S. Inoue, Characterization of single crystal silicon and electroplated nickel films by uniaxial tensile test with in situ X-ray diffraction measurement, Fatigue Fract. Eng. M. 30 (2006) 13-20.

[42] A. Uesugi, Y. Hirai, K. Sugano, T. Tsuchiya, O. Tabata, Effect of crystallographic orientation on tensile fractures of (100) and (110) silicon microstructures fabricated from silicon-on-insulator wafers, Micro. Nano. Lett. 10 (2015) 678 – 682.

[43] A. Uesugi, T. Yasutomi, Y. Hirai, T. Tsuchiya, O. Tabata, High-temperature tensile testing machine for investigation of brittle-ductile transition behavior of single crystal silicon microstructure, Jpn. J. Appl. Phys. 54 (2015) 06FP04.

[44] A. Wolter, H. Schenk, H. Korth, H. Lakner, Torsional stress, fatigue and fracture strength in silicon hinges of a micro scanning mirror, Proceedings of SPIE 5343 (2003) 176-185.

[45] T. Namazu, H. Yamagiwa, S. Inoue, Tension-torsion combined loading test equipment for a minute beam specimen, J. Eng. Mater. Technol. 135 (2013) 011004.

[46] A. Schifferle, T. Bandi, A. Neels, and A. Dommann, Where is the limit? Yield strength improvement in silicon microstructures by surface treatments, Phys. Status Solidi A 213 (2016) 102–107.

[47] M. Mitwally, T. Tsuchiya, O. Tabata, and S. Sedky, Improvement of tensile strength of freestanding single crystal silicon microstructures using localized harsh laser treatment, Jpn. J. Appl. Phys. 53 (2014) 06JM03.

[48] R. Hajika, S. Yoshida, Y. Kanamori, M. Esashi, S. Tanaka, An investigation of the mechanical strengthening effect of hydrogen anneal for silicon torsion bar, J. Micromech. Microeng. 24 (2014) 105014.

Chapter 2 Tensile Testing of Silicon Microstructure Fully Coated with PECVD DLC Film

2.1 Introduction

Diamond-like carbon (DLC) is a kind of amorphous film with outstanding mechanical properties, such as high elastic modulus, hardness, fracture toughness, and reliable tribological properties [1]. Its good chemical stability and biocompatibility [2] make DLC films attractive in various coating applications [3]. Furthermore, due to reliable adhesion on silicon surfaces [4], the use of DLC films is promising in micro electro-mechanical systems (MEMS) fabricated as silicon microstructures as the coatings enhance mechanical reliability and improve wear resistance.

However, DLC film has a relatively large compressive residual stress compared with other coating materials. The figure ranged from about 0.5 GPa to more than 10 GPa [5, 6], dominated by deposition method and coating parameters. Higher residual stress can cause the spalling of film from its substrate or the deformation of the microstructures [7]. On the other side, compressive residual stress can be used to prevent brittle fracture and toughen a structure [8]. Thus by full DLC coating, which means to deposit DLC film on all side of the structure, may take the best advantages and avoid the disadvantages of compressive residual stress, leading to an improvement in tensile strength.

In this chapter, a custom-made tensile test system was made up and the single crystal silicon (SCS) microstructure was manufactured by fundamental MEMS fabrication method. Released free-standing microstructure was subjected to plasma enhanced chemical vapor deposition (PECVD) DLC coating, to cover the whole surfaces and to avoid non-uniform coating causing deformation or fracture of SCS microstructure with 150 nm-thick DLC film. Then, the tensile strength between bare silicon and DLC coated microstructures were compared using the quasi-static tensile tester and the fracture mechanism difference between bare SCS and DLC coated microstructures was discussed.

2.2 Experiment

2.2.1 Tensile Test System

Figure 2-1 shows the sketch of tensile test system in this research. The chip was assembled on the top of sample stage driven by a piezoelectric stage (PI P-622.1cl) with the moving direction to the left. The stage displacement was measured using a built-in LVDT sensor. The free paddle of the microstructure was clamped using electrostatic gripping by a probe, and connected to a load cell (Kyowa LTS-50GA) for tensile force measurement. An X-Y axis manual stage and a Z axis motorized stage were used to align the specimen to the probe. A CCD camera (Fujix HC-300Zi) equipped on an optical microscope was used to observe the alignment of clamping as well as specimen fracture. The visual signal from CCD camera, force signal from loading cell and displacement from piezoelectric stage controller were delivered to a personal computer and recorded in the output data.

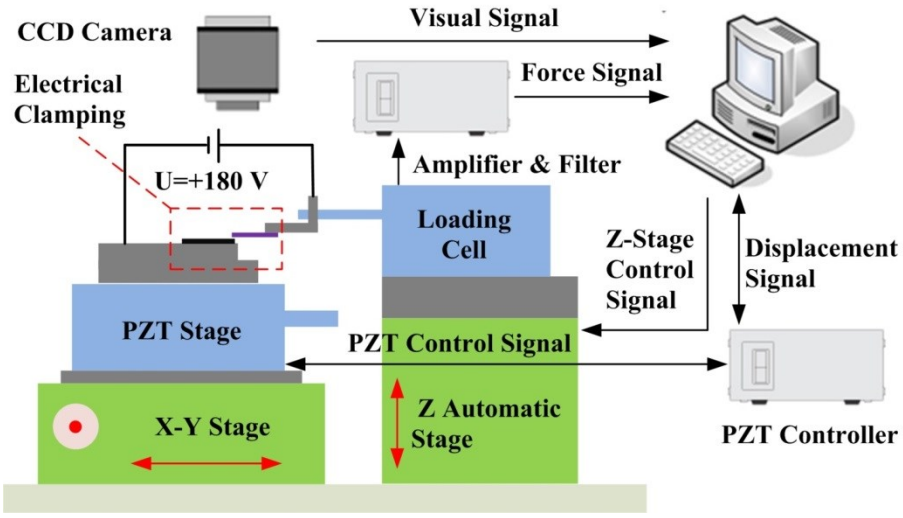

Figure 2-1 Sketch of tensile testing system.

The detail principle of electrostatic gripping is shown in Fig. 2-2. The silicon probe was diced to 10-mm-long and 1-mm-thick, and then was coated by a 200-nm-thick Si_3N_4 insulated film. The voltage was

applied between tensile microstructure and probe to produce electrostatic force, which was calculated through:

$$F_f = \mu \frac{\varepsilon_0 \varepsilon_{SN} S_p U^2}{2t_{SN}^2} \qquad (2-1)$$

where ε_0, ε_{SN} are the dielectric constant of vacuum and relative dielectric constant of Si_3N_4, respectively. μ is coefficient of friction (COF) between structure and probe. t_{SN} is the thickness of Si_3N_4 film and U is applied voltage. S_p is the area of paddle of the tensile specimen, which is introduced in next section. To ensure the fracture happen, the electrostatic force should be higher than the maximum tensile force of DLC coated microstructures, which was estimated as 6 GPa. Thus, the applied voltage should be more than 100 V. However, due to the probable debris existed between specimen and probe, the actual applied voltage was much higher than the theoretical value and smaller than 230 V, the dielectric voltage of Si_3N_4 [9].

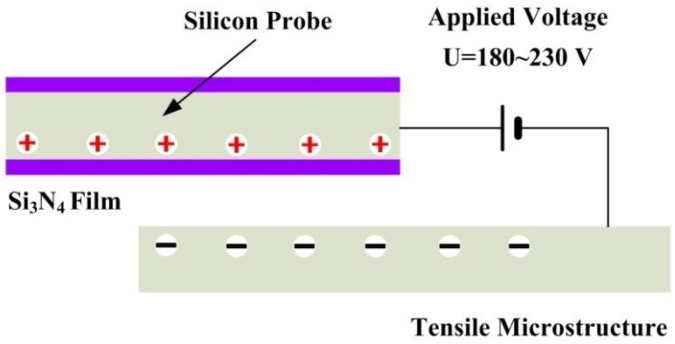

Figure 2-2 The principle for electrostatic gripping.

2.2.2 Microstructure Fabrication

Figure 2-3 shows the mask design of SCS tensile microstructure. The microstructure was composed of and thin gauge part, a large paddle part for electrostatic gripping. The concave corners of gauge part were rounded with a radius of 500 μm for avoiding stress concentration. The gauge part of normal

specimen was 120 μm long and 4 μm wide in design. Since several vibrations or shocking may happen during microstructure transportation and DLC coating, two stronger designs, with the width of 8 μm and 16 μm, were set as backups. One end of the gauge part was fixed to the substrate and the other was connected to a large paddle which was gripped by electrostatic force on tensile testing. The paddle was fixed by four beams to support during fabrication and cut by a laser cutter (Hoya HL-10) just before tensile testing.

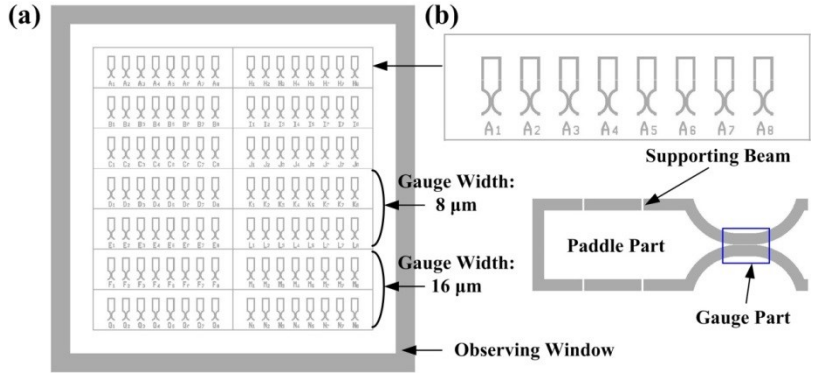

Figure 2-3 Mask design of tensile microstructure.

The SCS microstructure was fabricated from a single piece of silicon on insulator (SOI) wafer by a standard MEMS manufacturing technique. The surface orientation of SOI wafer was (100) and the thickness of device layer and handle layer were 5 μm and 400 μm, respectively. The fabrication was sketched in Fig. 2-4.

First, a 4 inch SOI with 1μm oxide layer on the back surface was cleaned in a piranha solution (H_2SO_4:H_2O_2=5:1). And then, photoresist (Tokyo Ohka Kogyo OFPR-800LB) was applied to the surface of the device layer and the microstructure pattern was formed with a using a double-sided mask aligner (Union Optics PEM-800). The device layer was then etched by a Bosch process using inductively coupled plasma reactive ion etching (ICP-RIE, Samco RIE-iPB800) at an etching rate of 118 nm/cycle. Next, the same resist was applied on the backside and patterned using the same mask aligner and the surface of etched handle layer was protected by the photoresist. The resist pattern was used for oxide layer pattern.

Then, The ICP-RIE was used to open windows on the handle layer at an etching rate of 3.5 μm/cycle. The resist layers on both surfaces were removed using an oxygen plasma assisted ashing process. Buried oxide layers were etched using buffered hydrofluoric acid and the structures were released from the handle wafer.

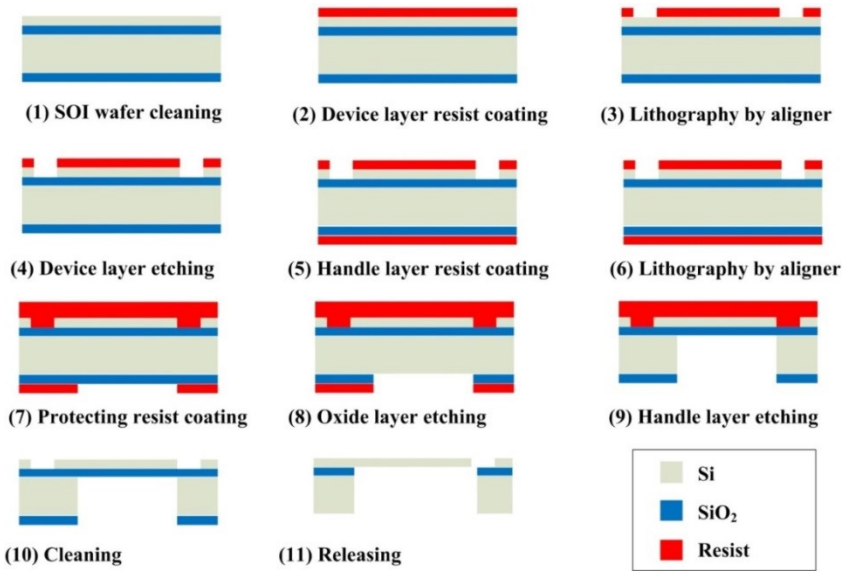

Figure 2-4 Fabrication flow of tensile microstructure.

2.2.3 DLC Deposition

The DLC film was deposited by PECVD method. PECVD is a chemical vapor deposition process used to deposit thin films from a gas state (vapor) to a solid state on a substrate. Chemical reactions are involved in the process, which occur after creation of plasma of the reacting gases. Compared with other coating methods such as sputtering, PECVD method can achieve full coating on all of the faces of microstructure since the particles in the plasma have less directionality and much easier to permeate between the narrow spaces in microstructure.

In this research, DLC film coating on the released microstructure was done using a penning ionization gauge PECVD machine (PIG-PECVD, Shinkoseiki ACV-1060) in Osaka Research Institute of

Industrial Science and Technology (ORIST). Figure 2-5 depicts the construction of PIG-PECVD. A filament was set about the deposition chamber, which was acted as a plasma gun. The medium gas, Ar and hydrogen (H_2) and the reaction gas, tetramethyl silane (TMS, $Si(CH_3)_4$) and acetylene (C_2H_2) were induced from the topside of chamber. A reflection electrode was set in the bottom of chamber to reflect the plasma from plasma gun, making the ionization process more effective. A pair of magnetic coils was set at the outer side of chamber, causing mirror-shaped plasma [10].

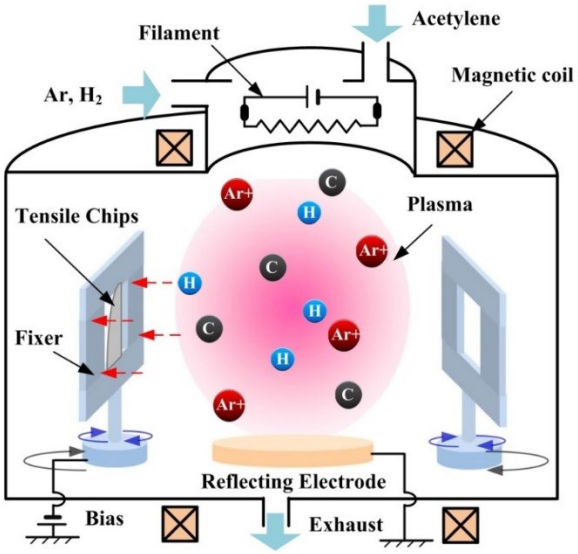

Figure 2-5 Full coating by adopting PECVD.

The released chip containing the structures was attached on a jig with an opening, and rotated on its own axis as well as on the center of plasma for a uniform and full coating at the gauge part. A bare (100) silicon wafer was put into the PECVD chamber at the same time with tensile chips for film characterization. Prior to film deposition, the chip underwent Ar^+ sputter cleaning for 1 min at a base pressure of about 8×10^{-4} Pa with a substrate DC bias voltage of -400 V to remove surface contaminants. And then, a mixture of H_2 (100 sccm) and TMS (30 sccm) was introduced into the chamber to form a 20 nm-thick SiC interlayer to enhance the adhesion between substrate and DLC film. C_2H_2 with a flow rate of 150 sccm was used in the deposition as the reaction gas with a working pressure of 0.04 Pa. The most

standard coating bias for the PIG-PECVD machine, −400 V were used at the same deposition time of 90 s, with the target film thickness of 150 nm. The detail working parameters of PECVD coating were shown in Table 2-1.

Table 2-1 Working parameters of PECVD

Substrate	Bias Voltage	-400 V	Current	0.38 A
Flow Rate	Ar	10 sccm	H_2	100 sccm
	TMS	30 sccm	C_2H_2	150 sccm
Coil Voltage	Left	7.0 A	Right	7.1 A
Plasma Gun	Voltage	63.2 V	Current	10.0 A

2.2.4 Tensile Test

The tensile test was conducted on the custom-made tensile test system introduced in section 2.2.1. Prior to test, the output and linearity of the load cell was confirmed through the standard weight and the result is shown in Fig. 2-6. It had a good linearity and the relationship between applied force and output voltage was described as:

$$F_t = 47.421U + 0.332 \qquad (2-7)$$

where F_t is tensile force, calculated in mN and U is output voltage of load cell. The above fitted formula was used in the following tensile test.

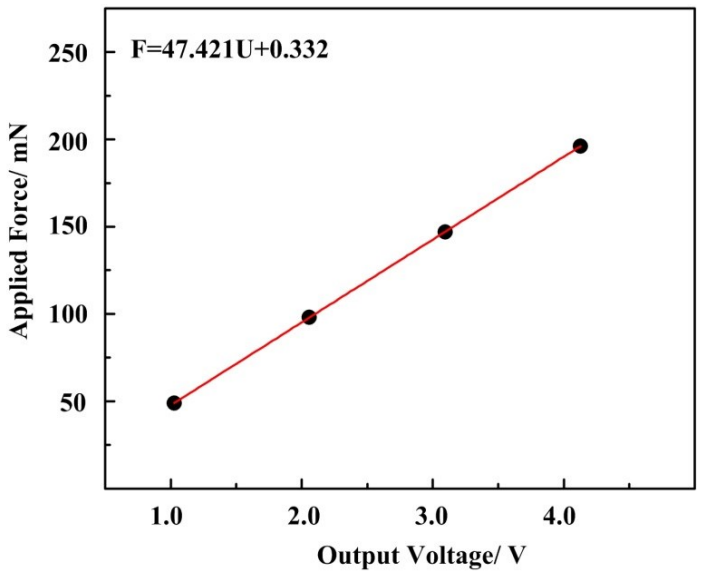

Figure 2-6 The output-force curve of the loading cell.

The chip was diced by hand along the dicing line before test. And then quasi-static tensile testing was conducted at room temperature (RT) for 20 SCS and 20 DLC coated microstructures. The loading rate was controlled at the stage speed of 0.75 μm/s. After fracture, surfaces were observed using field emission scanning electron microscope (FESEM, Hitachi SU-8020) and the nominal tensile stress was calculated by dividing the recorded tensile force by the cross sectional area measured by the FESEM.

2.3 Results

Figure 2-7 shows a FESEM image of DLC coated microstructures. The film was formally coated on the surface of microstructures and no deformation was observed even at the 4 μm-thick gauge and paddle part, confirming the validity of fully coating film by PECVD method. The size of gauge part was almost the same as designed value and the thickness of DLC film was around 152 nm.

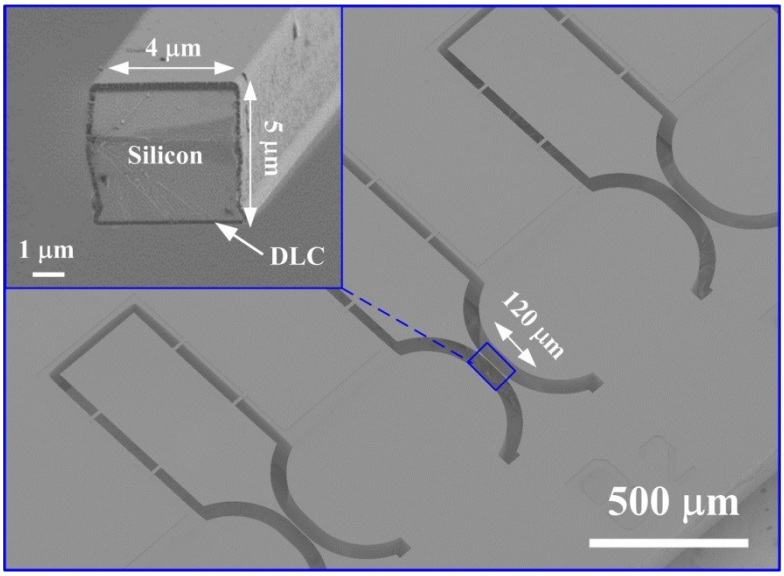

Figure 2-7 FESEM image of DLC coated tensile microstructures.

The tensile force-stage displacement curves of bare SCS and DLC coated microstructures measured by loading cell and LVDT sensor are depicted in Figure 2-8.

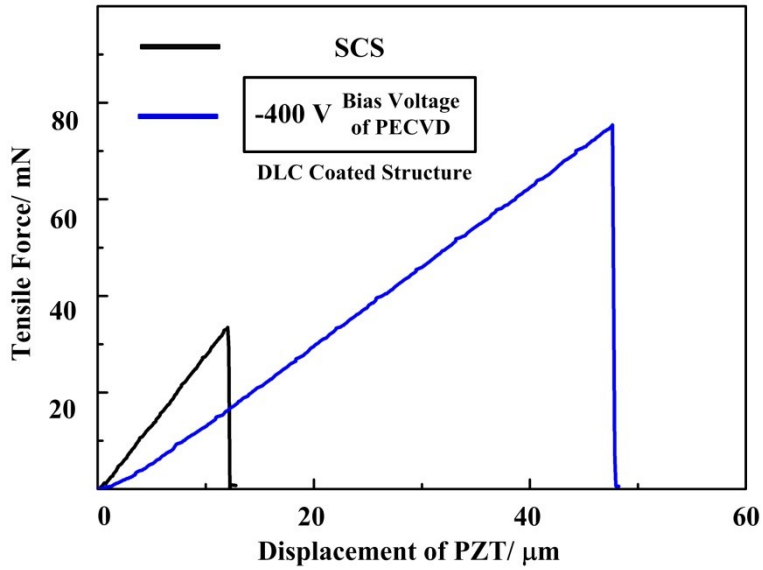

Figure 2-8 Tensile force-stage displacement curves of SCS and DLC coated microstructures.

Both of the tensile curve exhibited prefect linear plots and sudden drops of force, indicating elastic deformation and brittle fracture of silicon and DLC films. No redundant undulate was found near the sudden drop, which can be regarded as a proof of no spalling existence when the fracture happened.

The nominal tensile strength was calculated with tensile force at the sudden drop to cross sectional area. Figure 2-9 illustrates the tensile strength of bare and DLC coated microstructures. The bare SCS microstructures had the average tensile strength of 1.86 GPa. Compared with the bare silicon one, the average tensile strength of fully coated microstructure was 2.86 GPa, with an increasing of 53.5%.

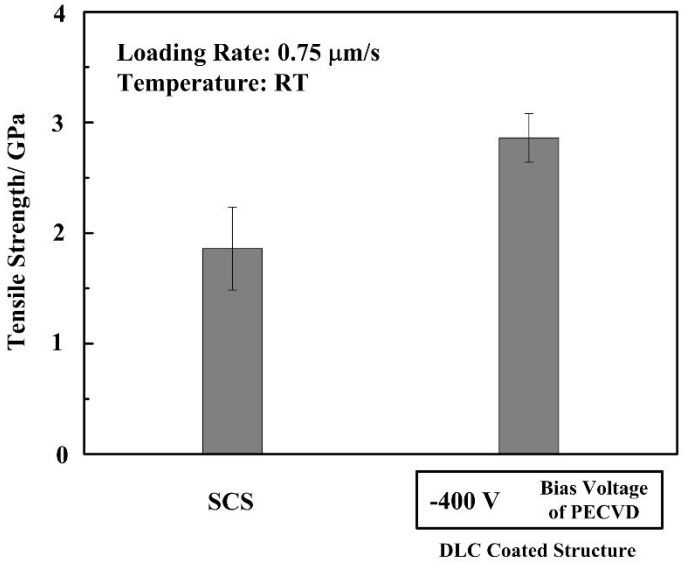

Figure 2-9 Tensile strength of SCS and DLC coated microstructures.

It has been proved in Fig. 2-8 that both of silicon and DLC are brittle materials, which means the structure may fracture at even at a relatively low applied force and thus result in a large scatter in the measured data. To evaluate the reliability of brittle MEMS structure, statistical analysis is crucial. In this research, the two-parameter Weibull analysis was conducted for evaluating the strength deviation. The cumulative distribution function of Weibull distribution is shown as follows:

$$F(\sigma) = 1 - e^{-(\frac{\sigma}{\eta})^m} \qquad (2-8)$$

where σ is measured tensile strength; η is the scale parameter which corresponds to the applied tensile stress at the fracture probability of 63.2%; m is the shape parameter, which is known as the Weibull modulus. With higher Weibull modulus, the strength deviation is smaller.

Figure 2-10 illustrates Weibull plots of bare and DLC coated microstructures with the fitted scale parameter and Weibull modulus. It could be concluded that the DLC coated microstructures had smaller scatterings than that of bare ones. DLC coated structures had two times higher Weibull modulus compared with the bare silicon ones, which would result in a better reliability of MEMS structures.

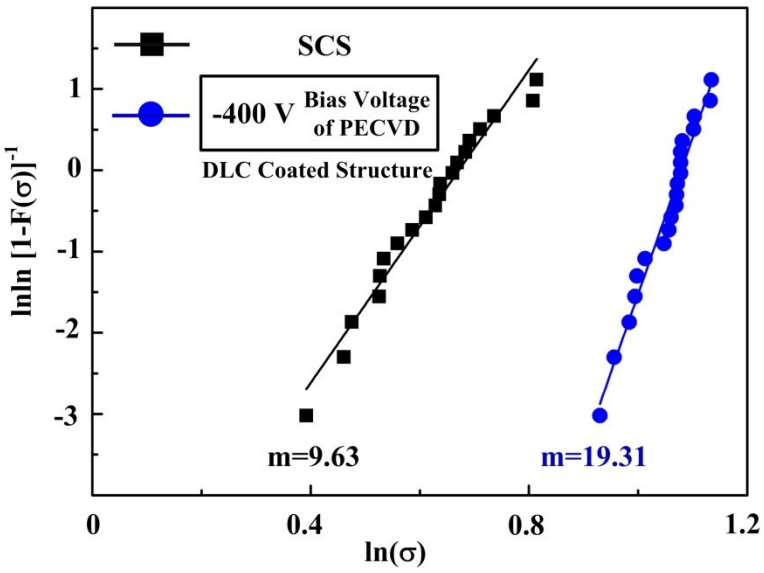

Figure 2-10 Weibull plots of SCS and DLC coated microstructures.

The typical fracture surfaces of bare and DLC at -400 V are shown in Figure 2-11. All of 20 bare silicon specimens had the same fracture surface of (111) plane, which agreed with our previous report [11]. The reason was considered that the lowest surface energy of in SCS happened in (111) plane with the value of only 1.44 J/m^2 [12]. Most of the fracture originated from a quite rough and inhomogeneous side wall of the gauge part due to the mixture influence from the photolithography as well as the ICP-RIE for specimen definition. The DLC coating did not change the fracture plane. However, about half of the coated structures fracture initiated from the top or bottom corner beside of side wall, which may due to an

improved side wall roughness achieved by DLC coating. It should be mentioned that no semicircular crack [7] was observed at the silicon and DLC interface by full coating, which may indicate a crack happened at the interface, leading to a decrease in yield strength according to Johansson`s theoretical work [13].

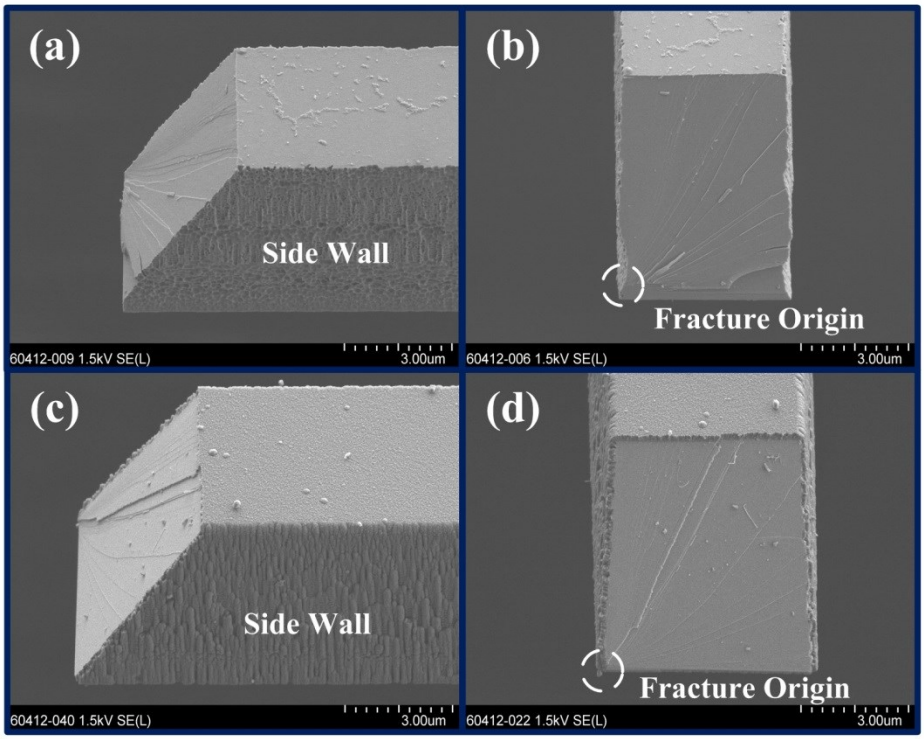

Figure 2-11 Typical fracture surface of microstructures observed at a tilt angle of 45°. (a, b) Fracture surfaces of bare silicon specimen; (c, d) Fracture surfaces of DLC coated specimen at the bias of -400 V.

2.4 Discussion

The tensile strength of silicon microstructure increased obviously by adopting conformal surface coating with DLC, which was quite different with the data reported in Isono et al.'s research [7]. The enhancement of the tensile strength might be mainly due to the two reasons. One is the improvement of the side wall morphology by DLC coating. MEMS manufacturing process would generate surface roughness and defects especially at the side wall, which may decrease the fracture strength of the silicon

structure. In order to enhance the mechanical strength, different kinds of surface treatment have been performed to achieve a better side wall condition and succeed in strength improvement [14-15]. In this work, DLC film may cover the defects of side wall as well as fill the defects on the silicon surface, causing a larger tensile strength.

Another reason may be the influence of compressive residual stress of the DLC film. In the single side of film coating, residual stress owning to one side DLC deposition may lead a deleterious effect on the reliability of the MEMS device such as structure deformation or film/substrate delamination with applied force. However, by adopting conformal coating on the structure, smaller deformation was generated on the microstructure. Thus, by the conformal coating, the compressive residual stress could be regarded as a kind of force to "seal" the crack from becoming serious to fracture. According to Tojek's theoretical derivation, in the same condition of defects distribution, the fracture toughness increased with the existence of the compressive residual stress [16].

The strength deviation was also improved by DLC coating. These results could be concluded as the residual stress suppressed defects activation. With higher residual stress, this suppression effect may become more distinct. Tandon et al. explained this phenomenon as the residual stress stabilized the crack and made the strength insensitive to the initial flaw size [16]. It should be mentioned that this improvement in strength deviation related directly with the initial flaw size as well as the residual stress distribution along the film thickness, and thus improvement only happened within specific conditions.

In this discussion, the mechanism of tensile properties (tensile strength, strength deviation) improvement in DLC coated SCS microstructure was concluded in two aspects: internal aspect, including the compressive residual stress and high fracture toughness of DLC film, and external aspect, mainly for the improved surface roughness. However, from data obtained in this chapter, the fracture mechanism cannot be further explained. The side wall roughness of microstructures was quite high because of the lithography machine resolution as well as the properties of the resist. Resist near the edge of

microstructure was not exposed formally and edge was in twists and turns. Thus, the side wall was quite rough and a standard scallop shape was not found in this work.

2.5 Conclusion

In this chapter, a tensile test system was set up and SCS tensile microstructures were manufactured through standard MEMS fabrication method. The released SCS structure was fully coated with 150 nm-thick DLC film at all surface by PECVD method with the deposition bias voltage of -400 V. Tensile properties of DLC coated SCS microstructure were evaluated. The tensile strength of SCS microstructures was improved by DLC coating up to 53.5% with the figure of 3.86 GPa. Furthermore, the Weibull analysis showed the coated SCS microstructures had smaller scatterings. The improvement in tensile properties may due to the compressive residual stress inside DLC as well as a relatively smooth side wall condition.

However, because of the lithography machine, the side wall of the microstructure was quite rough. Even this roughness can be proved by DLC coating, this roughness made it hard clarify the reason of tensile properties increasing, which need to be discussed in next chapter.

Reference

[1] J.K. Luo, Y.Q. Fu, J.A. Williams, S.M. Spearing, W.I. Milne, Diamond and diamond-like carbon MEMS, J. Micromech. Microeng. 17 (2007) S147-S163.

[2] A. Grill, Tribology of diamond like carbon and related materials: an updated review, Surf. Coatings Technol. 94-95 (1997) 507-513.

[3] J. Robertson, Diamond-like amorphous carbon, Mater. Sci. Eng. R 37 (2002) 129-281.

[4] J. Vetter, 60 years of DLC coatings: Historical highlights and technical review of cathodic arc processes to synthesize various DLC types, and their evolution for industrial applications, Surf. Coatings Technol. 257 (2014) 213-240.

[5] Y. Oda, M. Kirinuki, Y. Nishimura, K. Azuma, E. Fujiwara, M. Yatsuzuka, Measurement of residual stress in DLC films prepared by plasma-based ion implantation and deposition, Surf. Coatings Technol. 186 (2004) 141-145.

[6] J. In, Y. Kim, Y. Hwang, J.H. Choi, Control of residual stress of tetrahedral amorphous carbon thin film deposited on dielectric material by filtered cathodic vacuum arc source by using mid-frequency pulse bias voltage, 349 (2018) 909-916.

[7] Y. Isono, T. Namazu, N. Terayama, Development of AFM tensile test technique for evaluating mechanical properties of sub-micron thick DLC films, J. Microelectromech. Sci. 15 (2006) 169-180.

[8] S. Zhang, D. Sun, Y. Fu, H. Du, Toughening of hard nanostructural thin films: a critical review, Surf. Coatings Technol. 198 (2005) 2-8.

[9] T. Ataseven, A. Tataroglu, Temperature-dependent dielectric properties of Au/$S_{i3}N_4$/n-Si (metal insulator semiconductor) structures, Chin. Phys. B 22 (2013) 117310.

[10] 寺山暢之, PIG プラズマ CVD 法による DLC コーティング技術, J. Plasma Fusion Res. 87 (2011) 548-555 (in Japanese).

[11] A. Uesugi, T. Yasutomi, Y. Hirai, T. Tsuchiya, O.Tabata, High-temperature tensile testing machine for investigation of brittle–ductile transition behavior of single crystal silicon microstructure, Jpn. J. Appl. Phys. 54 (2015) 06FP04.

[12] R.C. Cammarata, Surface and interface stress effects in thin films, Prog. Surf. Sci. 46 (1994) 1-38.

[13] S. Johansson, F. Ericson, J.A. Schweitz, Influence of surface coatings on elasticity, residual stresses, and fracture properties of silicon microelements, J. Appl. Phys. 65 (1989) 122-128.

[14] M.M. Tojek, D.J. Green, Effect of residual surface stress on the strength distribution of brittle materials, J. Am. Ceram. Soc., 72 (1989) 1885-1890.

[15] R. Tandon, D.J. Green, Crack stability and T-curves due to macroscopic residual compressive stress profiles, J. Am. Ceram. Soc., 72 (1991) 1981-1986.

[16] R. Tandon, D.J. Green, The effect of crack growth stability induced by residual compressive stresses on strength variability, J. Mater. Res. 7 (1992) 765-771.

Chapter 3 Effect of Deposition Bias Voltage on Tensile Properties of DLC Coated Silicon Microstructure

3.1 Introduction

In last chapter, full diamond-like carbon (DLC) coating process was developed on free-standing single crystal silicon (SCS) microstructure and the tensile properties were employed by electrostatic gripping system. The results showed that fully DLC coating can increase the tensile strength and decrease the strength deviation [1].

However, there were still some questions needed to be further clarified. Since the fracture of coated microstructures seemed to start from the surface of DLC coating, the tensile properties may have a direct relationship with the properties of coated film, which was decided by deposition parameters, such as deposition bias voltage, gas material flow rate, and the intensity of plasma [2]. For this purpose, understanding the relationship between coating parameters and tensile properties is essential.

In this chapter, for optimum of tensile strength and reliability enhancement, SCS microstructure was fully coated by DLC film all-around by adopting plasma enhanced chemical vapor deposition (PECVD). Five deposition bias voltages, from -200 V to -600 V, were adopted to explore the influence on the mechanical properties of deposited DLC film. The chemical contents and mechanical properties of the DLC film were characterized and the relationship was discussed. Tensile test was conducted by adopting the quasi-static thin film tensile tester with an electrostatic gripping system. The measured tensile properties of microstructure were correlated with the chemical contents and mechanical properties of the DLC film. The mechanism of tensile properties enhancement was discussed in detail.

3.2 Experiment

3.2.1 Microstructure Fabrication

The SCS microstructure was fabricated from a single piece of silicon on insulator (SOI) wafer with a 100-nm-thick silicon dioxide (SiO_2) layer backside. The surface orientation of device layer was (100). Due to the resolution limitation of the double-side mask aligner (Union Optics PEM-800), the side wall of fabricated microstructures was quite rough and inhomogeneous, causing some problems in the analysis of fracture mechanism. In this research, a stepper (Nikon NSR2205i11D) was adopted to achieve smooth sidewalls. A stepper is a device used in the manufacture of integrated circuits (ICs) that is similar in operation to a slide projector or a photographic enlarger (5 times in this research). The term "stepper" is short for step-and-repeat camera. Stepper is an essential part of the complex process, which creates millions of microscopic circuit elements on the surface of tiny chips of silicon [3]. By adopting stepper, the tensile microstructures had better side wall and less individual difference among different structures, which was important for the mechanism analysis.

Figure 3-1 sketches the fabrication method revised from last chapter. First, photoresist (Tokyo Ohka Kogyo THMR-iP1800) was applied on the surface of 5-μm-thick device layer and the microstructure pattern was formed using the stepper. Second, the device layer was etched by inductively coupled plasma reactive ion etching (ICP-RIE, Samco RIE-iPB800) at an etching rate of 118 nm/cycle. Then, the etched patter was protected by a positive photoresist (Tokyo Ohka Kogyo OFPR-800LB) and was diced by a dicer (Disco DAD322). The SiO_2 film on 400-μm-thick handle layer of diced chips was coated by the same positive photoresist and patterned by a double-side mask aligner (Union Optics PEM-800) as well as buffered hydrofluoric (BHF) acid. Since the microstructures were only formed at the device layer, the fabrication precision was not so serious. Then, the handle layer was etched by the ICP-IRE at an etching rate of 3.5 μm/cycle through the SiO_2 hard mask. At last, the residual resist and SiO_2 hard mask were completely removed by wet etching and oxygen plasma assisted ashing (Samco FA-1).

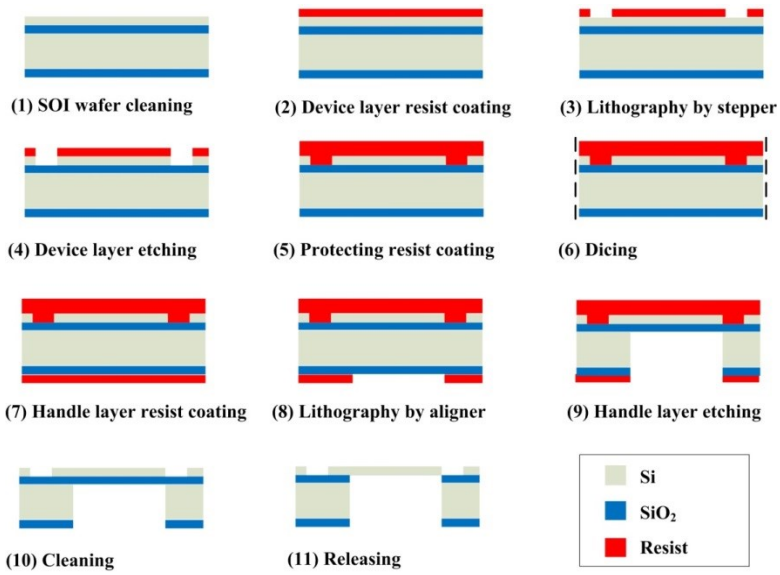

Figure 3-1 Fabrication flow of tensile microstructure.

DLC film was deposited on the released SCS microstructure by employing PECVD machine (Shinkoseiki ACV-1060) containing a sample stage that rotated around the center of plasma while also spun by itself, which was introduced in section 2.2.2. Bias voltages from -200 V to -600 V for every -100 V were used while deposition time was maintained at 90 s for a target film thickness of 150 nm. The other coating parameters and coating procedures were the same as last chapter.

3.2.2 Characterization of DLC

The deposition bias voltage influenced chemical contents (sp^2 carbon, sp^3 carbon and hydrogen) of DLC film and thus led to variable mechanical properties (roughness, hardness, elastic modulus, residual stress and fracture toughness), which influent the tensile properties of coated SCS microstructures.

The contents were qualitatively investigated by Raman spectroscopy (Horiba LabRAM-HR800) at a laser excitation with the wavelength of 488 nm, and recorded in the range 500-2400 cm^{-1}. The ratio of sp^2 and sp^3 phases (sp^2/sp^3) was quantitatively investigated by x-ray photoelectron spectroscopy (XPS, Ulvac

Phi 5000VersaProbeII) with a monochromatic Al Kα X-ray source. Hydrogen content was monitored using a thermal desorption spectrometer (TDS, ESCO TDS1200II). To ensure the releasing of hydrogen atoms and eliminate the influence caused by substrate silicon melting at the same time, samples were heated gradually up to 1200 °C in 1200 s by infrared radiation and kept for another 300 s. The analysis result of Raman spectroscopy was correlated with XPS and TDS results.

The thickness was measured at the edge of DLC film using a stylus profilometer (Veeco Dektak XT-S) with three different measurements. The residual stress was calculated from the measurement of wafer curvature and calculated through Stoney's formula [4].

$$\sigma_f = \frac{E_{si} d_{si}^2}{6(1-\upsilon) d_{DLC}} \left(\frac{1}{R_{post}} - \frac{1}{R_{pre}} \right) \qquad (3-1)$$

where E_{Si}, υ and d_{Si} are the elastic modulus, Poisson's ratio and thickness of the Si (100) substrate, respectively. d_{DLC} is the thickness of DLC film. R_{post} and R_{pre} were the curvature radii of substrate before and after deposition. For a silicon wafer, R_{pre} was considered as infinity and R_{post} can be approximatively considered as:

$$R_{post} = \frac{\left(\frac{L}{2}\right)^2}{2h} \qquad (3-2)$$

where L is the length of scanning, set as 15 mm in this work and h is the largest vertical deformation after DLC coating.

The surface roughness of the DLC film was measured using an AFM system (Atomic Force Microscope, Bruker Multimode 8) running at a tapping mode.

The elastic modulus and hardness were measured by a nanoindenter (Elionix ENT-2100) and calculated by Oliver–Pharr method [5].

$$E = \frac{S\sqrt{\pi}}{2\sqrt{A_c}} \quad (3-3)$$

$$H = \frac{P}{A_c} \quad (3-4)$$

where E and H are elastic modulus and hardness. S is initial unloading stiffness and P is the indentation load. A_c is the contact area of the indenter tip, which is fitted by the nanoindenter from the indentation depth. In the test, a Berkovich diamond indenter with a tip radius of 100 nm was used and the loading/unloading time was set as 20 s. The fracture toughness K_c of silicon and DLC/silicon system was calculated through Niihara's formula [6].

$$K_c = A\left(\frac{E}{H}\right)^{2/5}\frac{P}{L^{3/2}} \quad (3-5)$$

where E and H are the elastic modulus and hardness respectively. P is the indentation load and L is the crack length measured from the center of the indented area to the crack tip. A is an empirical constant depended on the indenter. Five maximum loads of 15 mN, 25 mN, 50 mN, 75 mN and 100 mN were used. After nanoindentation, the crack length was measured through a field emission scanning electron microscope (FESEM, Hitachi SU-8020).

3.2.3 Tensile Test

Tensile strength of microstructures was measured through the quasi-static tensile test system (section 2.2.1). The test was conducted at room temperature (24 °C) and relative humidity of 37%. To make a comparison to tensile test in last chapter, 20 microstructures per condition were fractured at a loading speed of 0.75 μm/s. The tensile strength value was the ratio of maximum applied tensile force before fracture and he cross sectional area obtained from FESEM.

3.3 Results

3.3.1 Characterization Results

3.3.1.1 Chemical Contents

The chemical contents (sp^2 phase, sp^3 phase and hydrogen contents) of DLC film influenced its mechanical properties directly. Thus, the Raman spectroscopy was conducted to exam the chemical contents difference with the different bias voltages. Figure 3-2 depicts the Raman spectra of DLC film with -200 V and -600 V bias voltages, respectively. A sharp silicon band was observed at 520 cm^{-1} [7] The spectra exhibited a composite band centered on 1500 cm^{-1} which could be divided into two bands, D Band at around 1350 cm^{-1} and G Band at around 1530 cm^{-1}[8]. D Band came from the breathing vibrations of rings of sp^2 bond, which was labelled "D" for "disorder" since it was found from the disordered graphite. G Band came from the bond stretching vibrations of all pairs of sp^2 atoms, with was labelled "G" for "graphite" [9, 10].

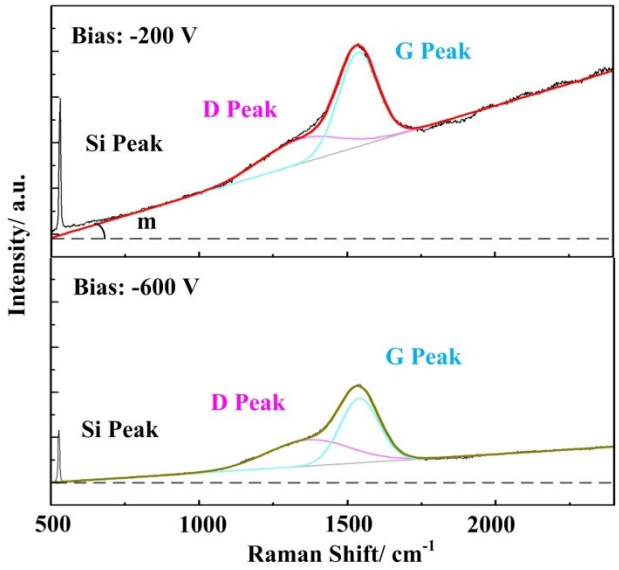

Figure 3-2 Raman spectra of DLC at bias of −200 V and −600 V.

The spectra region ranging from 1000 to 2000 cm^{-1} of all films were fitted to superposition of D and G bands using Breit–Wigner–Fano (BWF) function to calculate the integrated intensities of D band (I_D), G band (I_G), the gradient of the photo-luminescent background (k), and the wavenumber of G band (ω_G) as shown in Table 3-1. Robertson reported that the sp^2/sp^3 ratio was directly associated with the I_D/I_G. The greater I_D/I_G was, the larger sp^2/sp^3 ratio it had [11]. Therefore, it could be suggested that the sp^2/sp^3 ratio in the deposited DLC film also decreased with the increasing negative bias voltage.

Since the DLC film deposited by PECVD method using acetylene (C_2H_2), the film should contain hydrogen which influences the hardness, residual stress and COF [12]. According to Marchon`s research, the hydrogen content of DLC film could be evaluated from the ratio of slope parameter k to I_G, where the ratio is proportional to the hydrogen content [13]. The result shows the content of hydrogen decreased with increasing negative bias voltage.

The residual stress of DLC film was reflected from the wavenumber of G Band. Residual stress in the DLC film was compressive stress, which would decrease the interatomic distance and increase the spring constant of chemical bonding. Thus, the G Band moved to the high wavenumber [14]. In this research, with the increasing of bias voltage, the G Band moved from 1526 to 1537 cm^{-1}, indicating the increasing of residual stress.

The sp^2/sp^3 ratio was further qualitatively measured using high resolution XPS. As a typical example, the spectra and its deconvolution using -200 V coated DLC film is depicted in Fig. 3-3. The spectrum of carbon was decomposed into three Gaussian peaks near 284.8 eV, 285.8 eV and 288.7 eV, which were attributed the sp^2 phase (C=C), sp^3 phase (C-C) and (CO) bonds, respectively [15]. Figure 3-3(b) shows sp^2/sp^3 ratio of the C 1s peak at different deposition bias voltage. The sp^2/sp^3 ratio in PECVD DLC film was around 2.2 and decreased with higher bias voltage, which agreed with the Raman spectra.

The typical TDS spectrum acquired from -200 V coated DLC film is shown in Fig. 3-4. During the process time from 480 s to 1500 s, multiple peaks were observed mainly at the mass number 16, number

28 and number 2, which corresponds to methane (CH_4), ethylene (C_2H_4) and hydrogen (H_2), respectively. It was observed that methane and ethylene desorbed first while hydrogen generated later, which may be due to the difference of bonding energy between C-C bond (346 kJ/mol) and C-H bond (411 kJ/mol). After 300 s of holding time, desorption rate of three gases nearly dropped to zero.

Table 3-1 Fitting parameters for Raman spectra of DLC film.

Bias /V	$I_D\times10^5$	$I_G\times10^5$	k	I_D/I_G	$k/I_G\times10^{-6}$	ω_G/ cm^{-1}
-200	5.72	5.30	4.13	1.08	7.8	1526
-300	5.23	5.08	1.72	1.03	3.4	1533
-400	3.89	4.47	0.98	0.87	2.2	1536
-500	3.93	4.68	0.80	0.84	1.7	1537
-600	3.33	4.06	0.49	0.82	1.2	1537

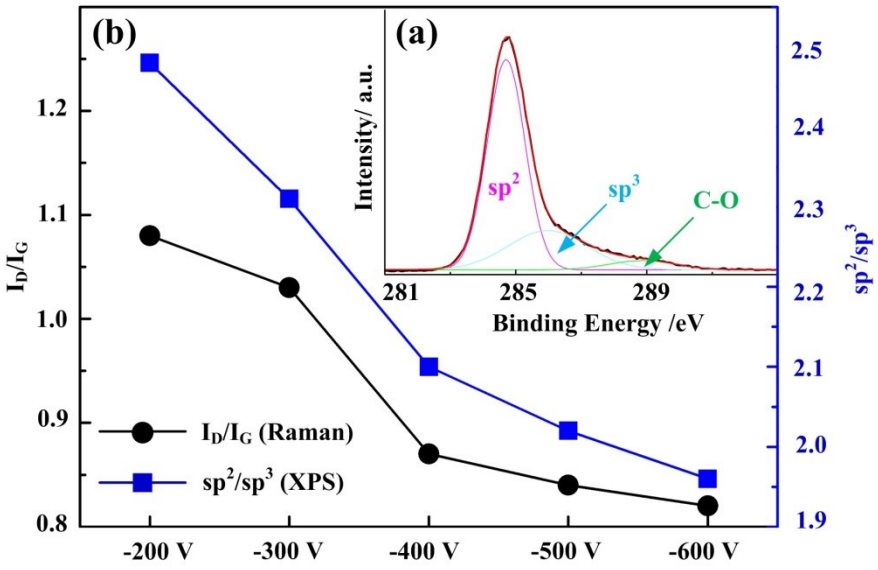

Figure 3-3 Comparison between Raman and XPS characterization: (a) C 1s XPS spectra of DLC at bias of −200 V. (b) Proportion of sp^2/sp^3 phase measured with XPS and Raman parameter I_D/I_G.

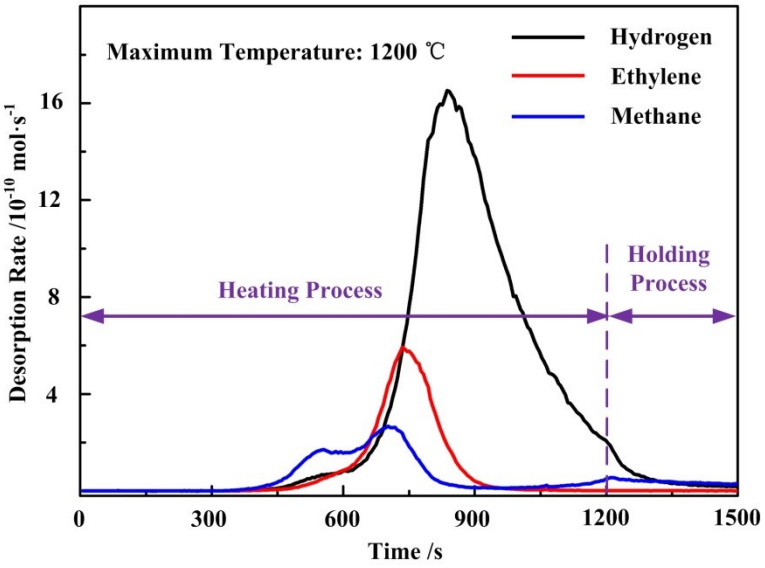

Figure 3-4 TDS spectra (methane, ethylene and hydrogen contents) of DLC at bias of −200 V.

The mole numbers of gases were obtained from the integrated intensities and the amount of hydrogen atoms inside DLC film was calculated. Figure 3-5 shows the hydrogen molar concentration measured by TDS and Raman with different deposition bias voltage. In this research, k/I_G value was proportional to the hydrogen molar concentration. The hydrogen content in the DLC film can be calculated from the following equation.

$$c_H = \frac{V_m}{V_m + (\rho - V_m \cdot M_H)/M_C} \qquad (3-6)$$

where M_H and M_C are the molar mass of hydrogen and carbon respectively. V_m is the molar concentration of hydrogen and ρ is the density of PECVD DLC film, which was 1.63±0.035 g/cm^3 according to LiBassi [16]. The average hydrogen content in our DLC film was around 35%, which is similar as other reports [17].

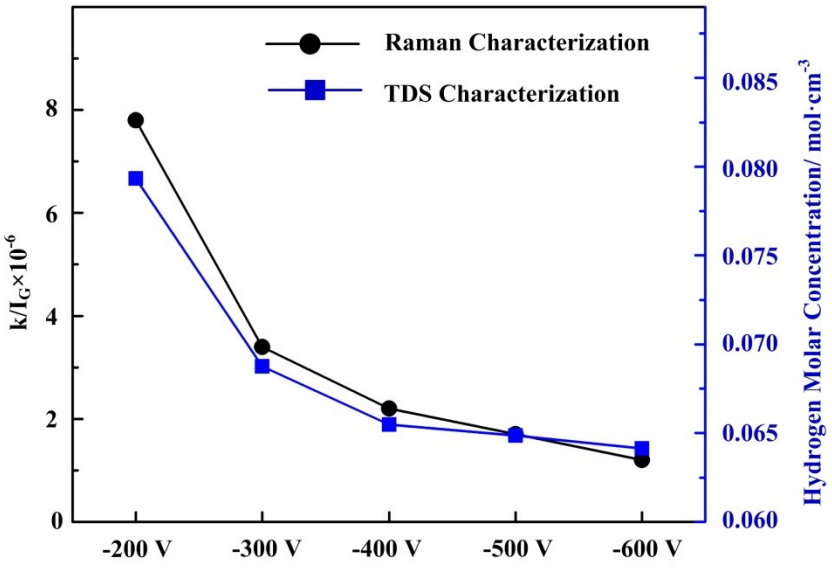

Figure 3-5 Hydrogen atomic density measured with TDS and Raman parameter k/I_G.

From the chemical content analysis, it could be referred that the both of the hardness and residual stress would increase with increasing bias voltage, since the sp^3 phase carbon increased and the sp^2 phase caron, hydrogen content decreased.

3.3.1.2 Thickness, Elastic modulus, Hardness, Residual Stress and Roughness

Table 3-2 lists the thickness of DLC films deposited at five different bias voltages. The thickness ranged from 150 nm to 165 nm and decreased with increasing of bias voltage, due to a competition between growth and etching during formation of DLC film [18].

Figure 3-6 shows the typical indentation force-displacement curves of DLC films. Since maximum penetration displacement exceeded 20% of the film thickness, the calculated elastic modulus and hardness values were considered as a mixture of film and substrate [19]. Table 3-2 displays the elastic modulus, hardness, residual stress and roughness of SCS substrate and DLC samples with different bias voltages. Both elastic modulus and hardness increased as bias voltage increased.

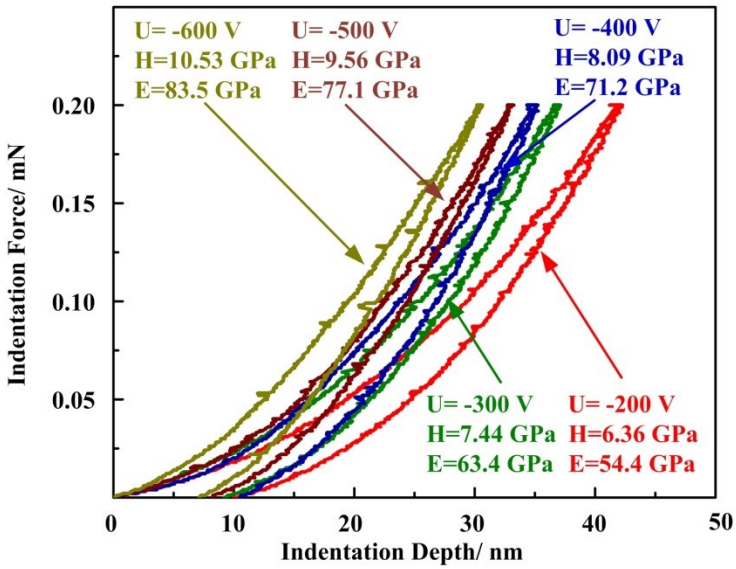

Figure 3-6 Nano-indentation curves for DLC film deposited at different bias voltages. Elastic modulus (*E*) and hardness (*H*) are shown in the plot.

Table 3-2 Hardness, elastic modulus, residual stress and roughness of SCS and DLC films.

Samples	DLC Film					SCS
	-200 V	-300 V	-400 V	-500 V	-600 V	
Thickness/ nm	165	155	150	150	150	N/A
Roughness/ nm	2.11	1.99	2.05	2.01	2.16	0.16
Modulus/ GPa	54±2	63±5	71±7	77±9	84±10	151±13
Hardness/ GPa	6.4±0.2	7.4±0.8	8.1±0.8	9.6±1.0	10.5±0.4	10.3±0.8
Residual Stress/ GPa	-0.68	-0.91	-1.13	-1.42	-2.03	N/A

The compressive residual stress ranged from 0.68 GPa to 2.03 GPa and also increased by raising bias voltage. The elastic modulus, hardness and residual stress values were smaller than those of film coated by sputtering method, probably because of relatively low coating energy in PECVD, as well as relatively high hydrogen content inside DLC film [20, 21]. The thickness, elastic modulus, hardness, and residual stress had the same values compared with chapter 2, indicating repeatable coating properties of PECVD.

Regarding the effect of surface quality to tensile fracture properties, the surface roughness of DLC coated microstructures was tested with AFM. Figure 3-7 shows the surface quality and roughness of microstructures deposited with coating bias voltages of −200 V and −600 V. The results indicate that roughness values were in the neighborhood of 2.08 nm and that increasing the bias voltage had little effect. Moreover, no large rough peak was observed and the film seemed to be essentially uniform. Thus, we feel that the effect of surface quality when comparing DLC coated microstructures can be neglected in this case.

In conclusion, with the increase of bias voltage, the elastic modulus, hardness and residual stress increased. The values were nearly the same as chapter 2. The deposition bias voltage did not affect the surface roughness of DLC film.

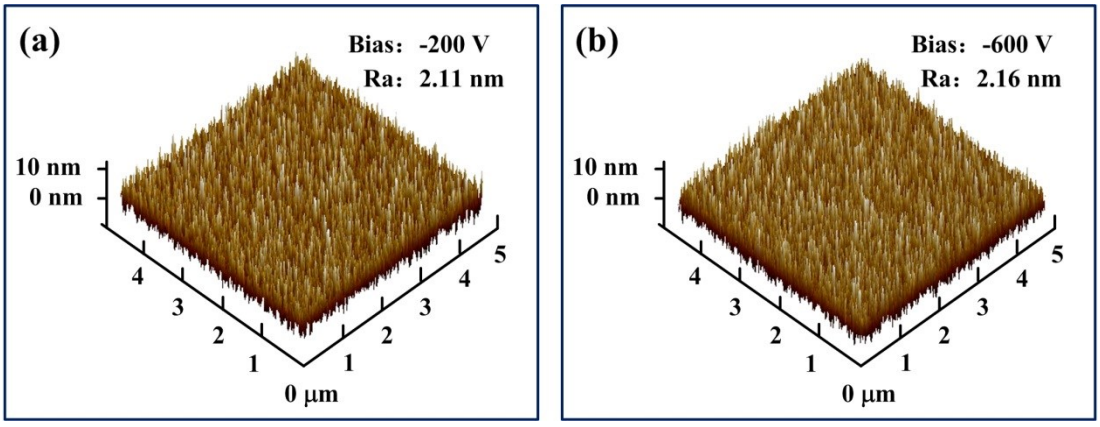

Figure 3-7 The surface quality and roughness of microstructures with different bias voltages of (a) bias voltage of −200 V (b) bias voltage of −600 V.

3.3.1.3 Fracture Toughness

The fracture toughness of silicon and the DLC/silicon system [22] was measured by a nanoindetation method. Figure 3-7(a, b, c) shows typical indentation cracks in silicon, for −200 V and −400 V coated DLC films indented with a maximum load of 25 mN. Obvious lateral cracks were observed in all samples and some radial cracks were present on coated samples. The sample coated at −400 V coated had the shortest crack length.

Since the DLC film thickness was roughly 150 nm and the indentation load had to be large enough to ensure the occurrence of a fracture, the fracture toughness we measured may also be influenced by substrate. To evaluate this influence, the crack lengths for different indentation loads, up to 100 mN were measured. As Fig. 3-8(d) illustrates, indentation load *P* was nearly proportional to the 1.5-th power of crack length *c*. Furthermore, no obvious discrepancy was found as the indentation load was incremented, which indicates that the influence from the substrate might be negligible for a sufficiently small indentation force.

The fracture toughness was calculated using Equation 3-5 and the value is shown in Table 3-3. The toughness of the silicon substrate was 1.18 MPa$\sqrt{m}$, which agrees with Nakao's research (1.28 MPa$\sqrt{m}$) [23]. The toughness of the DLC/silicon system ranged from 1.34 MPa$\sqrt{m}$ to 1.97 MPa$\sqrt{m}$, and the highest value was obtained in the sample subjected to a bias voltage of −400 V.

Table 3-3 Fracture toughness value of SCS and DLC film.

Samples	SCS	-200 V DLC	-300 V DLC	-400 V DLC	-500 V DLC	-600 V DLC
Toughness /MPa$\sqrt{m}$	1.16	1.34	1.71	1.97	1.65	1.80

In conclusion, with increasing the bias voltage, the deposition energy increased. Thus the sp^3 phase carbon increased and sp^2 phase carbon, hydrogen contents dropped, leading to an increase in hardness,

elastic modulus, and residual stress and influencing the fracture toughness with the highest value of 1.97 MPa$\sqrt{m}$.

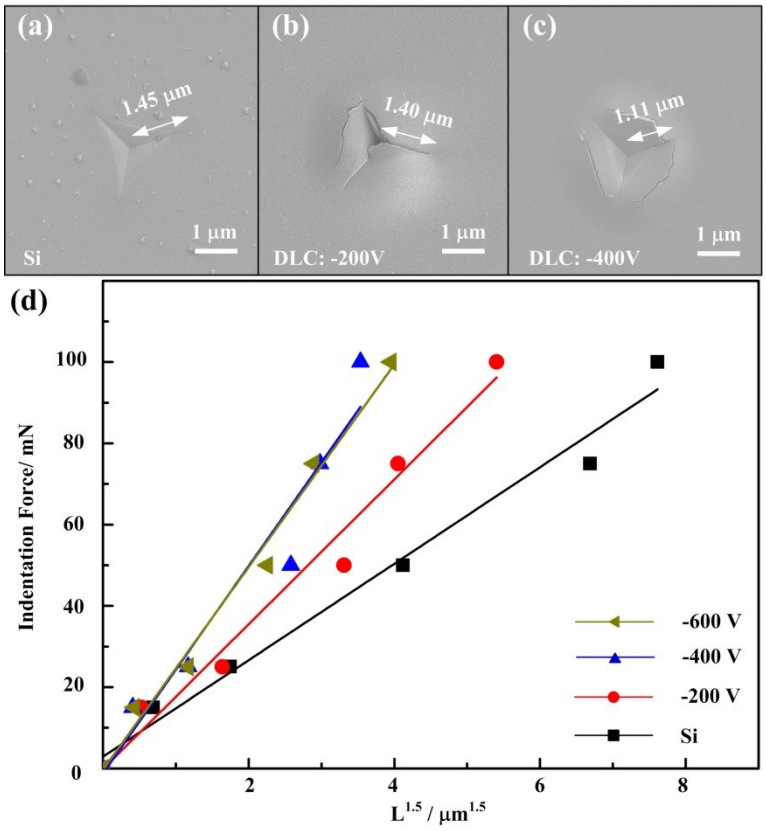

Figure 3-8 Fracture toughness measurement. (a) Typical indentation crack in silicon with a maximum load of 25 mN. (b) Typical indentation crack in DLC/silicon system coated at a bias voltage of −200 V and maximum load of 25 mN. (a) Typical indentation crack in DLC/silicon system coated at the bias voltage of −400 V and maximum load of 25 mN. (d) Relationship plot between indentation load P and the 1.5 power of silicon crack length for DLC/silicon system.

3.3.2 Tensile Properties

A summary of average tensile strengths for silicon and microstructures that were coated with DLC at different deposition bias voltages is provided in Fig. 3-9. The silicon structure had an average tensile strength of 3.04 GPa, which had a two-fold increase compared to previous report, due to the improvement in the surface patterning method. DLC coated structures revealed a 0.40~0.90 GPa increase compared with that of an uncoated silicon structure, which proved the reliability of full DLC coating method. The

tensile strength increased and, the highest strength of 3.94 GPa, was observed at a −400 V bias voltage. This value was slightly reduced when a voltage higher than −400 V was used.

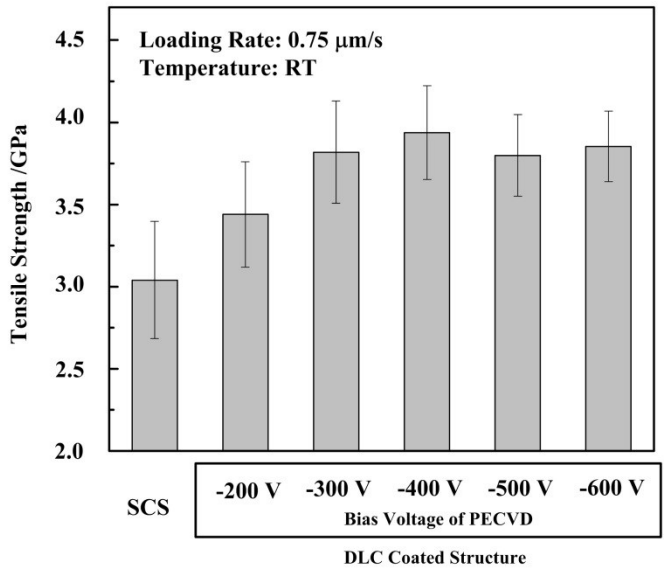

Figure 3-9 Tensile strength of SCS and DLC coated microstructures with different bias voltage.

Since both DLC and silicon are brittle materials, the measured tensile strengths showed a large distribution. A two-parameter Weibull analysis was used to estimate the relationship between tensile strength and cumulative tensile fracture rate. Figure 3-10 shows a fitted Weibull plot for silicon and a DLC coated microstructures, with shape parameter *m* acquired by linear approximation of the plot. It observed that DLC coated silicon microstructures have a narrower distribution then that of bare silicon one. For DLC coated structures, the deviation in tensile strength decreased with increasing bias voltage.

Figure 3-11 depicts the fracture surface of silicon and DLC coated microstructures at a −200 V bias voltage. The side wall of tensile microstructures shaped by stepper was relatively smooth than that shaped by double-side mask aligner. The typical scallop shape from ICP-RIE process was observed and the surface was quite homogeneous.

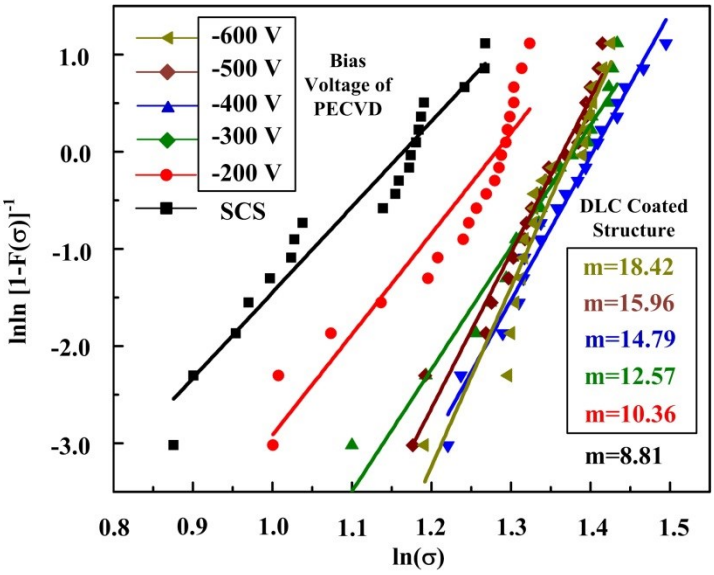

Figure 3-10 Weibull plot for tensile strength of silicon and DLC microstructures coated at different bias voltages. Shape parameter (Weibull Modulus, *m*) is shown in the plot.

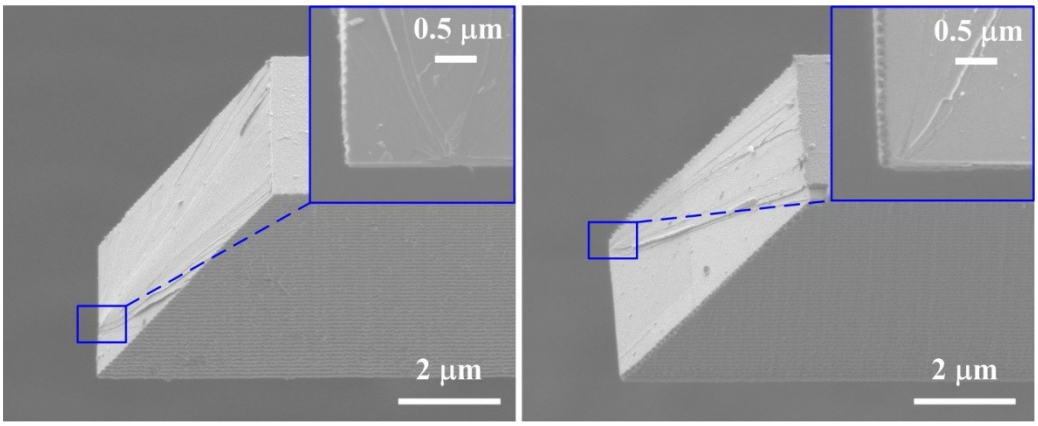

Figure 3-11 Typical fracture surfaces of microstructures observed at a tile angle of 45°. (a) Fracture surface of silicon microstructure. (b) Fracture surface of DLC microstructure coated at a bias of −200 V.

All of the silicon structures fractured in the same plane of (111). Most fractures originated from the bottom surface, due to initial defects in the raw SOI wafer. The fracture plane was unaltered by the DLC film surface, but more than 80% of the structures fractured from top or bottom corners, which have been formed by unevenness in the photoresist pattern as used the etching mask. Difference in the fracture

origin location revealed that DLC film covered the initially existing defects on the SOI wafer surface, leading to an improvement in tensile strength of the microstructures. Moreover, no spalling of the DLC was observed near the fracture origin (Fig. 3-11(b)) and the fracture was likely to be generated from the surface of the DLC film. In this way, tensile strengths of coated microstructures can be correlated with the fracture toughness of the DLC film.

3.4 Discussion

3.4.1 Tensile Strength Improvement

The influence of substrate bias voltage on tensile strength and strength deviation is discussed in this section. Figure 3-12 shows a comparison between fracture toughness and tensile strength of silicon and DLC coated microstructures. It is apparent that a good correlation exists between them since fracture happened on the surface of microstructures. The structure of bias -400 V show the highest fracture toughness. The reason could be explained qualitatively from the basic energy-balance concept proposed by Griffith, in which the fracture toughness of a material can be estimated from the elastic energy released during crack growth to the surface energy required to create new surfaces [24].

$$K_C = \sqrt{2\gamma E} \qquad (3-7)$$

where K_c is the fracture toughness. E is the elastic modulus and γ is the surface energy of DLC film, which can be calculated as:

$$\gamma = 0.5 N_{surf} \epsilon \qquad (3-8)$$

where N_{surf} is the density of bonds per unit area, which is about 1.23×10^{19} m^{-2} for DLC and ϵ is the bond energy between two adjacent atoms, which is 638 kJ/mol for sp^2 bond and 368 kJ/mol for sp^3 bond [25]. With increasing bias voltage, sp^3 content increased, leading to an increase in elastic modulus, whereas a decrease in surface energy. Hence, the increase in fracture toughness in -200 V, -300 V and -

400 V deposited DLC film was dominated primarily by the enhancement of the elastic modulus, while the slight decrease in the fracture toughness at higher bias voltages was mainly attributed to the reduction in the average surface energy.

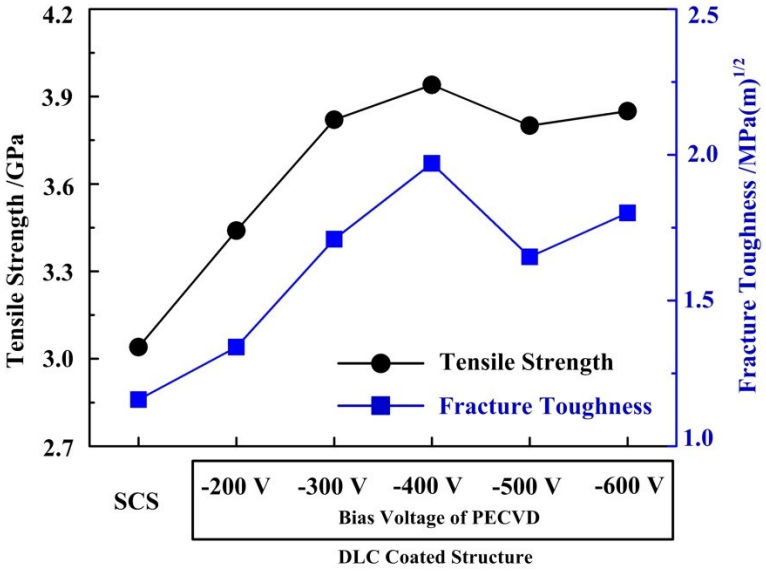

Figure 3-12 Average tensile strength and fracture toughness value for silicon and DLC/silicon system.

It should be pointed out that with the increment of bias voltage, the compression residual stress and deposition induced defects also increased [26, 27], causing another trade-off effect on the fracture toughness of DLC films. So it is difficult to decide the exact fracture toughness only using theoretical Formula 3-3 and Formula 3-4, and better to be measured experimentally.

The surface quality improvement of microstructure might be another reason for tensile stress enhancement as the discussion in section 2.4. The surface quality influence mainly reflected from two aspects: the side wall roughness and film roughness. The side wall roughness was improved significantly and the tensile strength of SCS microstructures was much higher than that described in chapter. However, the tensile strength still raised by 0.90 GPa in this work by achieving relatively smooth surface. On the other hand, DLC film may contain nanocrystals or defects, and thus change the fracture mechanism and affect the tensile strength of coated microstructure. Section 3.3.1 proved that there was no obvious

roughness difference within different bias voltages. Thus, the effect of quality improvement would be also negligible and the tensile strength improvement was mainly due to better anti-fracture properties of coated DLC film.

3.4.2 Strength Deviation

An evident relationship between deposition voltage and shape parameter was observed in Weibull analysis. This result can be considered as an effect of compressive residual stress [26] and analyzed through Tandon's model [27, 28]. For failure to occur, both the crack equilibrium and instability criteria have to be satisfied:

$$K_T = K_i - K_f \tag{3-9}$$

$$\frac{d(K_T)}{dc} \geq \frac{d(K_i - K_f)}{dc} \tag{3-10}$$

where K_T and K_f are the stress intensity factors due to the applied tensile stress and residual stress, respectively. K_i is the intrinsic toughness value of the film and c is the crack length. According to the classical fracture mechanics, K_T and K_f can be expressed as:

$$K_T = \psi\sigma c^{1/2} \tag{3-11}$$

$$K_f = \frac{\psi}{\pi c^{1/2}} \int_0^c \sigma_f(t) \frac{2c}{(c^2 - t^2)^{1/2}} dt \tag{3-12}$$

where σ was applied tensile stress, and ψ was a constant. $\sigma_f(t)$ was the residual stress profile along film thickness t. For the film under high-energy ion bombardment, the residual stress profile $\sigma_f(t)$ of PECVD DLC film would be simplified as a quadratic function, with the stress at the surface and interface zero and maximum at the center. The average value was measured residual stress. The reason could be interpreted as the stress releasing near the interface and surface, which was caused by substrate deformation, as well

as migration of embedded atoms and free surface, respectively [29]. Substituting Equation 3-9, 3-11 and 3-12 into inequality Equation 3-10, the failure condition was expressed as:

$$\beta(c) = 1 + \frac{2\psi\sigma_f c^{3/2}(8/\pi t + 4c/t^2)}{K_i} \geq 0 \qquad (3-13)$$

Figure 3-13 plots *β(c)* as a function of the crack length in DLC film with three different bias voltages. The crack length was normalized to the DLC film thickness *t*. At higher bias voltage, negative value of *β(c)* ($c_1<c<c_2$) exists, which indicates that a crack with its length smaller than c_2 showed stable propagation because of non-uniform compressive stress. Therefore the deviation of observed tensile strength would be suppressed by the effect [26]. With the increment of bias voltage, the stabilization effect became more distinct, leading to an increase in the shape parameter.

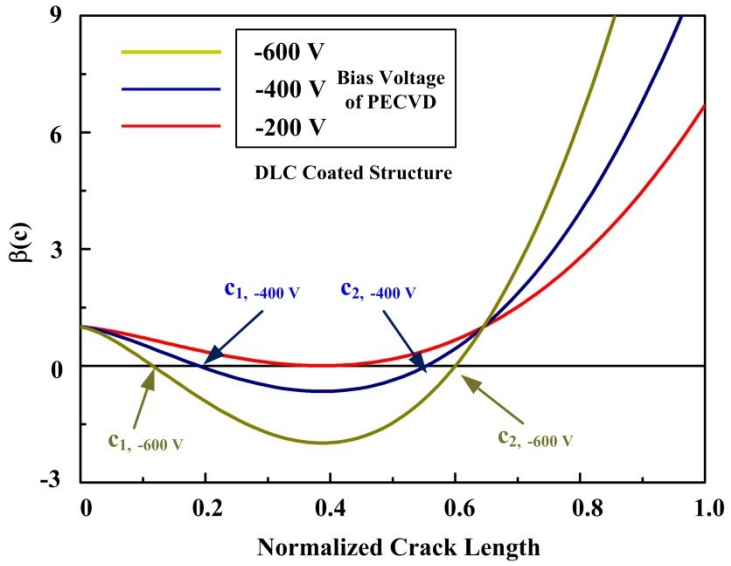

Figure 3-13 *β(c)* as a function of the normalized crack length (*c/t*) of DLC film.

The average initial crack length calculated from Equation 3-11 was 49.8 nm (normalized length: 0.33), using the measured average K_T and σ of DLC/silicon, as 1.64 MPa$\sqrt{\text{m}}$ and 3.7 GPa, respectively. The average initial size stood inside the region of stable crack growth (*β(c)<0*), which confirms the validity of using Tandon's model. However, the residual stress profile measurement of 150 nm thick film

is still a quite difficult task to verify the argument, and more research is needed on the actual stress profile of thin DLC film.

3.5 Conclusion

In this chapter, the SCS microstructure was fully coated by around 150-nm thick PECVD DLC film. The deposition bias voltage had a significant influence on the tensile properties of coated SCS structures. Chemical contents analysis showed that the ratio of sp^2/sp^3 phase carbon was 1.96~2.48, and hydrogen in our film was 32.5%~37.6%. With increasing the bias voltage, sp^3 phase and hydrogen increased, while sp^2 phase decreased, leading an increasing in film elastic modulus, hardness and residual stress. Average tensile strength of DLC coated microstructures was 13.2%~29.6% higher compared to SCS structures of 3.04 GPa. The value increased with increasing of bias voltage and slightly dropped when the bias was higher than -400 V, which was in good agreement with fracture toughness of DLC/silicon system. Weibull analysis showed the deviation in tensile strength reduced significantly with the increment of deposition bias. The compressive residual stress inside DLC film had high crack stability and made the strength value insensitive to the initial crack length. The observations and discussions reported in this article would contribute for a better understanding of the enhancement of MEMS components reliability through surface coating technology by DLC or even other hard, brittle coating material.

Reference

[1] W. Zhang, A. Uesugi, Y. Hirai. T. Tsuchiya, O. Tabata, Tensile test of a silicon microstructure fully coated with submicrometer-thick diamond like carbon film using plasma enhanced chemical vapor deposition method, Jpn. J. Appl. Phys. 56 (2017) 06GN01.

[2] K.J. Clay, S.P. Speakman, N.A. Morrision, N. Tomozeiu, W.I. Kapoor, Material properties and tribological performance of rf-PECVD deposited DLC coatings, Diamond Relat. Mater. 7 (1998) 1100-1107.

[3] C. Mack, Fundamental principles of optical lithography: the science of microfabrication, John Wiley & Sons Ltd., New York, 2007.

[4] J. Laconte, F. Iker, S. Jorez, N. Andre, J. Proost, T. Pardoen, D. Flandre, J.P. Raskin, Thin films stress extraction using micromachined structures and wafer curvature measurements, Microelectron. Eng. 76 (2004) 219-226.

[5] W.C. Oliver, G.M. Pharr, An improved technique for determining hardness and elastic modulus using load and displacement sensing indentation experiments, J. Mater. Res. 7 (1992) 1564-1583.

[6] K. Niihara, R. Morena, D.P.H. Hasselman, Evaluation of KIc of brittle solids by the indentation method with low crack-to-indent ratios, J. Mater. Sci. Lett. 1 (1982) 13-16.

[7] R. Wang, G. Zhou, Y. Liu, S. Pan, H. Zhang, D. Yu, Z. Zhang, Raman spectral study of silicon nanowires: high-order scattering and phonon confinement effects, Phys. Rev. B 61 (2000) 16827-16832.

[8] S. Prawer, K.W. Nugent, Y. Lifshitz, G.D. Lempert, E. Grossman, J. Kulik I. Avigal, R. Kalish, Systematic variation of the Raman spectra of DLC films as a function of sp^2:sp^3 composition, Diamond Relat. Mater. 5 (1996) 433-438.

[9] T.M.G. Mohiuddin, A. Lombardo, R.R. Nair, A. Bonetti, G. Savini, R. Jalil, N. Bonini, D.M. Basko, C. Galiotis, N. Marzari, K.S. Novoselov, A.K. Geim, A.C. Ferrari, Uniaxial strain in graphene by Raman spectroscopy: G peak splitting, Grüneisen parameters, and sample orientation, Phys. Rev. B 79 (2009) 205433.

[10] D.C. Elias, R.R. Nair, T.M.G. Mohiuddin, S.V. Morozov, P. Blake, M.P. Halsall, A.C. Ferrari, D.W. Boukhvalo, Control of graphene's properties by reversible hydrogenation: Evidence for graphane, Science 323 (2009) 610-613.

[11] J. Robertson, Diamond-like amorphous carbon, Mater. Sci. Eng. R 37 (2002) 129-281.

[12] A. Erdemir, The role of hydrogen in tribological properties of diamond-like carbon films, Surf. Coatings Technol. 146-147 (2001) 292-297.

[13] B. Marchon, J. Gui, K. Grannen, G.C. Rauch, J.W. Ager, S.R.P. Silva, J. Robertson, Photoluminescence and Raman spectroscopy in hydrogenated carbon films, IEEE Trans. Mag. 33 (1997) 3148-3150.

[14] Y. Miki, A. Nishimoto, T. Sone, Y. Araki, Residual stress measurement in DLC films deposited by PBIID method using Raman microprobe spectroscopy, Surf. Coatings Technol. 283 (2015) 274-280.

[15] M.H. Ahmed, J.A. Byrne, J.A.D. McLaughlin, A. Elhissi, W. Ahmed, Comparison between FTIR and XPS characterization of amino acid glycine adsorption onto diamond-like carbon (DLC) and silicon doped DLC, Appl. Surf. Sci. 273 (2013) 507-514.

[16] A. LiBassi, A.C. Ferrari, V. Stolojan, B.K. Tanner, J. Robertson, L.M. Brown, Density, sp3 content and internal layering of DLC films by X-ray reflectivity and electron energy loss spectroscopy, Diamond Relat. Mater. 9 (2000) 771-776.

[17] Y. Sun, X.Y. Huang, H. Wang, Influence of hydrogen content on optical and mechanical performances of diamond-like carbon films on glass substrate, J. Mater. Eng. Perform. 25 (2016) 1570-1577.

[18] N. Ravi, V.L. Bukhovets, I.G. Varshavskaya, G. Sundararajan, Deposition of diamond-like carbon films on aluminum, substates by RF-PECVD technique: Influence of process parameters, Diam. Relat. Mater. 16 (2007) 90-97.

[19] Z. Xu, Y. Zheng, F. Jiang, Y. Leng, H. Sun, N. Huang, The microstructure and mechanical properties of multilayer diamond-like carbon films with different modulation ratios, Appl. Surf. Sci. 264 (2013) 207-212.
[20] Y. Lin, A.W. Zia, Z. Zhou, P.W Shum, K.Y. Li, Development of diamond-like carbon (DLC) coatings with alternate soft and hard multilayer architecture for enhancing wear performance at high contact stress, Surf. Coatings Technol. 320 (2017) 7-12.
[21] Y.J. Jang, G.T. Kim, Y.J. Kang, D.S. Kim, J.K. Kim, A study on thick coatings of tetrahedral amorphous carbon deposited by filtered cathode vacuum arc plasma, J. Mater. Res. 31 (2016) 1957-1963.
[22] M. Nastasi, P. Kodali, K.C. Walter, J.D. Embury, R. Raj, Y. Nakamura, Fracture toughness of diamondlike carbon coatings, J. Mater. Res. 14 (1999) 2173-2180.
[23] S. Nakao, T. Ando, M. Shikida, K. Sato, Effect of temperature on fracture toughness in a single-crystal-silicon film and transition in its fracture mode, J. Microelectromech. Sci. 18 (2008) 015026.
[24] S. King, R. Chu, G. Xu, J. Huang, Intrinsic stress effect on fracture toughness of plasma enhanced chemical vapor deposited SiNx:H films, Thin Solid Films 518 (2010) 4898-4907.
[25] P.J. Kelly, R.D. Arnell, Magnetron sputtering: a review of recent developments and applications, Vaccum 56 (2000) 159-172.
[26] M.M. Tojek, D.J. Green, Effect of residual surface stress on the strength distribution of brittle materials, J. Am. Ceram. Soc., 72 (1989) 1885-1890.
[27] R. Tandon, D.J. Green, Crack stability and T-curves due to macroscopic residual compressive stress profiles, J. Am. Ceram. Soc., 72 (1991) 1981-1986.
[28] R. Tandon, D.J. Green, The effect of crack growth stability induced by residual compressive stresses on strength variability, J. Mater. Res. 7 (1992) 765-771.
[29] S. Zhao, H. Du, W. Hua, J. Gong, J. Li, C. Sun, The depth distribution of residual stresses in (Ti,Al)N films: Measurement and analysis, J. Mater. Res., 22 (2007) 2659-2662.

Chapter 4 Torsional Properties of DLC Coated Silicon Microstructure Using Resonant Vibration Testing

4.1 Introduction

In last two chapters, a custom-made tensile tester was set up and a full diamond-like carbon (DLC) coating process was developed on single crystal silicon (SCS) tensile microstructure. It was observed a significant improvement happened in both the tensile fracture strength and its deviation of DLC coated microstructures. And the improvement was directly decided by deposition bias voltages.

The tensile properties improvement is important not only in the tensile applications, but also in some other occasions such as bend and torsion, which is also quite common in micro electro-mechanical systems (MEMS). Since silicon and DLC film belong to the group of brittle material, the torsional fracture strength relates to its tensile fracture strength directly. Therefore, DLC coating is promising to be one of the candidates for improving the fracture strength of torsional application, for example, a scanning micro mirror resonator.

A scanning micro mirror resonator is one of the major optical devices in MEMS and plays an indispensable role in the fields of finger print sensing, light detection, laser printing and image display [1]. A MEMS mirror resonator mainly consists of a flame, torsional beams and a mirror plate [2], oscillated by electrostatic, electromagnetic, electrothermal or piezoelectric actuating [3]. These applications expect high reliability of the micro mirror including large scan angle and sufficient robustness against the possible damage from harsh environments, which are dominated by the fracture strength of torsional beams. Thus, seeking for the enhancement on torsional fracture strength by DLC coating and understanding its fracture mechanism are highly required.

Several studies have focused on the torsional fracture strength improvement by developing new material or surface modification based on the common silicon torsional beam. Among them, An et al. [4] fabricated a micro mirror resonator with carbon nanotubes-nickel nanocomposite (CNTs-Ni) beams by electroplating method and pointed out the potential applicability of CNTs-Ni torsional beam for its good mechanical properties. Hajika et al. [5] investigated the strengthening effect of hydrogen anneal for the silicon torsional beams. The authors concluded that the fracture strength and the strength deviation of SCS torsional beam was enhanced with longer anneal time. However, no one focused on the torsional properties of DLC coated silicon microstructure.

In this chapter, to study the effects of full DLC coating process on torsional fracture strength and deviation enhancement, a torsional test system was set up and torsional mirror resonator microstructure was designed. The SCS structure was fabricated thorough typical MEMS fabrication method and then coated with DLC film via a plasma enhanced chemical vapor deposition (PECVD) technique, from the top and bottom side simultaneously to minimize the deformations or damages caused by residual stress of DLC film. To analyze the relationship between torsional and tensile strength and optimize the coating parameter, three deposition bias voltages, -200 V, -400 V and -600 V, were adopted. Torsional test was conducted with the custom-made system and torsional properties, including torsional strength, strength deviation and torsional resonate frequency were compared with the characterization results of DLC films as well as tensile properties in our previous research [6, 7].

4.2 Experiment

4.2.1 Torsional Test System

Figure 4-1 shows the sketch of torsional test system in this research. A microstructure was attached on the top of a piezoelectric actuator (NTK Ceratec PAC166J) and was excited by the vertical movement of the actuator working at the resonant frequency. The angular amplitude was gradually increased by

increasing the input voltage to the actuator and adjusting the input frequency until the torsional beams were finally fractured. The maximum amplitude was recorded by detecting the reflected laser spot projected on a position sensitive detector (PSD, Hamamatsu Photonics S3270-01). A CCD camera (Hozan L-835) equipped on an optical microscope and X-Y axis, Z axis and θ linear stages were used to align the red laser beam (Global Laser 1260-03) on the mirror plate of the microstructure. Several filters were assembled in front of the laser source due with different structure material as well as the sensitivity of PSD.

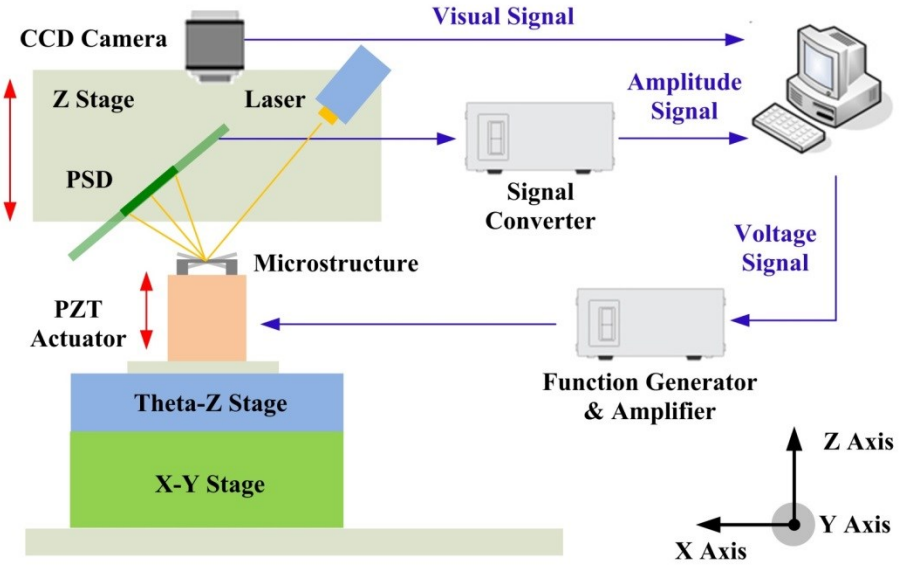

Figure 4-1 Sketch of torsional testing system.

Since the torsional microstructure was excited by a piezoelectric actuator, the linearity and maximum movable range were restrictive conditions for the resonator design. Figure 4-2 shows the displacement of piezoelectric actuator with increasing of applied voltage and different frequency, measured by a custom-made micro displacement measuring system (Fig. 4-3). A good linearity was observed even at a higher voltage of 80 V and the frequency did not affect the output displacement. However, since the friction heat from the polarization process of piezoelectric crystals became serious with higher applied frequency and

voltage, for example 2 KHz and 80 V in this research, and resulted in the damage to the actuator, the working frequency was restricted below 1 KHz for a safe operation.

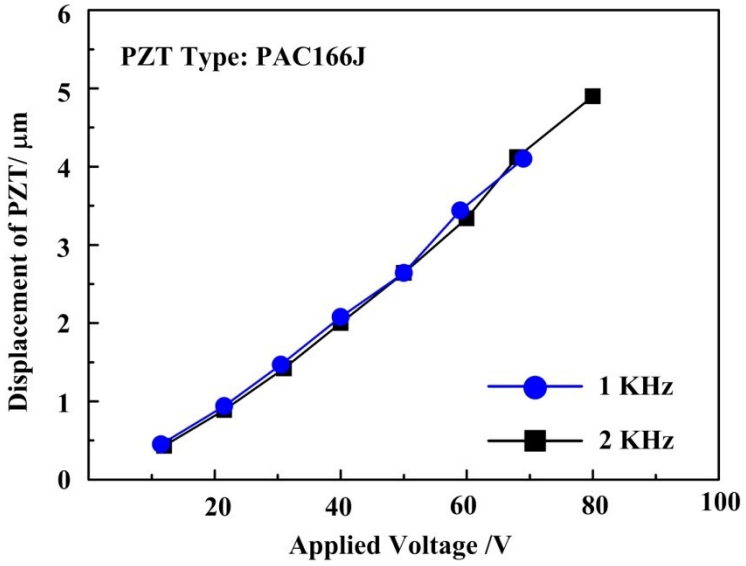

Figure 4-2 Displacement of piezoelectric actuator with increasing of applied voltage and working frequency of 1 KHz and 2 KHz.

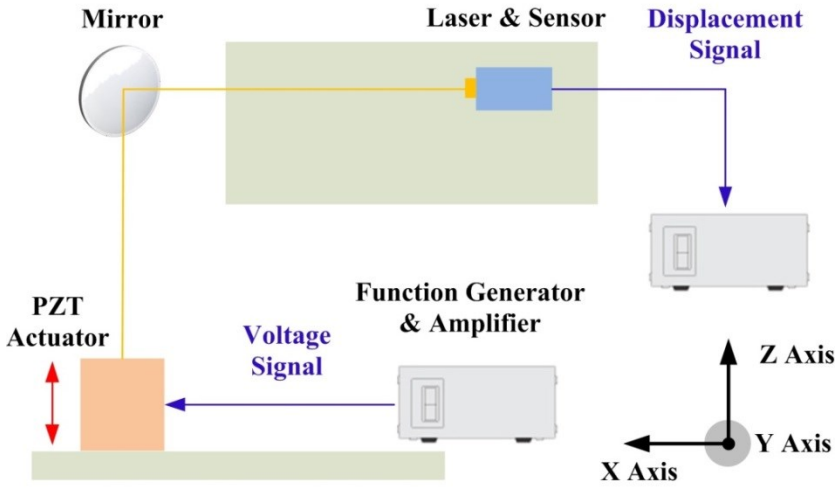

Figure 4-3 Sketch of micro displacement measuring system.

Prior to the torsion test, the test system was calibrated by a standard Gonio stage as Fig. 4-4 [8]. The result indicated a good calibration result when the torsional angle (mechanical angle) was smaller than 26° with the relationship below

$$U = 7.50 \tan \theta_{mech} \qquad (4-1)$$

where U is the output voltage from PSD and θ_{mech} is the torsional angle. Thus, the fracture angle of designed resonator should be designed smaller than 26°.

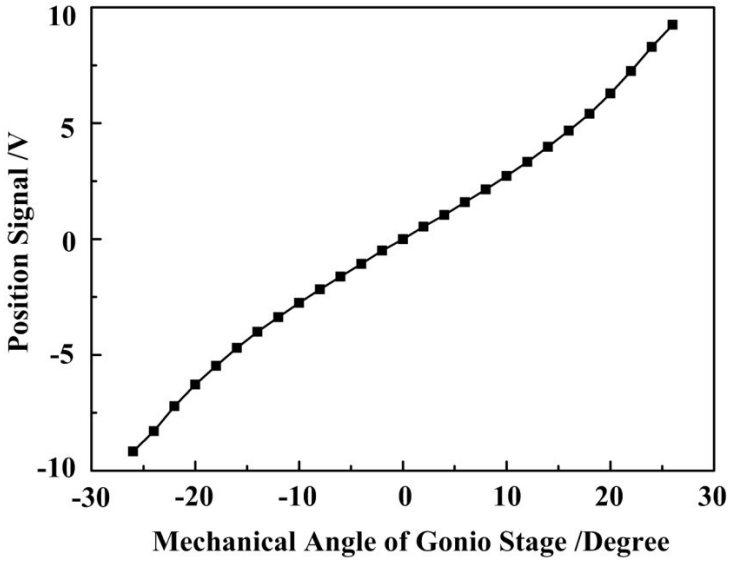

Figure 4-4 Calibration results from a standard Gonio stage (replotted) [8].

4.2.2 Silicon Torsional Microstructure Design

4.2.2.1 Design Target

The torsional microstructure was resonated by an outside piezoelectric actuator of the torsional test system described in last section. The sketch of torsional resonator is displayed in Fig 4-5, including an asymmetrically suspended mirror plate and a pair of torsional beams. Compared with other reported torsional structures excited by the actuator integrated inside the specimens [5, 9, 10], this design had the

advantages of easy fabrication, easy assembly without wire bonding and the gauge part suffering from less damage of surplus fabrication steps. And was suitable for material torsional properties test, which were asking for more test results as well as a good homogeneity of each structures.

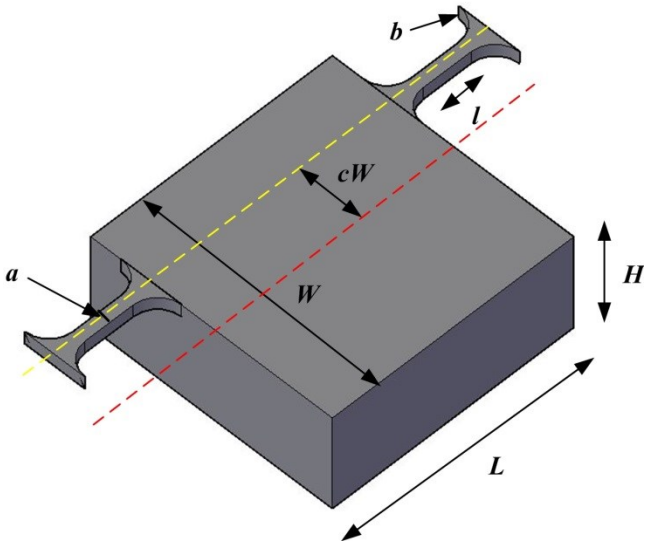

Figure 4-5 Sketch of torsional microstructure.

There were mainly seven parameters needed to be decided, including the dimensions of torsional beam with length l, width a, and height b; the dimensions of mirror plate with length L, width W, and height H, and offset parameter of the asymmetrically suspended mirror plate c.

The main design target of torsional microstructure was to make sure the chips could be tested on the torsional test system. And the restrictive conditions are concluded below: (1) fracture angle θ for silicon specimens was around 18° in case of DLC coated specimens have higher fracture angle; (2) the mirror plate was much larger than the laser spot, which was considered as 0.05 mm in radius; (3) the structure could be fractured with the displacement of piezoelectric actuator A smaller than 3.8 μm, with an applied voltage of 60 V; (4) torsional resonate frequency f was around or below 1 KHz; (5) the first modal of torsional microstructure was torsional modal, and much lower than other ones such as tensile and bending

modal; (6) the initial displacement (bending and torsion) of fabricated specimens should be much smaller than the fracture angle.

4.2.2.2 Design Detail

The torsional resonator was planned to be fabricated from 4 inch silicon on insulator (SOI) wafer with the 9-μm-thick device layer, 1-μm-thick sacrifice layer, and 400-μm-thick handle layer. Thus, the height of torsional beam b and mirror plate H was regarded as 9 μm and 400 μm, respectively. For an easier analysis of fracture strength, the cross section of torsional beam was considered as square, in which the width a was also 9 μm. The length of torsional beam l was decided by the expected fracture angle θ:

$$\theta = \frac{M_n l}{\beta G a b^3} \tag{4-2}$$

$$\tau = \frac{M_n}{\alpha a b^2} \tag{4-3}$$

where M_n is applied torque and τ is 3.3 GPa, the same with tensile strength of SCS [11]. α and β are torsional constant, which were 0.208 and 0.141 for the square cross section. G is shear modulus, which is calculated by the following equation [12].

$$G = \frac{E}{2(1+\nu)} \tag{4-4}$$

where E and υ are elastic modulus and Possion's ratio, which are assumed as 180 GPa and 0.30 for silicon, respectively [13]. Thus, since the maximum fracture angle was 18°, the length of torsional beam should no longer than 40.21 μm and was set as 40 μm in the consideration of design and measurement.

Since the mirror plate should be much larger than the spot size, in this research, the length and width of mirror plate was considered as 1 mm, with the same dimensions of commercialized micro mirror

resonator. And the displacement of piezoelectric actuator A for fracture happening was calculated from the offset of the asymmetrically suspended mirror plate d with the following principle: at the resonant frequency, the scanning amplitude of the resonator is Q-factor times amplified with the respect to the static condition [14]. Thus the relationship between torsional angle and displacement of piezoelectric actuator was described as:

$$\theta = \frac{QAcW}{\frac{2}{3}H^2 + (c^2 + \frac{1}{6})W^2} \qquad (4-5)$$

where Q is Q-factor of torsional microstructure, which was set as 200 according to other experimental results with the similar structures [4, 14]. Fracture angle θ was expected as 18°, in compliance with torsional beam design.

Figure 4-6 draws the curve from Equation 4-5 with the offset parameter c, ranging from 0.1 to 0.5. It was found that the required displacement of piezoelectric actuator for fracture had a minimum value of 1.6 μm when the c value was around 0.2~0.3. For an easier fabrication and measurement, c was set as 0.25.

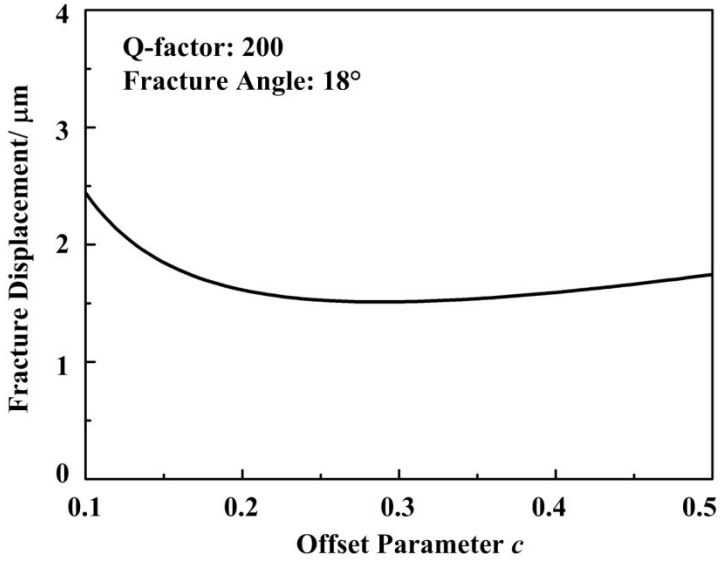

Figure 4-6 The relationship between required displacement and offset parameter.

The resonate frequency of torsional resonator was examined. Considering the mirror plate as grid, there were mainly three kinds of modals when the resonator was excited: torsion, bending and compression [15]. The frequency was calculated as follow:

$$f_t = \frac{1}{2\pi}\sqrt{\frac{2\beta G a b^3}{l J_p}} \tag{4-6}$$

$$f_b = \frac{2.267\pi^2}{4l^2}\sqrt{\frac{Ea^2}{12\rho}} \tag{4-7}$$

$$f_c = \frac{1}{2\pi}\sqrt{\frac{2Ea}{\rho l W H}} \tag{4-8}$$

where f_t, f_b and f_c are resonate frequency of torsion, bending and compression modal. ρ is density of SCS and J_p is the moment of inertia about the longitudinal axis of torsional beam. The f_t, f_b and f_c value of three frequencies were 695.5 Hz, 38227.7 Hz and 73104.2 Hz, respectively. The torsional frequency was the smallest and much smaller than the bending frequency, which confirmed that the when the vibration happened, the modal was pure torsion.

The torsional microstructure had a pair of torsional beams and a relatively large, asymmetrical mirror plate, which may lead to an initial angle on the torsional beams. Thus, the initial angles, including bending angle θ_b caused by the weight of mirror plate and the torsional angle θ_t caused by the asymmetrical mirror plate calculated below:

$$\sigma_b = \frac{3g\rho WHLl}{a^3} \tag{4-9}$$

$$\theta_b = tan^{-1}(\sqrt{\left(1+\left(\frac{\sigma_b}{E}\right)^2-1\right)^2} \tag{4-10}$$

$$\theta_t = \frac{0.25 g \rho W^2 L H l}{2 \beta G a^3 b} \qquad (4-11)$$

The initial bending and torsional angle were 0.25° and 0.02°, which was only around 1.3% of the expected fracture angle. Thus, the influence of initial angle could be neglected.

The main parameters of torsional structure are listed in Table 4-1, which were used as the dimensions of the resonator in this chapter.

Table 4-1 Main parameters of torsional microstructure.

Mirror Plate Length *L*	1000 μm	Torsion Beam Length *l*	40 μm
Mirror Plate Width *W*	1000 μm	Torsion Beam Weight *a*	9 μm
Mirror Plate Height *H*	410 μm	Torsion Beam Height *b*	9 μm
Offset Parameter *c*	0.25	Radius of Corners *r*	15 μm

It should be pointed out that in order to avoid stress concentration, all of the concave corners of torsional beams were rounded with a radius of 15 μm. The effect of round corners on the resonate frequency and fracture angle need to be discussed further.

4.2.2.3 FEM Simulation

FEM method was adopted in this research mainly for two proposes: examining the effect of round corners on the fracture angle as well as the stress distribution along the torsional beam.

The FEM simulation was conducted on Femtet (Murata Software) and the simulation model is shown in Fig. 4-7. One of the torsional beams was modeled with 15-μm-radius rounded corners and 20-μm-long gauge part, according to the experience of our previous torsional test [8]. The mesh density was

set as 1 μm and elements number was 55751. One end of the torsional beam was defined as an anchor with a solid fix situation, while another end was regarded as the mirror plate with an applied angular displacement of 18°. Silicon (100) was adopted in the model and the mechanical parameters from the built-in data base of the software.

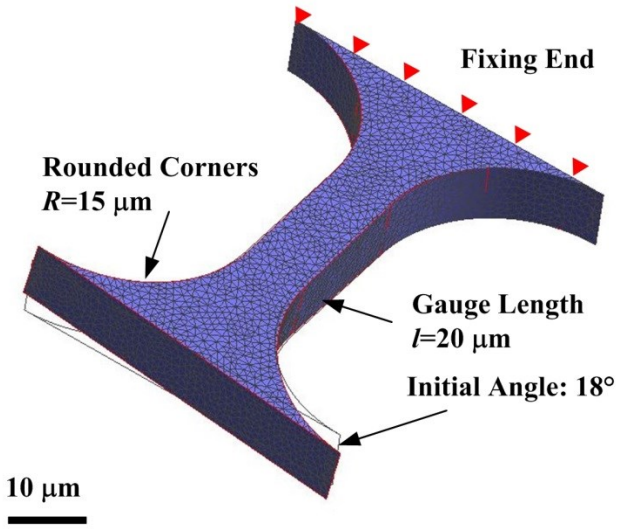

Figure 4-7 FEM simulation model of torsional beam.

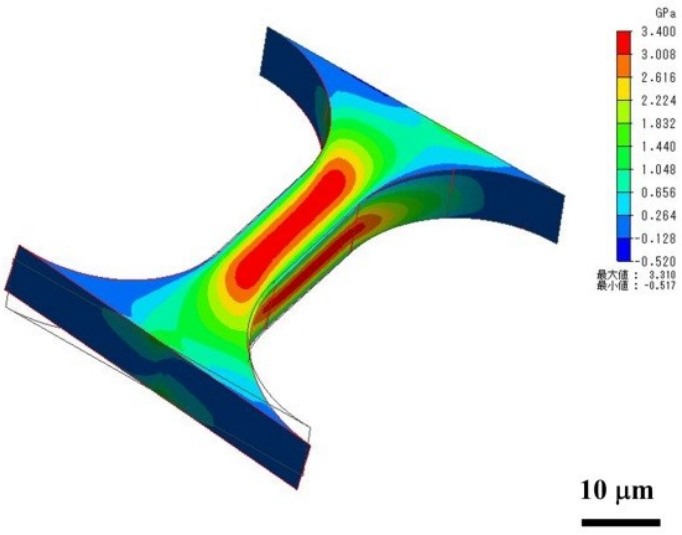

Figure 4-8 Stress distribution along the torsional beam.

The torsional stress and stress distribution were calculated. Figure 4-8 shows the stress distribution along the torsional beam and cross-section. It could be found that the maximum principle stress in the torsional beam was around 3.31 GPa, which had a similar value of tensile strength of silicon [11, 16, 17], proving that the torsional beam could be fractured with a torsional angle around 18°. The largest value happened at the center of each surface, showing a good agreement with Namazu et al.'s report [18].

4.2.3 DLC Coated Torsional Microstructure Fabrication

The SCS torsional microstructure was fabricated from a 4-inch silicon on insulator (SOI) wafer with (100) surface orientation. Unlike last chapter, the SOI wafer had no oxide layer at the surface of handle layer. Figure 4-9 illustrates the fabrication process of torsional microstructure. For a better side wall and less individual difference among different structures, the device layer was patterned in a stepper introduced in last chapter and the DLC film was fully coated on all side of torsional beam by the same PECVD instruments. The fabrication processes are listed in detail.

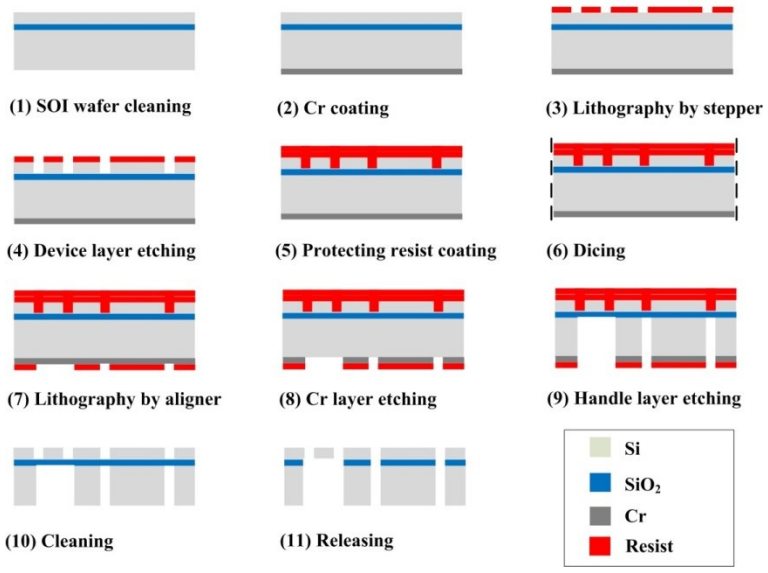

Figure 4-9 Fabrication process of torsional microstructures.

First, a 100-nm-thick chromium (Cr) film was deposited by an electron beam deposition on the backside handle layer (Canon Anelva EB1200). And then 9-μm-thick device layer was patterned by a stepper (Nikon NSR2205i11D) and then etched by inductively coupled plasma reactive ion etching (ICP-RIE, Samco RIE-iPB800) at an etching rate of 118 nm/cycle. The backside Cr film was patterned using a double-sided mask aligner (Union Optics PEM-800) and wet etching process. The 400-μm-thick handle layer was etched by the ICP-IRE at an etching rate of 3.5 μm/cycle. The residual resist, Cr, and fluorocarbon passivation film from ICP-RIE were completely removed by piranha solution wet etching and oxygen plasma assisted ashing (Samco FA-1), and then the resonator was released from the handle layer by etching the buried oxide layer with buffered hydrofluoric (BHF) acid. DLC film was coated by a PECVD tool (Shinkoseiki ACV-1060) with a sample holder spinning on its own axis as well as on the center of plasma to achieve full coating on the torsional resonator. To make the torsional fracture strength comparable with the tensile strength, three different deposition bias voltages: -200 V, -400 V and -600 V were studied, and the deposition time was maintained as 180 s for a target film thickness of 300 nm, to make the nominal DLC/Si volume ratio same with our previous research on tensile specimens [6, 7].

Figure 4-10 shows the mask design for the torsional microstructure.

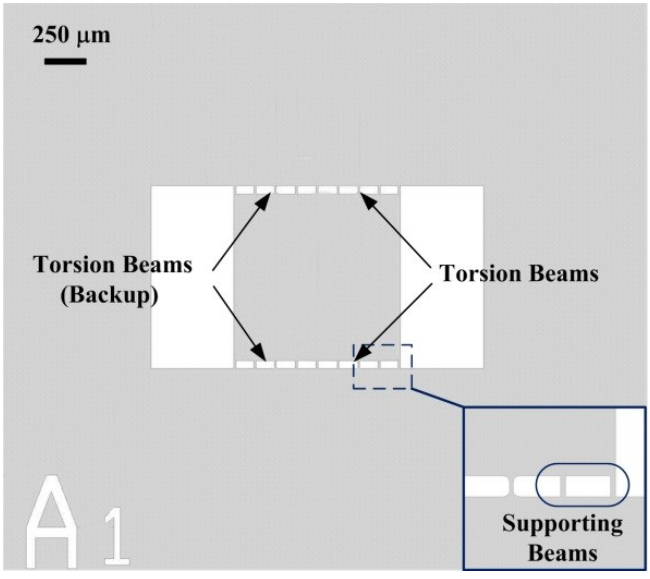

Figure 4-10 Mask design for one torsional microstructures.

The structure had an asymmetrically suspended mirror plate, seven pairs of supporting beams to prevent damage during fabrication, a pair of torsion beams and another pair of backup torsional beams, which were also acted as supporting beams. The FESEM photograph of one fabricated microstructure is shown in Fig. 4-11.

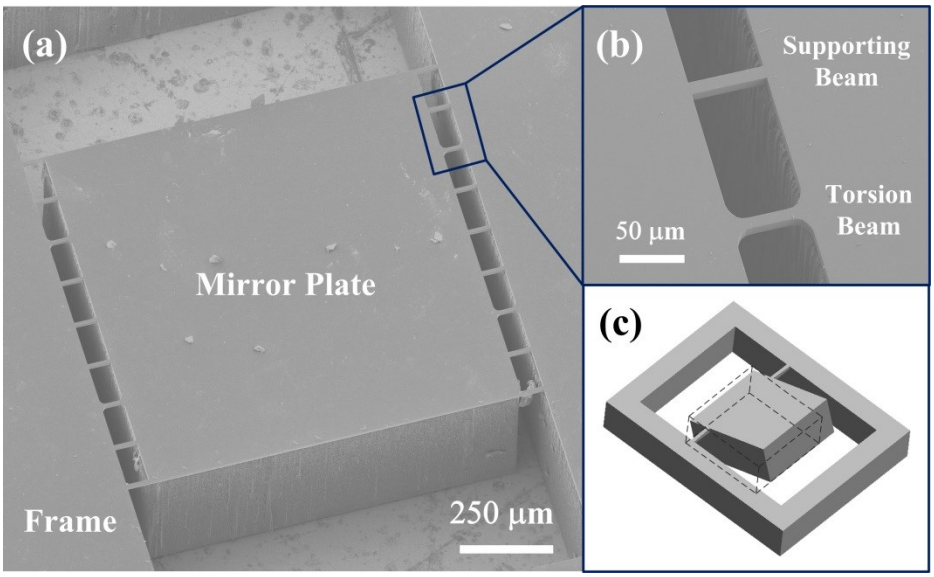

Figure 4-11 DLC coated torsional microstructure. (a) The mirror structure coated with DLC at bias of -400 V. (b) Local enlarged image of supporting and torsional beam. (c) Schematic drawing of the vibration of microstructure.

4.2.4 Characterization of DLC

The bias voltage affected the deposition rate and chemical contents (sp^2 carbon, sp^3 carbon and hydrogen) of the DLC films and thus affected their thickness, modulus, residual stress and fracture toughness. And the properties of fabricated DLC film may be even changed by the maintaining of PECVD machine in same occasions. Thus, to make a clear understanding on the properties of DLC film and torsional strength, the most important properties, such as chemical contents, elastic modulus and residual stress were characterized again in this chapter.

The chemical contents were qualitatively analyzed by Raman spectroscopy (Horiba LabRAM-HR800) at a laser excitation wavelength of 488 nm, recorded in the range 400-2600 cm^{-1}. The film

thickness and curvatures of coated samples were measured with a profilometer (Veeco DektakXT-S), and the residual stress was calculated from the curvatures result through Stoney's formula [19]. The film hardness and elastic modulus were measured using nanoindention method (Elionix ENT-2100) and calculated by the Oliver-Pharr method [20] with an average of four different indentations. In the test, 0.3 mN was set at the maximum indentation force and a 100-nm-radius Berkovich diamond tip was used.

4.2.5 Torsional Test

The torsional test was carried out at atmospheric pressure and room temperature with 10 microstructures for each deposition condition. Each of the torsional test was completed within 3 min and the maximum vibration cycle before fracture was 1.2×10^5 cycles estimated from the average resonant frequency of 624 Hz. Such low cycles probably caused insignificant fatigue effects to the torsional fracture strength [5]. The fracture surface was observed using a field emission scanning electron microscope (FESEM, Hitachi SU-8020).

4.3 Results

4.3.1 Characterization Results

The Raman spectra acquired from -200 V, -400 V and -600 V coated DLC film are depicted in Fig. 4-11. A sharp silicon band was observed at 520 cm^{-1} [21]. All of the spectra show a broad composite band around 1500 cm^{-1}, comprised of two Gaussian peaks corresponding to the D peak at 1350 cm^{-1} and G peak at 1530 cm^{-1} [22]. Table 4-2 summarized the fitting parameters, the ratios for the integrated intensity of the D peak to the G peak (I_D/I_G) and the photo luminescent background gradient to intensities of the G peak (k/I_G). Our result shows that higher negative bias voltage increased both I_D/I_G and k/I_G

value, indicating a reduction in sp^2/sp^3 ratio and amount of hydrogen according to Robertson and Marchon's work [23, 24].

Table 4-2 Fitting parameters of Raman spectra of DLC films.

Bias/ V	I_D	I_G	k	I_D/I_G	$k/I_G\times10^{-6}$
-200	3.52×10^5	2.04×10^5	1.58	1.72	7.7
-400	2.66×10^5	1.76×10^5	0.46	1.52	2.7
-600	1.60×10^5	1.34×10^5	0.27	1.20	2.0

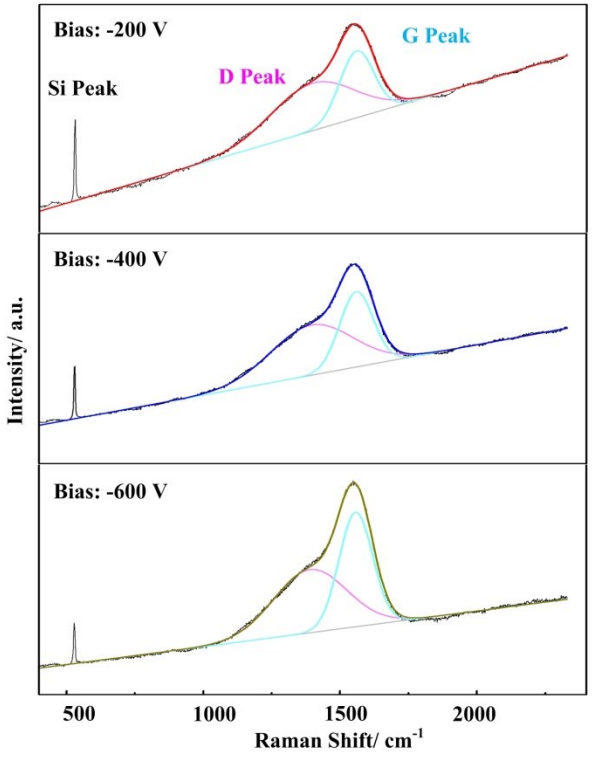

Figure 4-12 Raman spectra of DLC films with different bias voltages.

It should be mentioned that the I_D/I_G ratio was 25% larger than the data reported in last chapter. Although the sp^2/sp^3 ratios in DLC film cannot be derived directly from the Raman analysis, it could be referred that the film was slightly softer than last DLC coating.

Table 4-3 lists the thickness, elastic modulus, hardness and residual stress values of the SCS substrate and DLC samples obtained when using different bias voltage. The typical indentation force-displacement curves are shown in Fig. 4-13. Since the thickness became much larger and all of the maximum penetration depths were smaller than 1/7 of the film thickness, substrate influences on the calculated elastic modulus and hardness values were negligible [25].

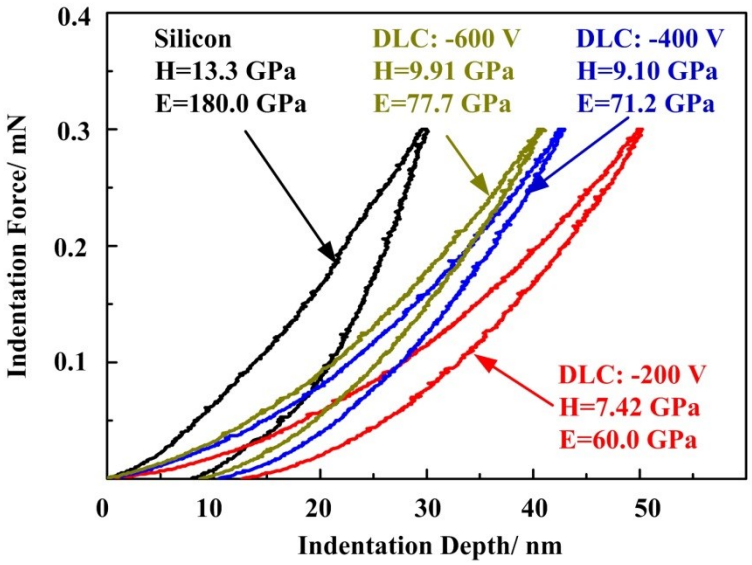

Figure 4-13 Nano-indentation curve of DLC films. Elastic modulus (E) and hardness (H) are shown in the graph.

The elastic modulus, hardness and compressive residual stress increased by raising the bias voltage while the deposition rate decreased, due to a competition between growth and etching during formation of DLC film [26]. The mechanical properties results show a good agreement with chemical composition analysis.

Table 4-3 Mechanical properties of SCS and DLC films.

Samples	DLC film			SCS
	-200 V	-400 V	-600 V	
Thickness/ nm	350	310	283	N/A
Elastic modulus/ GPa	60±3.0	71±3.0	78±2.7	180±11.0
Hardness/ GPa	7.4±0.5	9.1±1.2	9.9±0.8	13.3±0.3
Residual stress/ -GPa	0.44	0.83	1.06	N/A

4.3.2 Torsional Properties

The resonant frequency, torsional strength and strength deviation of SCS and DLC coated torsional microstructure were investigated in detail.

The frequency response for SCS and typical DLC coated structure are depicted in Fig. 4-14, and their Q-factors were calculated by half width method:

$$Q = \frac{f}{\Delta f} \qquad (4-12)$$

where *f* and *Δf* are the resonant frequency and bandwidth of its peak, respectively. The average resonant frequency of DLC coated microstrures was 10 Hz higher compared to that of silicon structure, while no apparent tendency was observed between coated one. A relatively high Q-factor of the mirror resonator, approximately 1200, was achieved in this research compared with other similar microstructures [4, 14]. DLC coating did not affect the Q-factor**.**

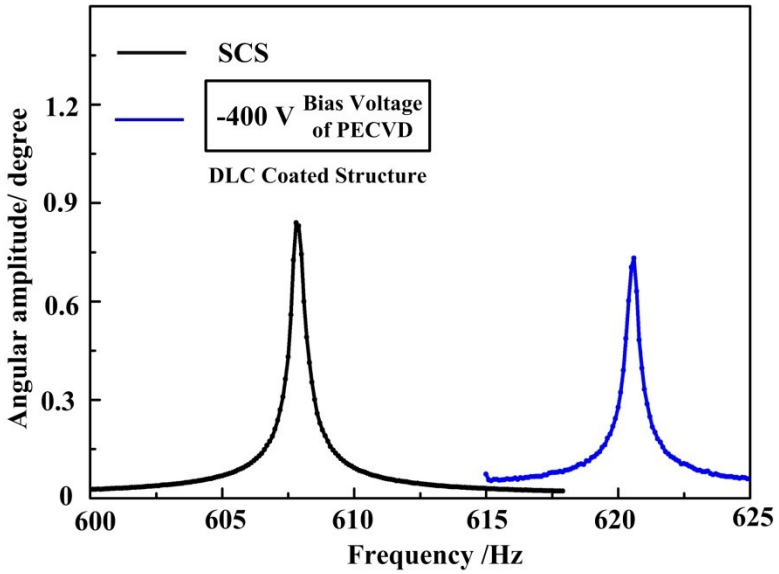

Figure 4-14 Typical frequency response of SCS and -400 V coated torsional microstructures.

Typical temporal plots of angular amplitude for bare and DLC coated SCS microstructures are shown in Fig. 4-15. T The loading curve is not smooth or linear, due to the nonlinearity of the resonator. The nonlinearity cased resonant frequency shift [27] and oscillation became unstable. The average fracture angle of SCS resonator was 17.98°, which was nearly the same as designed value.

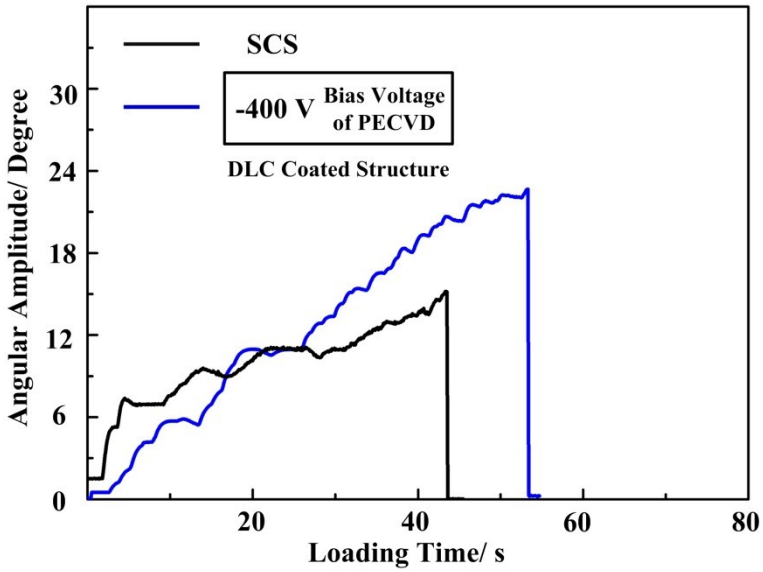

Figure 4-15 Typical loading curves of torsional test of bare and DLC coated SCS microstructures.

It is obvious that the maximum angular amplitude for DLC coated torsional microstructures were larger than that of bare silicon one. However, since the thickness of DLC film was around 300 nm, there was a 13.7% increment in the cross-sectional area of the torsional beams by adopting surface coating. The effect in dimensions change should be taken into consideration by using nominal torsional strength.

The torsional strength τ was defined as the total torque applied on the torsion beam divided by the dimension changed from Equation 4-2 and Equation 4-3:

$$\tau = \frac{M_n}{\alpha(d+t)^3} \qquad (4-13)$$

M_n can be considered as the sum of M_{Si} and M_{DLC}, torques applied on silicon and DLC films, and were calculated as follows:

$$M_{Si} = \frac{\beta G_{Si}\theta d^4}{l_e} \qquad (4-14)$$

$$M_{DLC} = \frac{G_{DLC}\theta t(d+t)^3}{l_e} \qquad (4-15)$$

where θ is measured from the maximum angular amplitude at the sudden drop. G_{Si} and G_{DLC} are shear modulus of silicon and DLC film, Since the torsion beams had fillets at the ends, the effective length of torsion beams l_e had to be obtained from the measured resonant frequency of silicon torsional beams:

$$l_e = \frac{\beta G_{Si} d^4}{2\pi^2 f^2 J_p} \qquad (4-16)$$

Figure 4-16 provides a summary of average torsional fracture strengths for bare and DLC coated SCS microstructures with different deposition bias voltages. The bare structure had average torsional fracture strength of 2.93 GPa. The strength was improved by DLC coating with an increase of 0.56~0.88 GPa, and the higher the negative bias voltage was, the higher the fracture strength was obtained.

Temporal plots proved brittle properties of DLC film and silicon during torsional fracture process, and thus a large distribution was observed in the fracture strengths result. The two-parameter Weibull analysis was conducted to estimate the relationship between torsional fracture strength and cumulative fracture probability [16].

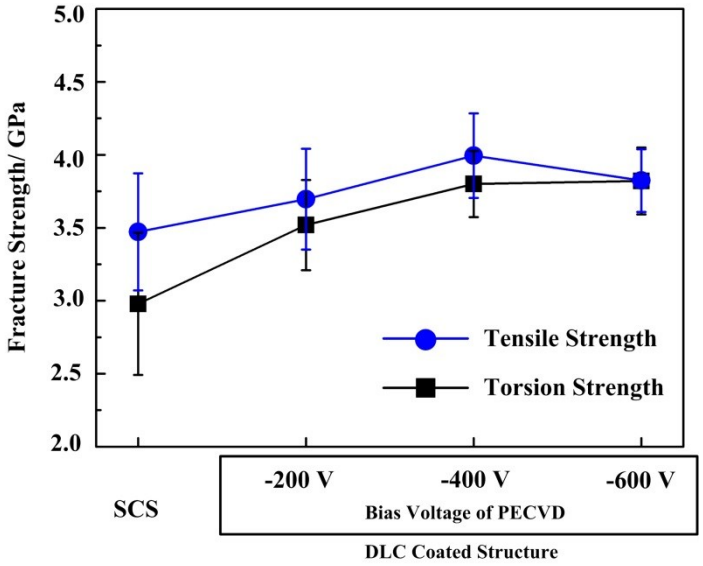

Figure 4-16 Average torsional fracture strength and tensile fracture strength values of SCS and DLC coated microstructures with different deposition bias voltages.

Figure 4-17 shows fitted Weibull plot for bare and DLC coated SCS microstructures with shape parameter *m* acquired by linear fitting. It is clear that DLC coated microstructures had higher Weibull modulus, representing a narrower distribution than those of bare silicon one. For the DLC coated ones, the deviation in torsional fracture strength decreased with increasing bias voltage.

Figure 4-18 shows the fracture surface of bare and DLC coated SCS microstructures at the deposition bias of -400 V.

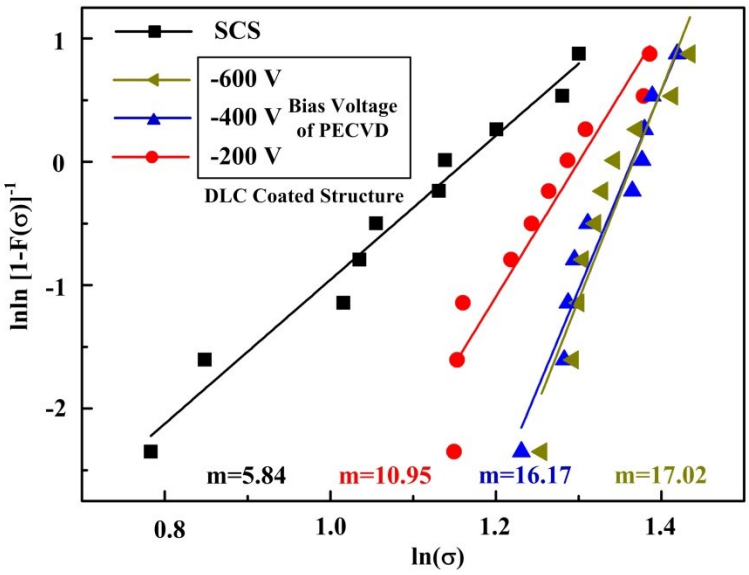

Figure 4-17 Weibull plot of torsional fracture strength of SCS and DLC coated microstructures with different deposition bias voltages. Shape parameter (Weibull Modulus, *m*) is shown in the plot.

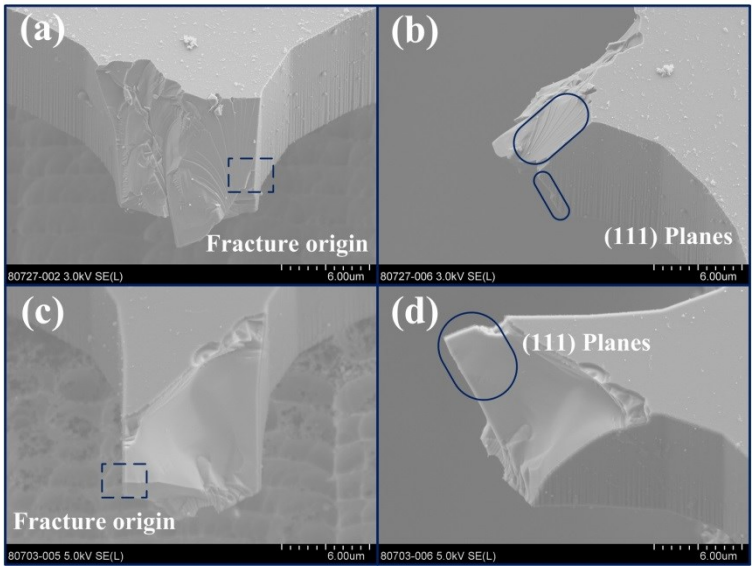

Figure 4-18 Typical fracture surfaces of torsional beam observed at a tile angle of 45° with the fracture origin and fracture planes. (a,b) SCS torsional beam. (c, d) Fracture surface of DLC coated torsion beam at the bias of -400 V.

Both of the structures had an acicular shaped surface alike the results of Namazu et al.'s research [18]. The fracture seemed to initiate from near the center of the side wall surface where the maximum

principal stress generated [29], as well as side wall roughness from ICP-RIE induced stress concentration. And then running along two (111) planes, leaving a quite smooth, brittle fracture surface near the origin. The fracture was likely to be generated from the surface of the DLC film since no spalling between DLC and silicon substrate was observed near the fracture origin.

4.4 Discussion

Here we discuss the effect of full DLC coating process on resonant frequency, torsional strength and its deviation of SCS torsional resonator. A 10 Hz increase in resonant frequency was observed by DLC coating, while no difference was observed by the different bias voltages. A quantitative explanation on the surface effects can be discussed based on Wang's sandwich beam model [30], in which the resonant frequency ratio of the coated/uncoated microstructures can be obtained as:

$$\frac{f_{DLC}}{f_{Si}} = \sqrt{(1+\alpha_1)(1+\alpha_2)} \qquad (4-17)$$

where f_{Si} and f_{DLC} are resonant frequency of bare and DLC coated SCS torsional microstructures. α_1 and α_2 are two dimensionless parameters standing for the effects of surface elasticity and surface residual stress, respectively. They are defined by:

$$\alpha_1 = \frac{E_{DLC} t d^3}{2 E_{Si} J_B} \qquad (4-18)$$

$$\alpha_2 = -\frac{2\sigma_r t d l_e^2}{\pi^2 (E_{Si} J_B + \frac{E_{DLC} t d^3}{2})} \qquad (4-19)$$

where σ_r, t and J_B are the compressive residual stress, thickness of DLC film and inertia moment of the torsion beam. Table 4-4 lists the value of α_1, α_2 and f_{DLC}, calculated from the properties obtained by nanoindentation. The difference between theoretical and experimental resonant frequency was smaller than 1.5%. α_1 and α_2 did not change significantly with different deposition bias voltage because of the

similar elastic modulus and thickness. Moreover, since α_1 was more than 10 times of α_2, it can be referred that the surface elasticity had much larger effect on the resonant frequency the than the compressive residual stress of the DLC film.

Table 4-4 Resonance properties of bare and DLC coated microstructures with different deposition bias voltages.

Structures	DLC-coated			Bare
	-200 V	-400 V	-600 V	
Measured resonate frequency/ Hz	625±5.6	624±9.0	629±10.0	616±11.0
Surface elasticity parameter α_1	0.0576	0.0624	0.0641	N/A
Residual stress parameter α_2	0.0024	0.0041	0.0049	N/A
Frequency ratio (Measured)	1.015	1.013	1.021	1
Frequency ratio (Calculated)	1.027	1.028	1.029	N/A

The torsional fracture strength of SCS microstructure increased substantially by a full DLC coating. The value shows a clear relationship with the deposition bias of the DLC film. Figure 4-15 shows a comparison between of the torsional fracture strength to the tensile strength measured in the previous report [7].

A good correlation exists between the two strengths. Since fractures occurred on the sidewall surface instead of the film interface and the brittle properties of both silicon and DLC film, the torsional fracture strength exhibited a strong relationship with tensile fracture strength, dominated by fracture toughness of

the DLC/silicon system [7]. This relationship was described by a limiting strain energy strength theory (LSEST) raised by Liu [31]. For brittle materials, the failure condition is defined as:

$$\sqrt{(\frac{\sigma_1}{\sigma_t})^2 + (\frac{\sigma_3}{\sigma_c})^2} \geq 1 \qquad (4-20)$$

where σ_t and σ_c are tensile and compressive strength of the material. σ_1 and σ_3 are the first and third principal stress. In the occasion of pure torsion:

$$\sigma_1 = -\sigma_3 = \tau \qquad (4-21)$$

The relationship between torsional strength and tensile strength is:

$$\frac{\tau}{\sigma_t} = \sqrt{\frac{1}{1+(\sigma_t/\sigma_c)^2}} \qquad (4-22)$$

As for SCS, the tensile strength and compressive strength was 3.0 GPa [7] and 7.0 GPa [32], respectively. The theoretical torsional strength was 0.92 time of the tensile strength, which agreed well with our experimental results.

The torsional strength deviation was improved by DLC coating and adopting higher deposition bias voltage, which had a similar tendency compared with our previous report on the tensile strength [6, 7]. It was reported that the compression residual stress inside DLC film not only improved the fracture toughness of DLC/silicon system, but also suppressed the defects activation and made the strength insensitive to the initial flaw size, causing a decrease in strength deviation [33, 34]. With higher deposition bias voltage, the sp^2/sp^3 ratio and the amount of hydrogen of DLC film reduced, and thus the compressive residual stress increased. Higher residual stress may enhance the crack stabilization, leading to a higher shape parameter. Another interesting finding was that the Weibull modulus increment between -400 V and -600 V coated microstructures were smaller than that between -200 V and -400 V. This may be attributed to the unexpected low residual stress of -600 V DLC film from some uncontrolled factors,

such as substrate current, in the deposition process. This finding also confirmed the validity of relationship between fracture strength and residual stress.

4.5 Conclusion

This chapter investigated the effects of fully DLC coating, aiming to improve the torsional fracture strength of SCS resonator for MEMS mirror usage. The torsional test system, driving by a piezoelectric actuator, was built and SCS torsional microstructure was designed to meet with the requirement of tester. The SCS structure was fully coated by a 300-nm-thick PECVD DLC film with three different deposition bias voltages. With the increase of bias voltage, the sp^2/sp^3 ratio and hydrogen amount decreased, resulting in an overall increase in film elastic modulus, hardness and compressive residual stress. DLC coating increased the resonant frequency by 10 Hz because of the change in the surface elasticity of mirror resonator. The average torsional fracture strength of SCS microstructure was 2.93 GPa and improved by DLC coating by 19.1~30.0%. A good agreement between torsional and tensile fracture strength, dominated by the fracture toughness of DLC/silicon system, was further confirmed. DLC coated microstructure showed a smaller deviation in torsional fracture strength compared to that of SCS ones. The deviation was further reduced as deposition bias voltage increased, related to the high crack stability caused by of compressive residual stress of DLC film. Our observations and discussions may contribute to the reliability enhancement of a MEMS torsional mirror through DLC surface coating technology, as well as a better understanding between torsional and tensile fracture strength for brittle, micro materials.

Reference

[1] S.T.S. Holmstrom, U. Baran, H. Urey, MEMS laser scanners: A review, J. Microelectromech. Syst. 23 (2014) 259-275.

[2] L. Ye, G. Zhang, Z. You, 5 V compatible two-axis PZT driven MEMS scanning mirror with mechanical leverage structure for miniature LiDAR application, Sensors 17 (2017) 1-13.

[3] R. Maeda, J.J. Tsaur, S.H. Lee, M. Ichiki, Piezoelectric microactuator devices, J. Electrocream. 12 (2004) 89-100.

[4] Z. An, L. He, M. Toda, G. Yamamoto, T. Hashida, T. Ono, Microstructuring of carbon nanotubes-nickel nanocomposite, Nanotechnology 26 (2015) 195601.

[5] R. Hajika, S. Yoshida, Y. Kanamori, M. Esashi, S. Tanaka, An investigation of the mechanical strengthening effect of hydrogen anneal for silicon torsion bar, J. Micromech. Microeng. 24 (2014) 105014.

[6] W. Zhang, A. Uesugi, Y. Hirai, T. Tsuchiya, O. Tabata, Tensile test of a silicon microstructure fully coated with submicrometer-thick diamond like carbon film using plasma enhanced chemical vapor deposition method, Jpn. J. Appl. Phys. 56 (2017) 06GN01.

[7] W. Zhang, Y. Hirai, T. Tsuchiya, O. Tabata, Effect of substrate bias voltage on tensile properties of single crystal silicon microstructure fully coated with plasma CVD diamond-like carbon film, Appl. Surf. Sci. 443 (2018) 48-54.

[8] 帯谷和敬, ねじり梁を用いた振動型ミラーの共振疲労試験, bachelor thesis, Kyoto University, 2018 (in Japanese).

[9] A. Arslan, D. Brown, W.O. Davis, Comb-actuated resonant torsional microscanner with mechanical amplification, J. Microelectromech. Syst. 19 (2010) 936-943.

[10] F. Filhol, E. Defay, C. Divoux, C.Zinck, M.T. Delaye, Resonant micro-mirror excited by a thin-film piezoelectric actuator for fast optical beam scanning, Sens. Actuators A Phys. 123-124 (2005) 483-489.

[11] A. Uesugi, T. Yasutomi, Y. Hirai, T. Tsuchiya, O.Tabata, High-temperature tensile testing machine for investigation of brittle–ductile transition behavior of single crystal silicon microstructure, Jpn. J. Appl. Phys. 54 (2015) 06FP04.

[12] J.J. Wortman, R.A. Evans, Young's modulus, shear modulus, and Poisson's ratio in Silicon and Germanium, J. Appl. Phys. 36 (1965) 153-156.

[13] M.A. Hopcroft, W.D. Nix, T.W. Kenny, What is the Young's modulus of Silicon, J. Microelectromech. Syst. 19 (2010) 229-238.

[14] C.L. Pan, Y.T. Ma, J. Y, F.R. Kong, Z.H. Feng, Miniature orthogonal optical scanning mirror excited by torsional piezoelectric fiber actuator, Sens. Actuators A Phys. 165 (2011) 329-337.

[15] 中村友哉, シリコンナノワイヤを用いたねじり梁型共振ミラー, bachelor thesis, Kyoto University, 2017 (in Japanese).

[16] T. Tsuchiya, O. Tabata, J. Sakata, Y. Taga, Specimen size effect on tensile strength of surface-micromachined polycrystalline silicon thin films, J. Microelectromech. Syst. 7 (1998) 106-113.

[17] T. Tsuchiya, T. Hemmi, J. Suzuki, Y. Hirai, O. Tabata, Tensile strength of silicon nanowires batch-fabricated into electrostatic MEMS testing device, Appl. Sci. 8 (2018) 880.

[18] T. Namazu, H. Yamagiwa, S. Inoue, Tension-torsion combined loading test equipment for a minute beam specimen, J. Eng. Mater. Technol. 135 (2013) 011004.

[19] W.C. Oliver, G.M. Pharr, An improved technique for determining hardness and elastic modulus using load and displacement sensing indentation experiments, J. Mater. Res. 7 (1992) 1564-1583.

[20] J. Laconte, F. Iker, S. Jorez, N. Andre, J. Proost, T. Pardoen, D. Flandre, J.P. Raskin, Thin films stress extraction using micromachined structures and wafer curvature measurements, Microelectron. Eng. 76 (2004) 219-226.

[21] R. Wang, G. Zhou, Y. Liu, S. Pan, H. Zhang, D. Yu, Z. Zhang, Raman spectral study of silicon nanowires: high-order scattering and phonon confinement effects, Phys. Rev. B 61 (2000) 16827-16832.

[22] J. Vetter, 60 years of DLC coatings: Historical highlights and technical review of cathodic arc processes to synthesize various DLC types, and their evolution for industrial applications, Surf. Coat. Tech. 257 (2014) 213-240.

[23] J. Robertson, Diamond-like amorphous carbon, Mat. Sci. Eng. R 37 (2002) 129-281.

[24] B. Marchon, J. Gui, K. Grannen, G.C. Rauch, J.W. Ager, S.R.P. Silva, J. Robertson, Photoluminescence and Raman spectroscopy in hydrogenated carbon films, IEEE Trans. Mag. 33 (1997) 3148-3150.

[25] B. Jonsson, S. Hogmark, Hardness measurements of thin films, Thin Solid Films, 114 (1984) 257-269.

[26] N. Ravi, V.L. Bukhovets, I.G. Varshavskaya, G. Sundararajan, Deposition of diamond-like carbon films on aluminum, substates by RF-PECVD technique: Influence of process parameters, Diam. Relat. Mater. 16 (2007) 90-97.

[27] T. Izawa, T. Sasaki, K. Hane, Scanning micro-mirror with an electrostatic spring for compensation of hard spring nonlinearity, Micromachines 8 (2017) 240.

[28] N. Savvides, T.J. Bell, Hardness and elastic modulus of diamond and diamond-like carbon films, Thin Solid Films 228 (1993) 289-293.

[29] H. Yamagiwa, T. Fujii, T. Namazu, M. Saito, K. Yamada, T. Miyatake, Influences of specimen size and deformation mode on the strength of single-crystal silicon micro-beam structures, MEMS 2012, Pairs, 2012.

[30] G. Wang, X. Feng, Effects of surface elasticity and residual surface tension on the natural frequency of micro beams, Appl. Phys. Lett. 90 (2007) 231904.

[31] G. Liu, A novel limiting strain energy strength theory, Trans. Nouferrous Met. Soc. China 19 (2009) 1651-1662.

[32] B. Moser, K. Wasmer, L. Barbieri, J. Michler, Strength and fracture of Si micropillars: A new scanning electron microscopy-based micro-compression test, J. Mater. Res. 22 (2007) 1004-1011.

[33] M.M. Tojek, D.J. Green, Effect of residual surface stress on the strength distribution of brittle materials, J. Am. Ceram. Soc. 72 (1989) 1885-1890.

[34] R. Tandon, D.J. Green, The effect of crack growth stability induced by residual compressive stresses on strength variability, J. Mater. Res. 7 (1992) 765-771.

Chapter 5 Conclusion

5.1 Overview

In this thesis, to enhance the reliability, including tensile and torsional properties, of silicon microstructures for electro-mechanical systems (MEMS) applications, one layer of diamond-like carbon (DLC) film was coated on the single crystal silicon (SCS) microstructures with thickness around 150~300 nm. DLC film is a kind of amorphous film with outstanding mechanical properties, but with relatively large compressive residual stress. To prevent the palling of film or the deformation of microstructures caused by unbalanced stress, a DLC film was fully coated on the entire surfaces of silicon microstructures by plasma enhanced chemical vapor deposition (PECVD) method.

Tensile and torsional test systems were built and the microstructures were designed and fabricated through standard MEMS technology. The tensile, torsional strength and strength deviation of bare and DLC coated SCS microstructures were investigated respectively. For further understanding of the fracture mechanism and confirming the repeatability of DLC coated microstructure, the influence of deposition bias voltage on tensile and torsional properties were explored, with taking consideration of chemical contents, hardness, elastic modulus, residual stress and fracture toughness of DLC film. Some mechanical models also were used for a theoretical understanding of residual stress effect on strength deviation, resonate frequency, and the relationship between tensile strength and torsional strength. The main conclusions of this thesis were listed as follows:

(1) The tensile strength of SCS microstructure was around 1.86~3.04 GPa, and strongly depended on the sidewall condition of microstructure; The torsional strength of SCS microstructure was 2.98 GPa.

(2) Fully DLC coating increased 13.2%~53.5% of the tensile strength and 18.1-27.9% of the torsional strength compared to those of uncoated SCS microstructures; No DLC spalling or substrate deformation happened on the coated microstructures.

(3) Fully DLC coating decreased the tensile and torsional strength derivation significantly.

(4) By increasing of deposition bias voltage, the sp^2 phase carbon, hydrogen decreased and sp^3 phase carbon increased, leading to an increasing of film elastic modulus, hardness and compressive residual stress. Bias voltage had no effect on film roughness.

(5) A good agreement existed among tensile strength, torsional strength of DLC coated microstructures and fracture toughness of Si/DLC system, due to their brittle properties.

(6) With increasing of deposition bias voltage, the tensile and torsional strength deviation decreased.

5.2 Chapter Summary

In Chapter 1, in addition to the overview and motivation, the fundamental knowledge of DLC film and MEMS reliability has been reviewed. DLC film is a kind of multipurpose material with excellent mechanical properties, good chemical stability, biocompatibility and adhesion with silicon. By using different deposition methods, adjusting coating parameters and elements doping, the properties of DLC film can be controlled and even some completely new properties can be investigated. Then, some typical usages of DLC films on traditional industry and MEMS industry were introduced. However, due to the large compressive residual stress, few report was done on the reliability improvement by using DLC film. Finally, the unclear things related to the reliable DLC coating method for MEMS usage and lack of mechanical properties of DLC coated silicon structures were emphasized, with the relevant work carried out in this thesis.

In Chapter 2, a custom-made tensile test system was built up and one layer of DLC film was coated on released SCS microstructure with the dimensions of 120 μm long, 4 μm wide and 5 μm thick, from the top and bottom side simultaneously. The thickness of DLC coating was around 150 nm and the deposition bias voltage was set as -400 V. The tensile strength of DLC coated microstructure was around 2.86 GPa, showing a 53.5% increment compared with uncoated ones. The strength derivation also decreased by adopting fully DLC coating. This study proved the feasibility of full DLC coating method on the tensile properties enhancement. However, due to the relatively rough and inhomogeneous side wall conditions, the detail fracture mechanism still remained unknown.

In Chapter 3, to explore the influence of coating parameters and the mechanism of film fracture, the SCS microstructure was fully coated by PECVD DLC film at five different bias voltages, ranging from -200 V to -600 V. After the depositions, Raman spectroscopy, X-ray photoelectron spectroscopy (XPS), thermal desorption spectrometry (TDS), surface profilometry, atomic force microscope (AFM) measurement, and nanoindentation methods were used to study the chemical and mechanical properties of the deposited DLC film. Tensile test indicated that the average strength of coated microstructure was 13.2~29.6% higher than that of the SCS one. The microstructure fabricated with a −400 V bias voltage was strongest. The fracture toughness of the DLC film was dominant factor in the observed tensile strength. Deviations in strength were reduced with increasingly negative bias voltage. The effect of residual stress on the tensile properties is discussed by adopting Tandon's model.

In Chapter 4, the torsional properties of DLC coated microstructure were studied. A custom-made torsional test system was built up and the 300 nm thick DLC film was adopted to enhance the torsional fracture strength of the SCS microstructure for micro mirror application. The SCS torsional beam of the resonator had dimensions of 20 μm long, 9 μm wide and 9 μm thick, and was fully coated using PECVD with three different deposition bias voltages, -200 V, -400 V and -600 V. The microstructure was driven by a piezoelectric actuator and evaluated from a custom-made torsional test system. Average torsional fracture strength of DLC coated microstructure was 18.1~27.9% higher than that of the SCS one, with

figure of 2.98 GPa. The torsional fracture strength exhibited a good agreement with the tensile fracture strength. Deviations in torsional fracture strength were also reduced with increasing of deposition bias voltage, due to the compressive residual stress of DLC film.

5.3 Practical Application

For the MEMS engineering researchers, the results we obtained in this thesis can provide useful information for the optimal design and production of DLC coated silicon microstructures serving as MEMS components working in tough conditions. The fully coating method reported in this thesis is not only useful for DLC film, but also important for other hard, brittle coating materials with high residual stress. Moreover, this work may inspire more research and usage of DLC film on MEMS for reliability enhancement as well as functional usage.

For the material science researchers, this work provide another engineer application of DLC films on MEMS field and a new evolution method for the on-chip material properties test. All the time along, the mechanical properties of DLC film was tested on a piece of sample coated silicon wafer instead of real microstructure. This kind of testing method can obtain some mechanical properties like hardness, indentation properties, and scratch properties, which are too abstract to be directly used for the engineering application. Our work is trying to build a bridge between material properties to the reliability of MEMS components, and make better understanding of the fracture mechanism of coating/substrate system.

For the industrial producers, even though the data reported in this thesis still cannot make DLC film fully accepted in MEMS industry, at least provided some idea of exploring new surface coating material to improve the reliability of their productions.

5.4 Future Work

This work reported the tensile and torsional properties of DLC coated microstructures; optimized the best coating conditions and discussed their fracture mechanism. Still, there is much space and interesting spaced to be improved. For example, this thesis discussed the mechanism of strength deviation by adopting Tandon's model in section 3.4.2. As it is mentioned in the text, the strength deviation inside DLC film is too hard to be tested and was assumed as a quadratic function. However, by controlling the penetration depth of Raman spectrum, this experiment may come true. And the reliability of using Tandon's model on this work can be further confirmed.

Another big research topic is that this paper still cannot provide a good method for DLC film pattern, including lift-off and etching. And also, the influence from tradition MEMS fabrication, such as lithograph, hard mask coating, wet etching, on the properties of DLC film remains unknown. I believe by corssing these barriers between academic research and industrial production, DLC film is hopefully to be a shining star in the sky of MEMS.

List of Publications

Journal Papers

[1] W. Zhang, A. Uesugi, Y. Hirai. T. Tsuchiya, O. Tabata, Tensile test of a silicon microstructure fully coated with submicrometer-thick diamond like carbon film using plasma enhanced chemical vapor deposition method, Jpn. J. Appl. Phys. 56 (2017) 06GN01.

[2] W. Zhang, Y. Hirai, T. Tsuchiya, O. Tabata, Effect of substrate bias voltage on tensile properties of single crystal silicon microstructure fully coated with plasma CVD diamond-like carbon film, Appl. Surf. Sci. 443 (2018) 48-54.

[3] W. Zhang, K. Obitani, Y. Hirai. T. Tsuchiya, O. Tabata, Fracture strength of a silicon torsional mirror resonator fully coated with submicrometer-thick PECVD DLC film, Sens. Actuators A Phys. In Process.

Conference Paper

[1] Wenlei Zhang, Akio Uesugi, Yoshikazu Hirai, Toshiyuki Tsuchiya, Osamu Tabata, Tensile properities of single-crystal-silicon fully coated with submicrometer-thick PECVD DLC, Micro Electro Mechanical Systems (IEEE-MEMS), 2017 IEEE 30th International Conference on (pp. 732-735).

Conferences

[1] 張文磊, 上杉晃生, 平井義和, 土屋智由, 田畑修, サブミクロン厚のプラズマ CVD-DLC 薄膜で全面被覆されたシリコンマイクロ構造の引張試験, 日本機械学会 2016 年度年次大会, 福岡, 日本, 2016.

[2] Wenlei Zhang, Akio Uesugi, Yoshikazu Hirai, Toshiyuki Tsuchiya, and Osamu Tabata, Tensile test of a silicon microstructure fully coated with submicrometer-thick DLC film using PECVD method, 29th International Microprocesses and Nanotechnology Conference (MNC 2016), Kyoto, Japan, 2016.

[3] Wenlei Zhang, Akio Uesugi, Yoshikazu Hirai, Toshiyuki Tsuchiya, and Osamu Tabata, Tensile properties of single-crystal-silicon fully coated with submicrometer-thick PECVD DLC, Micro Electro Mechanical Systems (IEEE-MEMS), Las Vegas, USA, 2017.

[4] 張文磊, 上杉晃生, 平井義和, 土屋智由, 田畑修, プラズマ CVD により DLC を全面被膜した単結晶シリコンマイクロ構造体の引張特性に及ぼす成膜バイアスの影響, 日本機械学会 2017 年度年次大会, 琦玉, 日本, 2017.

[5] Wenlei Zhang, Yoshikazu Hirai, Toshiyuki Tsuchiya, and Osamu Tabata, Tensile strength and deviation analysis of micro-scaled silicon structure with full-coated PECVD DLC film, 8th Micro/Nano Engineering Symposium (MNM 2017), Hiroshima, Japan, 2017.

[6] Wenlei Zhang, Yoshikazu Hirai, Toshiyuki Tsuchiya, and Osamu Tabata, Tensile properties of single crystal silicon microstructure fully-coated by plasma CVD diamond-like carbon with different substrate bias voltages, 2017 Materials Research Society Fall Meeting & Exhibit (MRS 2017 FALL), Boston, USA, 2017.

[7] 土屋智由, 張文磊, 中野優, 笠井隆, 吉村知浩, 佐野浩二, MEMS マイクロホンのダイアフラム用多結晶シリコン膜の引張強度評価, 日本機械学会 2018 年度年次大会, 大阪, 日本, 2018.

[8] 帯谷和敬, 張文磊, 平井義和, 土屋智由, 田畑修, ねじり梁を用いた振動型ミラーの信頼性評価, 日本機械学会 2018 年度年次大会, 大阪, 日本, 2018.

[9] Wenlei Zhang, Kazutaka Obitani, Yoshikazu Hirai, Toshiyuki Tsuchiya, and Osamu Tabata, Fracture strength of a silicon torsional mirror resonator fully coated with submicrometer-thick PECVD DLC film, 31st International Microprocesses and Nanotechnology Conference (MNC 2018), Sapporo, Japan, 2018.